DEVELOPMENT OF A COMPUTATIONAL MODEL FOR SHOE-FLOOR-CONTAMINANT FRICTION

by

Kurt Edward Beschorner

BS Mechanical Engineering, University of Illinois Urbana-Champaign, 2004

Submitted to the Graduate Faculty of

Swanson School of Engineering in partial fulfillment

of the requirements for the degree of

Doctor of Philosophy

University of Pittsburgh

2008

UNIVERISTY OF PITTSBURGH

SWANSON SCHOOL OF ENGINEERING

This dissertation was presented

by

Kurt Edward Beschorner

It was defended on

December 1, 2008

and approved by

Michael R. Lovell, Ph.D., Professor, Department of Mechanical Engineering, University of Wisconsin-Milwaukee

C. Fred Higgs III, Ph.D., Associate Professor, Department of Mechanical Engineering, Carnegie Mellon University

Rakié C. Cham, Ph.D., Associate Professor, Department of Bioengineering, University of Pittsburgh

Richard E. Debski, Ph.D., Associate Professor, Department of Bioengineering, University of Pittsburgh

Dissertation Director: Mark S. Redfern, Ph.D., Professor, Department of Bioengineering, University of Pittsburgh

DEVELOPMENT OF A COMPUTATIONAL MODEL FOR SHOE-FLOOR-CONTAMINANT FRICTION

Kurt Edward Beschorner, Ph.D.

University of Pittsburgh, 2008

Slip and fall accidents are a serious occupational and public health problem. While shoe-floor-contaminant friction is known to be critical to slip risk, no method of measuring shoe-floor-contaminant friction is widely accepted as being relevant to human slips. In addition, the tribological mechanisms of the shoe-floor-contaminant interface are poorly understood. This dissertation studies slips and falls from a biomechanical and tribological perspective. Heel contact control was investigated during human slipping experiments. Knee joint torques were found to be the primary contributor to heel acceleration during contact with the floor. For the tribology portion of this research, experimental testing was performed using a novel whole shoe slip testing method and a pin-on-disk tribometer. The experiments revealed that shoe-floor-contaminant friction could be described with the theoretical Stribeck curve. The lubrication regime that was determined to be most relevant to shoe-floor-contaminant friction was the mixed-lubrication regime. A computational model was developed to describe this mixed-lubrication regime, simulating the hydrodynamic and contacting pressures at the shoe-floor-contaminant interface applied to pin-on-disk experiments. The model-predicted friction values showed good agreement with experimental data. Because the custom code was limited to simple geometries, FEA was examined for its ability to simulate mixed-lubrication of an entire shoe heel against a floor surface. Limitations were discovered in current FEA software packages that prevented their use in shoe-floor-contaminant friction modeling. Therefore, a hybrid model that used FEA software to simulate the contact and custom modeling to simulate the lubrication effect was proposed. The research presented in this dissertation may be the first step towards developing a comprehensive shoe-floor-contaminant friction model, which will be useful for

evaluating slip potential of shoes and flooring, designing safer shoes and floor surfaces, and understanding the biomechanics of slipping.

TABLE OF CONTENTS

PREFACE xiii

NOMENCLATURE: xiv

For Section 5.1 xiv

For Section 5.2: xvv

1.0 PROPOSAL/SPECIFIC AIMS 1

1.1 LONG TERM PURPOSE 1

1.2 PURPOSE 2

1.3 SPECIFIC AIMS 2

1.3.1 Specific Aim #1 2

1.3.2 Specific Aim #2 2

1.3.3 Specific Aim #3 3

1.4 SUMMARY OF CHAPTERS 3

2.0 BACKGROUND 5

2.1 PROBLEM STATEMENT AND SIGNIFICANCE 5

2.2 CONTRIBUTING FACTORS TO SLIP AND FALL ACCIDENTS 7

2.3 MEASURING SLIPPERINESS 11

2.3.1 Devices 12

2.3.2 Human centered approaches 12

2.4 SHOE-FLOOR-CONTAMINANT FRICTION 14

2.5 THIN FLUID FILM MODELING TECHNIQUES 15

2.6 SUMMARY 20

3.0 HUMAN FACTORS: IMPACT OF JOINT TORQUES ON HEEL ACCELERATION AT HEEL CONTACT, A CONTRIBUTOR TO SLIPS AND FALLS 22

3.1 ABSTRACT 22

3.2 INTRODUCTION 23

3.3 METHODS 25

3.3.1 Subjects, experimental conditions and protocol 25

3.3.2 Data processing 27

3.4 RESULTS 31

3.4.1 Overview of general gait differences between recoveries and falls 32

3.4.2 Contribution of heel acceleration at heel contact to slip outcome 34

3.4.3 Heel contact heel acceleration determined by joint torques 35

3.4.4 Relationship between heel acceleration at heel contact and general gait variables ... 37

3.5 DISCUSSION 38

4.0 EXPERIMENTAL STUDIES 41

4.1 EFFECTS OF SLIP TESTING PARAMETERS ON MEASURED COFFICIENT OF FRICTION 41

4.1.1 Abstract 42

4.1.2 Introduction 42

4.1.3 Methods 45

4.1.3.1 Equipment 45

4.1.3.2 General protocol and data processing 47

4.1.3.3 Experiment #1 48

4.1.3.4 Experiment #2 49

4.1.4 Results 49

4.1.4.1 Force and COF profiles 49
4.1.4.2 Experiment #1 52
4.1.4.3 Experiment #2 55
4.1.5 Discussion 56
4.1.6 Conclusion 58
4.2 SHOE-FLOOR FRICTIONAL PROPERTIES FOR VARYING SLIDING SPEED, PRESSURE AND CONTAMINANT 59
4.2.1 Abstract 59
4.2.2 Introduction 60
4.2.3 Methods 61
4.2.4 Results 62
4.2.5 Discussion and Conclusions 64
4.3 SUMMARY 64
5.0 SHOE-FLOOR FRICTION MICRO-MODEL 65
5.1 MODELING MIXED-LUBRICATION OF A SHOE-FLOOR INTERFACE APPLIED TO A PIN-ON-DISK APPARATUS 66
5.1.1 Abstract 66
5.1.2 Introduction 66
5.1.3 Analytical Model 69
5.1.3.1 Contact Modeling 71
5.1.3.2 Hydrodynamic Modeling 72
5.1.3.3 Friction Model 75
5.1.4 Experimental Testing 76
5.1.5 Results 79
5.1.5.1 Experimental Results 79
5.1.5.2 Analytical Model Results 79

5.1.6 Discussion 84

5.1.7 Conclusions 86

5.2 SOLUTION OF REYNOLDS EQUATION IN POLAR COORDINATES APPLICABLE TO NON-SYMMETRIC ENTRAINMENT VELOCITIES 86

5.2.1 Abstract 86

5.2.2 Introduction 87

5.2.3 Methodology 88

5.2.4 Case Study I: Pin-on-Disk 91

5.2.5. Case Study II: Chemical-Mechanical Polishing (CMP) 97

5.2.6 Conclusions 101

5.3 SUMMARY 101

6.0 SHOE-FLOOR FRICTION MACRO-MODEL 102

6.1 PRELIMINARY SHOE-FLOOR-CONTAMINANT FINITE ELEMENT MODELING 102

6.1.1 Methodology 103

6.1.1.1 Implicit analysis 103

6.1.1.2 Explicit Analysis 107

6.1.2 Results 108

6.1.3 Limitations of Current FEA Modeling Approaches 111

6.1.4 Using Finite Element Analysis for Modeling Shoe-Floor-Contaminant Friction 112

6.2 PROPOSED HYBRID SHOE-FLOOR-CONTAMINANT FRICTION MODEL: CUSTOM MODELING UTILIZING FINITE ELEMENT ANALYSIS 113

6.3 SUMMARY 116

7.0 DISCUSSION AND CONCLUSIONS 117

7.1 FUTURE DIRECTIONS FOR SHOE-FLOOR-CONTAMINANT FRICTION MODEL 118

7.1.1 Necessary Improvements in the Model 118

7.1.2 Long Term Plan for Model 119

7.2 INTEGRATED TRIBOLOGY AND BIOMECHANICS APPROACH TO HEEL CONTROL DURING SLIPPING 121

7.3 CONCLUSIONS 123

BIBLIOGRAPHY 124

LIST OF TABLES

Table 3.1. Subject population characteristics stratified by age group 26

Table 3.2. General gait characteristics stratified by slip outcome and age group 33

Table 3.3. Pearson correlation coefficients relating gait variables of interest 36

Table 3.4 R^2 values of $HeelAcc_{HC}$ regressed on each joint torque individually and simultaneously 36

Table 4.1. List of whole shoe slip-testing devices and their testing conditions 44

Table 4.2. Correlation coefficients for regression analyses 53

Table 5.1. Testing Conditions 78

Table 5.2. Simulation parameters for pin-on-disk 92

Table 5.3. Comparison of Cartesian (Eq. 5.25c) and polar (Eq. 5.31) Reynolds equation results 95

Table 5.4. Simulation conditions for CMP 98

Table 6.1. Loading conditions for the implicit analysis simulation 106

LIST OF FIGURES

Figure 2.1. Flow chart for the slipping process 8

Figure 2.2. Slip initiation process 9

Figure 2.3. Stribeck curve 17

Figure 2.4. Chemical Mechanical Polishing 18

Figure 3.1. Heel velocity and acceleration average time series plots for normal gait 28

Figure 3.2. Typical heel position (a) and ground reaction forces (b) for baseline and slip trials . 30

Figure 3.3. Typical heel acceleration time series plots from dry (solid) and slip (dashed) trials . 33

Figure 3.4. Heel acceleration stratified by slip outcome and age group 34

Figure 3.5. Regression plot of $HeelAcc_{HC}$ against $KneeTorq_{HC}$ 37

Figure 4.1. Slip-testing device 46

Figure 4.2. Normal and shear force profiles for slow speed (a) and fast speed (b) 51

Figure 4.3. Examples of linear and quadratic correlations with low and high r^2 values 54

Figure 4.4 COF-normal force regression plots stratified by fluid contaminant and shoe angle across a range of testing speeds 55

Figure 4.5. Effect of speed on COF for two contaminants 56

Figure 4.6. Theoretical Stribeck curve 57

Figure 4.7. Pin-on-disk apparatus 61

Figure 4.8. Stribeck curve for polyurethane. Low and high pressures represented as solid and hollow symbols. High, medium and slow speeds are circles, squares and triangles, respectively 63

Figure 4.9. Stribeck curve for polyvinyl chloride Low and high pressures represented as solid and hollow symbols. High, medium and slow speeds are circles, squares and triangles. 63

Figure 5.1. Iterative method for determining fluid and contact forces on pin 70

Figure 5.2. Profile of pin surface with polynomial curve fit 71

Figure 5.3: Pin-on-disk setup with coordinate system labeled 73

Figure 5.4. Tribometer Device 78

Figure 5.5. Model COF plotted against experimental COF values for PU (a) and PVC (b) 80

Figure 5.6. Representative hydrodynamic (a) and contact pressures (b) across the pin surface as predicted by Reynolds equation and Hertzian contact mechanics. The motion of the disk relative to the pin is in the +X direction. 82

Figure 5.7. Model estimates for percent contact area plotted across speed for PU (a) and PVC (b) 83

Figure 5.8. Diagram of pin-on-disk with the polar coordinate system labeled 93

Figure 5.9. Pressure profile from side (left) and top view (right) for pin on disk for three forms of Reynolds equation (a-c) 96

Figure 5.10 Orientation of wafer on pad with polar coordinate system labeled 98

Figure 5.11. Solution to developed (a) and traditional (b) polar Reynolds equation applied to CMP 100

Figure 6.1. Geometry and meshing of the shoe heel, floor surface and fluid for implicit analysis 104

Figure 6.2. Geometry of shoe heel and applied boundary conditions 106

Figure 6.3. Geometry and meshing of shoe-floor model for explicit analysis 108

Figure 6.4. Stresses in the heel material (left) and of the contact (right) from implicit analysis simulations 109

Figure 6.5. Plots of utilized COF, velocity, shoe angle and normal force across the simulation 110

Figure 6.6. Material stresses of shoe-floor contact simulation using explicit solution techniques 111

Figure 6.7 Iterative scheme for determining force supported by contact and fluid regions 114

PREFACE

I owe my modest success to the many wonderful influences in my life. I want to thank my committee members, Mark Redfern, Rakié Cham, Richard Debski, Fred Higgs and Michael Lovell, who have greatly contributed to the quality of this work and my professional development. They are outstandingly talented both as scholars and mentors. I could not have asked for a better advisor than Mark Redfern who allowed me to maximize my opportunities by creating an environment that was challenging but also instructional and supportive. I would like to thank my co-workers, past and present, who have made working at the Human Movement and Balance Laboratory an enjoyable and rewarding experience. I am delighted to have many of these co-workers as friends and look forward to enjoying their friendship for a very long time. This work would not have been possible without the unwavering support of my friends and family. I want to thank my friends in Pittsburgh and elsewhere who have always inspired me to strive to be a better person. I also would like thank my parent for being so supportive of me, both academically and personally. I want to thank my siblings, who have been tremendous roommates and friends over the years. Finally, I would like to thank Alex, who has been calming force through tumultuous times, a best friend all of the time, and has made every bit of this work worthwhile.

NOMENCLATURE

For Section 5.1

B: Curvature coefficient

D: Distance from center of pin to center of disk

E^*: Effective modulus of elasticity

F: Force

R': Radius of curvature of pin

U: Sliding velocity of disk relative to pin

a: Radius of contact region

d: diameter of pin

h: Film thickness

$\bar{h}$: Average gap film thickness

$\bar{h}_{0.75}$: Average gap film thickness where 75% of asperities are in contact

r: Cylindrical coordinate, r

v: Entrainment velocity

θ: Cylindrical coordinate, θ

μ: Coefficient of friction

σ: RMS Roughness

ν: Viscosity

ω: Angular velocity of disk

$_{con}$: Refers to region of shoe-floor contact

$_{fl}$: Refers to region where lubricant is present

$_{i,j}$: discrete levels of r and θ

$_{r}$: Refers to in the radial direction

$_{t}$: Refers to total (combined fluid and contact regions)

$_{\theta}$: Refers to in the angular direction

For Section 5.2:

B: Pin curvature parameter

H: Normalized film thickness parameter

U: Sliding velocity of disk relative to pin

R: Maximum radius

V: Average sliding speed

d: Center-to-center distance of the pad and disk

h: Film thickness

h_0: Minimum film thickness

h_m: Term used to normalize fluid thickness of Reynolds equation. Represents either minimum or mean film thickness

h_M: Mean film thickness

p: Pressure

p^*: Normalized pressure

p_{atm}: Atmospheric pressure

r: Radial polar coordinate

r*: Normalized radial polar coordinate

x*: Normalized Cartesian coordinate

y*: Normalized Cartesian coordinate

α: Roll angle

β: Pitch Angle

θ: Polar angular coordinate

η: Viscosity

ν: Velocity

ω_p: Rotation speed of the pad

ω_w: Rotation speed of the wafer

$_a$: refers to bottom surface bordering fluid film, z = 0

$_b$: refers to top surface bordering fluid film, z = h

$_r$: Refers to in the radial direction

$_\theta$: Refers to in the angular direction

1.0 PROPOSAL/SPECIFIC AIMS

This dissertation investigates the frictional properties of the shoe-floor-contaminant interface from a theoretical perspective and using computational modeling techniques. Slip and fall accidents are the cause of numerous injuries both in the public sector and in the workplace. Often, slips are caused by an inadequate amount of friction from a liquid contaminant between the shoe and floor surfaces. Relatively little is understood about the shoe-floor-contaminant interface and what is known tends to be empirical in nature. Thus, the primary objective of this research is to gain a greater understanding of the interactions between shoes and floors under contaminant conditions through applying tribological theory and implementing computational models. Shoe-floor-contaminant friction, however, is not the sole contributing factor in whether a low-friction surface leads to a fall. Therefore, the secondary objective is to examine the contribution of lower leg dynamics as well as heel kinematics as they affect the outcome of slipping accidents. The long term goal is to reduce slip injuries by developing models that can be used in the design of shoes and floors.

1.1 LONG TERM PURPOSE

The long-term purpose of this work is to generate a computational shoe-floor-contaminant friction model that is capable of predicting shoe-floor-contaminant friction based on user inputs, which may include shoe design, floor design, fluid contaminant and loading conditions. The intent of this fully developed shoe-floor-contaminant friction model is to reduce slip and fall accidents by serving as a tool for improving design of shoes and floor surfaces as well as increasing understanding of the shoe-floor-contaminant interface. Through understanding the critical lubrication mechanisms relevant to slip accidents, researchers may be better equipped to

develop improved slip testing devices and determine the effect of biomechanical factors on shoe-floor-contaminant friction. This dissertation represents a starting point toward accomplishing these long-term goals. The required steps and anticipated difficulties of expanding the shoe-floor-contaminant friction models that are developed in this dissertation towards a comprehensive shoe-floor-contaminant friction model are described in Chapter 7.

1.2 PURPOSE

The purpose of this research is to improve understanding of slip and fall accidents by studying the shoe-floor-contaminant interface from a theoretical perspective and by developing a computational tool to model this interface. Experimental testing techniques are employed to identify critical information regarding the lubrication effect of the fluid between shoe and floor surfaces. A computational model is then developed to simulate this lubrication effect between shoe and floor surfaces and predict friction coefficient. Because the shoe-floor-contaminant interface is part of a larger system (i.e. the whole body), the contribution of lower-leg dynamics to the kinematics of the foot as well as slip outcome are also analyzed.

1.3 SPECIFIC AIMS

1.3.1 Specific Aim #1

Experimental testing techniques at both the whole shoe level and with a precision pin-on-disk device will be used to identify the lubrication effects critical to slipping accidents.

1.3.2 Specific Aim #2

A computational shoe-floor-contaminant friction model will be developed for shoe and floor samples separated by a fluid contaminant applied to a pin-on-disk device. This preliminary

modeling effort will have predictive capabilities and be based on the measurable inputs: shoe material properties, shoe and floor roughness, fluid viscosity, shape of the shoe material, sliding speed and normal force.

1.3.3 Specific Aim #3

The ability of the ankle, knee and hip joint torques to control the slipping foot and their contribution to the resulting slip outcome will be analyzed.

1.4 SUMMARY OF CHAPTERS

This dissertation is composed of 7 chapters. The first chapter outlines the purpose of this proposal. Chapter 2 gives readers a background on current literature for: biomechanics of slip and fall accidents, slip testing techniques for the shoe-floor-contaminant interface, theoretical understanding of shoe-floor-contaminant interface, and tribological modeling techniques that may be applicable to shoe-floor-contaminant friction. Chapter 3 is an analysis of the contribution of heel acceleration at heel contact to falls during a slipping accident. Chapter 4 reports the results of two experimental studies. The first section (Section 4.1) examines the effects of slip testing parameters on measured coefficient of friction for an entire shoe. Analysis of how friction coefficient varies as testing parameters are changed yields information of the lubrication mechanisms that are critical to developing a shoe-floor-contaminant friction model. The second section (Section 4.2) shows that these same lubrication mechanisms can be seen for a pin-on-disk setup. Chapter 5 shows the development of the shoe-floor-contaminant micro-model, which models shoe-floor-contaminant friction for shoe and floor samples using a pin-on-disk apparatus. The first section (Section 5.1) shows this preliminary shoe-floor-contaminant friction model and compares model output with experimental data. The second section (Section 5.2) is the derivation of polar Reynolds equation using assumptions appropriate to the pin-on-disk shoe-floor-contaminant friction model. Chapter 6 describes preliminary attempts to model shoe-floor-contaminant friction for an entire shoe heel. This chapter describes the current limitations of

commercially available finite element analysis software to simulate shoe-floor-contaminant friction. Chapter 7 provides discussion and summarizes this dissertation. Special emphasis is placed on the future directions of this project.

2.0 BACKGROUND

Slip and fall accidents are a serious health concern; accounting for large portions of injuries in the work place and among older adults. Numerous researchers have studied slip and fall accidents either from a biomechanical perspective or by developing slip-testing devices. This chapter reviews the problem and significance of slip and fall accidents (Section 2.1), the contributing factors to slip and fall accidents (Section 2.2), current methods of measuring slipperiness (Section 2.3), current tribological understanding of shoe-floor-contaminant friction (Section 2.4) and other tribological modeling techniques that are applicable to shoe-floor-contaminant friction (Section 2.5).

2.1 PROBLEM STATEMENT AND SIGNIFICANCE

Falls continue to be among the leading causes of work-related injuries. Great Britain ranked slips, trips and falls as the most frequent event leading to fatal and non-fatal major accidents, accounting for 30% of all job-related injuries in 1997/1998 [1]. In Sweden, 22% of all occupational accidents were attributed to falls, once again the most numerous type of job-related accidents [2]. The US Bureau of Labor Statistics (BLS) reported that falls accounted for an average 21% of non-fatal injuries and 13% of deaths [3]. Injuries from falls are often severe. More than 25% of workers that sustain falling injuries miss 31 days at work or more [4]. Falls are often listed as the cause of the most disabling conditions (e.g. fractures and multiple injuries), affecting, in nearly 2/3 of the cases, the trunk (mostly back) and lower extremities [4]. The severity of fall-related injuries is partly responsible for their high economical costs. An estimated 24% of the direct cost of all claims filed during 1989/1990 was attributed to falls [5].

Falls also represent a serious health concern in the geriatric community where these falls often result in an injury. More than one in three adults over 65 years old experience a fall each year in the United States [6, 7] and 20-30% of falls lead to moderate to severe injuries [8, 9]. The most recent statistics available from the CDC indicate that falls were the leading cause of both fatal injuries in 2005 (15,800 reported cases) and non-fatal injuries in 2006 (over 1.8 million reported cases) among adults over 65 years old [10]. Thus falls are clearly a major issue among older adults in the general population as well.

Falls are often initiated by slip events. The US National Health Interview Survey questionnaire administered by the National Center for Health Statistics in 1997 revealed a clear majority (64%) of the work-related falls attributed to slipping, tripping or stumbling. Investigations of occupational falls occurring on the same level from 1992-1998 indicated that slipping was the most common triggering event (43% of the cases), followed by tripping (18%) and loss of balance (14%) [11]. Injuries due to slips affect most industries. Construction has some of the highest levels of reported slip/fall injuries; however, other industries also have significant levels of injury. For example, slips and falls in the restaurant industry account for about 25 % of all reported injuries [12], and are perceived by workers as the leading cause of injury [13].

Shoe design has been implicated as an important factor in slips and falls for the occupational setting and for the geriatric community. In the occupational setting, improper or worn footwear and floor surfaces have been determined to increase fall risk in the postal and farming industries [14, 15]. Footwear is also a contributing factor to falls among the geriatric community [16]. While comfortable shoes (athletic or canvas shoes) may decrease the risk of falling [16, 17], all shoes that were tested by Menz et al. had inadequate slip resistance under certain contaminant conditions [17]. Despite the large problem that slips and falls represent in the occupational and public settings and indications that shoe design is critical to this risk, little is known about shoe-floor-contaminant friction from a fundamental tribological perspective.

Thus, the injuries due to slips and falls are a significant public health and occupational problem. Research into methods of preventing and thus reducing these injuries is needed. This dissertation approaches the problem by examining the biomechanics of heel control and studying the tribological interactions of the shoe-floor-contaminant interface. This research improves the understanding of the biomechanics of slips and of the shoe-floor-contaminant friction, while also

developing a computational tool that may lead to improved shoe and floor slip resistance evaluation and design.

2.2 CONTRIBUTING FACTORS TO SLIP AND FALL ACCIDENTS

The events leading to a slip and fall accident are dependent on numerous contributing factors including environmental conditions, gait style and post-slip postural responses. A slip accident can be broken sequentially into three regions: slip initiation, slip severity and slip outcome (fall, recovery) (Figure 2.1). The initiation of a slip is determined by person-specific factors such as choice of footwear and gait style (i.e. cadence, step length) as well as environmental factors such as flooring, the presence of a contaminant and floor sloping. The severity of a slip is also affected by person-specific and environmental factors but also can be attributed to the post-slip postural response. Finally, a fall occurs when the post-slip postural response cannot adequately overcome the severity of the slip.

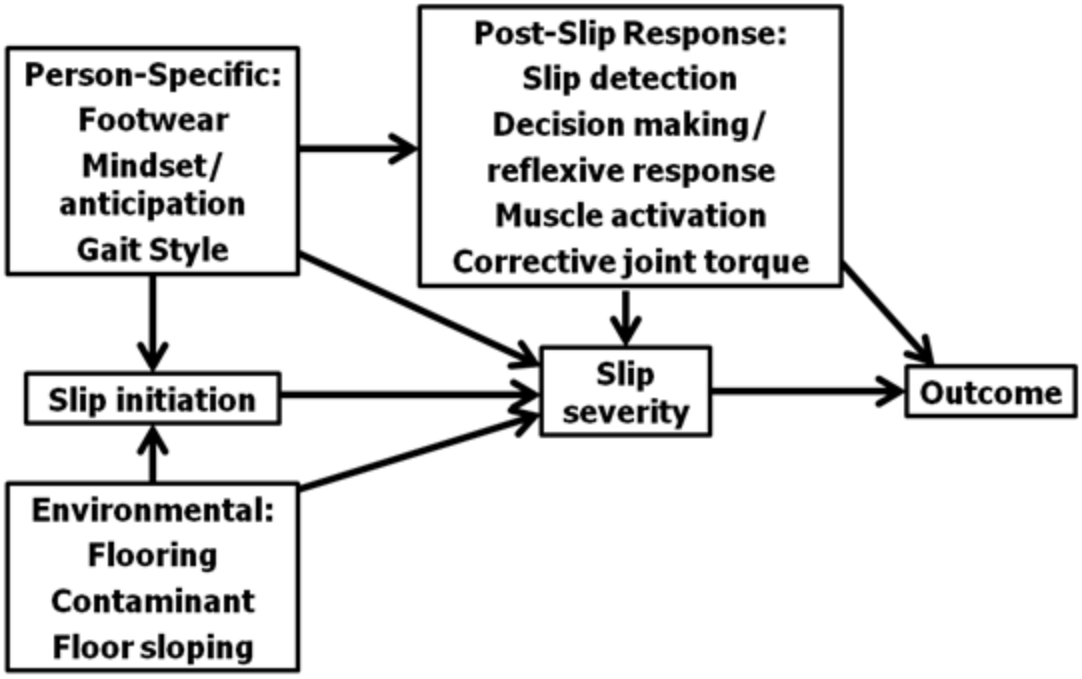

Figure 2.1. Flow chart for the slipping process

Slip initiation, which occurs when frictional requirements for walking exceed the available friction [18, 19], is dependent on numerous different person-specific and environmental factors. For example, frictional requirements have been shown to increase when walking with a greater gait speed [20] and decrease when a person anticipates a slippery surface [21]. Frictional requirements have also been shown to be dependent on a person's footwear [22]. In addition to the person-specific factors, floor sloping has also been shown to affect required friction with larger frictional requirements being associated with steeper ramp angles [23]. Person-specific and environmental factors also affect the amount of available friction. For example, biomechanical factors contribute to the amount of available friction including normal force and heel velocity [24-27]. The choice of footwear including the shoe material [22, 25, 28-30] and tread design [31, 32] has also been determined to contribute to the amount of available friction. Environmental factors such as the flooring, especially its surface roughness and waviness, along

with the presence of a contaminant are known to be critical to the amount of available friction [28, 33-38]. Thus, many different person-specific and environmental factors have been shown to contribute to slip initiation by affecting either the amount of available or required friction.

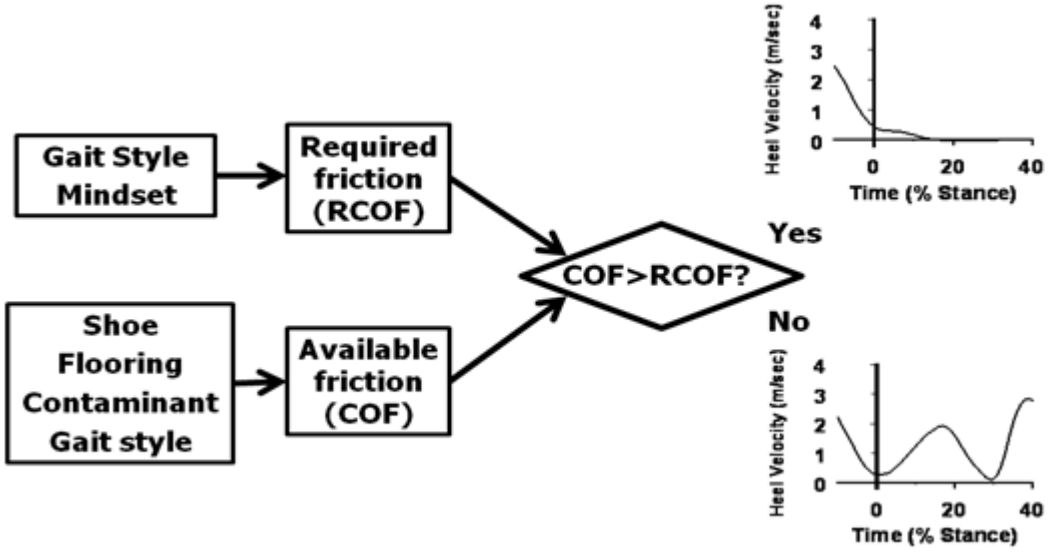

Figure 2.2. Slip initiation process

Once a slip is initiated, numerous factors affect the progression of a slip including its severity and whether the slip results in a fall. The primary measures for slip severity are heel displacement and the maximum heel velocity. In fact, much research has been conducted to establish thresholds of slip distance and maximum heel velocity that differentiates between severe and non-severe slips. For example, some researchers have set the slip distance threshold for severe slips at 10 cm [39, 40], while others have set a threshold of maximum slipping velocities at levels of 0.5 m/s [40], 0.8 m/s [41], and 1.0 m/s [42]. While the exact value of the maximum heel velocity threshold varies from study to study, Moyer et al. argues that heel

displacement and maximum heel velocity should be treated as a continuum where larger slip distances and slip velocities indicate the most severe slips [43]. Previous research has demonstrated that a decreased required friction is coupled with a decrease in slip severity [21], therefore, it is reasonable to expect that the same factors that affect slip initiation are also likely to contribute to the slip severity, especially as the gap between required and available friction becomes larger. In addition, other person-specific factors have been directly correlated with slip severity. For example, a larger step length and a smaller cadence increases subjects likelihood of a severe slip [43]. Heel velocity at heel contact has also been shown to correlate with slip distance early on in the slip [44]. The severity of the slip is critical to determining whether a slip will result in a fall. Lockhart et al. determined that younger adults may be more capable of recovering from large slipping perturbations; his analysis stated that a fall is likely when maximum slipping velocity exceed the thresholds for young and older adults of 1.44 m/s and 1.07 m/s, respectively [45]. In addition, Pai and Patton defined a stability region that combined heel position and velocity relative to the center of mass relative for a sit-to-stand task [46]. This measure was later shown to also predict the slipping perturbations that are likely to lead to a fall during walking [47]. While numerous person-specific and environmental factors affect slip severity, which is critical to the likelihood of a fall, the body is also capable of generating a postural response in order to reduce the severity of the slip and improve the chances of recovery from the slip.

In response to the slipping perturbation, the body generates a coordinated postural response in order to reduce the severity of a slip and recover balance. The leg ipsilateral (on the same side) to the slip reacts by generating hip extension moments and knee flexion moments [48, 49]. Marigold et al. indicated that both the unperturbed leg and arms are also involved in the postural response as part of a whole-body coordinated effort [50]. The unperturbed limb may play a role in reestablishing the base of support, which is supported by the finding that joint moment onset times of this limb are correlated with the type of foot landing strategy [51]. In addition, the role of the upper body during slips may be to break a fall in the case of a severe slip or to help recover from the slip in the case of a non-severe slip [52]. The post-slip postural response also requires a complex neurological process in order to properly detect the slip [53], react to the slip either cognitively or reflexively and activate muscles [54] in a coordinated manner to produce joint torques [48-50] that will increase the chance of recovery from the slip

perturbation. The post-slip postural response is a whole-body coordinated effort that requires a complex neurological process and is essential to regaining balance after a slip perturbation.

Many factors contribute to the severity of a slip and the resulting outcome. The factors contributing to the slip and fall process can be divided into the categories of person-specific, environmental and post-slip response. Chapter 3 of this dissertation aims to identify another person-specific gait measure, heel acceleration at heel contact, which may contribute to slips and fall accidents. Additionally, the long-term goal of this dissertation, to develop a shoe-floor-contaminant friction model, may improve our understanding of how certain person-specific and environmental factors affect shoe-floor friction and thus slip initiation and slip severity.

2.3 MEASURING SLIPPERINESS

Shoe-floor-friction testing is a common empirical method for evaluating the slip resistance of the shoe-floor-contaminant interface. Given the theoretical complexity of the interface, slip resistance testing devices provide a straight-forward way to evaluate slip and fall risk for existing environments. However, controversy exists regarding the quality of measures from the various devices that are used. Measurements across different testing devices often disagree, depending upon the shoe, floor and contaminant involved. Experts have agreed that these tests should be performed under conditions that closely resemble what occurs during a human slip (i.e. biofidelic) [11]. Slip testers have used a variety of approaches to measure slip resistance including small portable devices for use in the field and large laboratory devices capable of exerting high loads and fast speeds. Slip testing devices can be categorized by whether they test an entire shoe specimen, whole shoe slip testing devices, or whether they use just a small sample of shoe material, which are typically small portable slip testing devices. In addition, human-centered approaches to measuring slip-resistance have been developed in order to account for the dynamic and transient nature of walking. Chang et al. provides an overview of commonly used slip-resistance testing methods [55].

2.3.1 Devices

A large number of devices have been developed to quantify shoe-floor friction. A survey of many of these devices can be found in [55]. The most commonly used portable devices at this time are the English XL and the Brungraber Mark II. Both of these devices allow for a collision between a shoe material and the floor at varying angles and the COF is determined by the angle that the shoe material transitions from sticking to the floor to slipping out. The difference between these devices is the English XL is pneumatically driven and the Brungraber Mark II is gravity driven [28]. One limitation of this method is that while studies have shown that the amount of tread has a significant effect on COF, there is often little or no tread on the pads [31]. Another limitation is that the circular shape of the pads may not resemble the actual contact area or loading profile between a shoe and the floor.

Lab devices often test an entire shoe at higher loading levels under more controlled loading conditions with increased flexibility in shoe angle, loading levels, and sliding velocity. Numerous lab devices have been developed including the SATRA device [26], the slip simulator [56] and the High Payload Slipmeter [57]. Many of these devices are capable of applying the large forces experienced by the shoe during walking. In addition, these devices typically choose sliding velocities and shoe-floor angle that are considered most relevant to walking. Unfortunately, a wide range of normal forces, sliding speeds, and shoe angles are considered to be appropriate. As discussed in Chapter 4 of this dissertation, friction coefficient is dependent on the testing parameters [57]. Therefore, it can be confusing and difficult to isolate a single coefficient of friction value that best represents the slip-resistance of a shoe-floor-contaminant combination. In addition, it is well known that the normal force, shoe angle and sliding speed are transient during walking and particularly during a slip. None of the devices, however, currently have the capabilities to reproduce these transient loading conditions during testing.

2.3.2 Human centered approaches

Because the primary goal of measuring friction is to reduce injuries that result from slipping, several human centered methods have been developed to evaluate shoes and floors. One approach for quantifying COF was developed by Skiba et al. having subjects walk on a surface

with continuously increasing inclination until the subject fell or felt unsafe [58]. This angle could then be used to determine the maximum available friction. This method was adopted as a German standard for determining slip resistance of a floor [59]. The use of inclination angle, while allowing for simple quantification of the COF from subject-based data, probably does not resemble a hazardous and dangerous slip precisely because of the anticipation factors that can affect gait [60]. In addition, the method is restricted to laboratory investigation and limited in its use for design.

Unexpected slips, which are more likely to lead to dangerous falls, can be produced in the laboratory by concealing the condition of the floor from the subject and determining the severity of the slip that incurs. The amount of friction required to prevent slipping is a relevant measure described by Redfern and colleagues as the Required COF (RCOF), and defined as the amount of shear force utilized per normal force [19, 23, 61, 62].This is often used as a threshold to determine whether a condition is likely to lead to a fall (i.e. when Required COF is greater than available COF, a slip is likely). The difference between Required COF and measured COF has been used to determine the probability of a slip [19]. This method of evaluation has also been used in another study with success [18]; however, has not been effective at showing differences between younger low-risk groups and older higher-risk groups [45]. Slip distance and slip velocity are often used as indicators to determine the severity of a slip by categorizing slips as hazardous (i.e. slips likely to lead to a fall) or non-hazardous (unlikely to lead to a fall) [43, 45, 60, 63, 64].

2.4 SHOE-FLOOR-CONTAMINANT FRICTION

As part of an effort to design safer shoe-floor-contaminant combinations, numerous studies have attempted to determine shoe and floor features that affect and can potentially increase shoe-floor-contaminant friction. Contributing factors to shoe-floor-contaminant friction can divided into the categories of: shoe design (material, surface micro-structure and tread patterns), floor design (floor material and micro-structure), environment (contaminant), and biomechanical (loading pattern, heel velocity and shoe-floor angle). Current research typically uses empirical approaches to identify which of the above factors contributes to increase shoe-floor-contaminant friction. Previous studies have attempted to identify factors that affect shoe-floor-friction presumably with the intent of understanding how to maximize friction. The complex interactions between these factors, however, make the results of these studies difficult to understand and apply. A basic understanding of the contributing factors to shoe-floor-contaminant friction, however, also provides guidance for which factors need to be included in computational modeling approaches.

The effect of floor roughness has been widely studied to determine surface features that yield higher friction. Studies have shown that both floor surface roughness [28, 33-37], floor surface waviness [37, 38], and contaminant condition [33-37] significantly contribute to COF. Chang explored the correlation between common surface parameters and COF that quantify either surface roughness or surface waviness by using different cut-off lengths [37]. This study showed that in the presence of a liquid contaminant when viscosity is low, surface roughness is the more important factor but when viscosity is high, surface waviness dominates. While most efforts to determine the effects of roughness on friction have focused on the floor surface, interlocking of shoe asperities with floor asperities also have an effect, particularly under dry conditions and therefore both the surface roughness of the shoe and the floor need to be considered [65, 66]. Kim and Smith also demonstrated that during repeated testing, large asperities are worn off, which alters shoe-floor-contaminant friction levels [67].

Features of the shoe including the outer sole material and tread style are also known to contribute to shoe-floor-contaminant friction. While shoe-floor-contaminant friction is clearly dependent on shoe-material [22, 25, 28-30] with some studies indicating that harder shoe materials are associated with a smaller friction coefficient, it remains unclear what mechanisms are predominantly responsible for this change in friction. The design of tread, however, has a

more direct effect on friction. Both increasing the size of tread width and tread depth were found to increase the amount of available friction [31, 32]. While it is apparent that shoe design affects its slip-resistant properties, the friction mechanisms that cause these changes are poorly understood.

Biomechanical factors such as the normal loading of the shoe, shoe-floor angle, and the sliding velocity of the shoe may affect shoe-floor friction. Larger speeds have consistently been shown to result in lower COF values [24-26]. While studies have been more inconclusive regarding the effects of normal force and shoe angle on shoe-floor-contaminant friction [25, 27], shoe angle and normal force would likely affect the size of the shoe-floor contact region, which could potentially alter the shoe-floor-contaminant friction. In a simplified modeling approach, Proctor and Coleman likened the shoe-floor-contaminant friction to a slider bearing in order to demonstrate the importance of sliding speed and normal force on the lubrication of the shoe-floor-contaminant interface [68].

While a large number of factors are known to contribute to shoe-floor-contaminant friction, few attempts have been made to determine how these factors interact and collectively contribute to the overall slipperiness of a shoe-floor-contaminant combination. Modeling attempts that include the micro-structure of the shoe and floor surfaces, shoe material, tread design, and biomechanical factors will provide an opportunity to better understand the contributions from each of these factors. In addition, shoe-floor-contaminant friction may provide opportunities to identify an optimal combination of conditions to maximize shoe-floor-contaminant friction.

2.5 THIN FLUID FILM MODELING TECHNIQUES

Computational modeling of the shoe-floor-contaminant interface provides the opportunity to better understand the lubrication effect of the contaminant and how this effect varies across different shoe and floor conditions as well as different loading conditions. However, there is a paucity of research that has attempted to develop such models for shoe and floor surfaces. Sun et al. used finite element analysis to examine the traction of different boots on soil [69]. This modeling attempt did not include the presence of a fluid and therefore is not applicable to the

current application of modeling fluid lubrication effects in the shoe-floor-contaminant interface. The lubrication effect from a thin film fluid, however, has been extensively studied in the other applications, particularly among researchers specializing in chemical-mechanical-polishing and mixed-lubrication. Therefore, a review of the state-of-the-art thin-film lubrication research may provide insight that is critical for developing a computational model for shoe-floor-contaminant friction.

Numerous types of tribological models have been developed for interacting surfaces separated by a thin film. The governing equations for these models tend to be dependent on the type of lubrication, often referred to as lubrication regimes. The different lubrication regimes are often described using the Stribeck curve. The Stribeck curve (Figure 2.3) shows that friction is high in boundary lubrication when the film thickness is small and most of the normal force is transmitted through asperity interaction. As film thickness and hydrodynamic pressure increase, the friction coefficient rapidly decreases as the normal force is transferred from contacting asperities to the fluid. In the elastohydrodynamic lubrication regime, the hydrodynamic pressure causes substantial deformation of the contacting surfaces which results in a larger fluid film separating the surfaces. Once the film thickness is great enough to fully separate the surfaces, all of the normal force is supported by the fluid in the lubrication region known as hydrodynamic lubrication. Friction coefficient tends to be very small during hydrodynamic lubrication. As film thickness continues to increase in the hydrodynamic lubrication regime, friction coefficient increases slightly due to increased amounts of frictional force required to shear the fluid. For shoe-floor-contaminant friction, the regions of most interest are mixed-lubrication and elastohydrodynamic lubrication because they represent the transition from safe high-friction conditions to dangerous low-friction conditions.

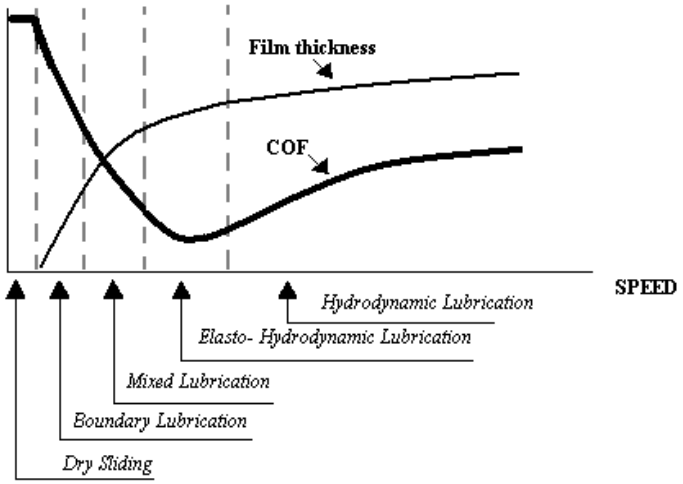

Figure 2.3. Stribeck curve

Chemical-mechanical polishing (CMP) is a process that smoothes silicon wafers with a polyurethane pad and a slurry of fluid and small abrasive particles. CMP models may provide insight into shoe-floor-contaminant modeling because both CMP and shoe-floor-contaminant interfaces have a mixed-lubrication interaction between a soft material and a hard material where both the fluid and surface roughness play a major role (Figure 2.4). Research in the field of CMP has yielded models of mixed-lubrication, which represents the region where a normal force is partly supported by asperity-to-asperity interaction and partly supported by fluid pressure [70, 71]. CMP modeling often employs the Greenwood and Williamson approach of approximating the average fluid thickness from average contact pressure and the distribution of asperities [72]. For example, if an exponential distribution is assumed for the asperities, the film thickness is:

$$\mathbf{h(x) = s * ln}\left(\frac{\sqrt{\pi}\eta \mathbf{E R}^{1/2}\mathbf{s}^{3/2}}{\left(1-\nu^2\right)\sigma(\mathbf{x})}\right) \qquad \text{Eq. (2.1)}$$

In Eq. (2.1), E is the elastic modulus, R is the average radius of the asperities, s is the pad roughness and η is the density of asperities, v is Poisson's ratio and σ is the contact pressure. The film thickness as determined by the Greenwood and Williamson equation is input into the Reynolds equation to determine fluid pressure for 1D as:

$$\frac{d}{dx}\left(\phi_x h^3 \frac{dp}{dx}\right) = 6\mu U \frac{dh}{dx} \qquad \text{Eq. (2.2)}$$

In order to account for flow disturbances due to the roughness of the surfaces, flow factors, originally developed by Patir and Cheng, can be used by defining φ_x in Eq. (2.2) as [73]:

$$\phi_x = 1 - 0.9 * \exp\left(-0.56\frac{h}{s}\right) \qquad \text{Eq. (2.3)}$$

CMP modeling efforts provide insight for using statistical approaches to represent roughness effects while modeling fluid and contact pressure at the macro-scale. One limitation of applying CMP modeling directly to shoe-floor-contaminant friction is the underlying assumption regarding lubrication regime. CMP assumes that the entire interface is under mixed-lubrication, while during shoe-floor-contaminant interaction; different regions of the shoe may be in different lubrication regions. To illustrate this point, consider a region of the shoe surface that is completely separated from the floor and has a film thickness of 1mm. Because this region of the shoe is outside of the contact region, the contact stress is 0 ($\sigma(x)=0$). Equation 2.1 would estimate the film thickness to approach infinity, which would of course be incorrect. Thus the current form of CMP modeling cannot be directly applied to shoe-floor-contaminant modeling.

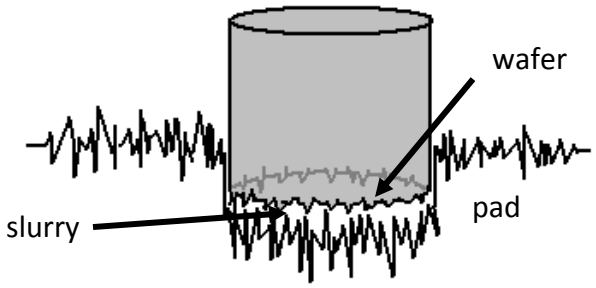

Figure 2.4. Chemical Mechanical Polishing

Elastohydrodynamic mixed-lubrication (EHL) modeling techniques are similar to mixed-lubrication models but also account for the deformation of the contacting surfaces from contact and hydrodynamic pressure. Therefore, EHL modeling techniques may provide insight for shoe-floor-contaminant friction because shoe materials tend to be soft and compliant and regions of the shoe may be in contact while other regions of the shoe may have a fluid separating the surfaces. EHL analyses typically calculate film thickness as a function of the undeformed geometries of the surfaces, the deformation due to fluid pressure, and deformation due to contact pressure [74, 75]. Generically, the equation for film thickness is:

$$\mathbf{h = h_{fl} + h_s} \qquad \text{Eq. (2.4a)}$$

$$\mathbf{h_{fl} = d_0 + h_{und} + uz_{fl}} \qquad \text{Eq. (2.4b)}$$

$$\mathbf{h_s = uz_s} \qquad \text{Eq. (2.4c)}$$

In Eqs. (2.4), h is the total film thickness and is the sum of the h_{fl} and h_s. The film thickness due to only fluid effects, h_{fl}, is a function of an offset between the surfaces, d_0, the undeformed geometry of the surfaces, h_{und}, and deformation due to hydrodynamic pressures, uz_{fl}. The film thickness resulting from solid contact, h_s, is a function of the deformation due to solid contact pressure, uz_s. The film thickness as determined by Eqs. (2.4) is then used with Reynolds equation to determine the fluid pressure across the 2D surface.

$$\mathbf{\frac{d}{dx}\left(h^3\frac{dp}{dx}\right)+\frac{d}{dy}\left(h^3\frac{dp}{dy}\right)=6\mu U\frac{dh}{dx}} \qquad \text{Eq. (2.5)}$$

Elastohydrodynamic mixed-lubrication models may also provide insight on how to treat the transition between the fluid region and the solid contact region. Because the Reynolds equation models hydrodynamic pressure, it cannot be used inside the contact regions. Some researchers have therefore applied boundary conditions to the Reynolds equation at this boundary that prevents fluid from flowing into the contact region using the condition:

$$\mathbf{q_x = -\frac{h^3}{12\eta}\frac{\partial p}{\partial x}+\frac{\nu_x}{2}h = 0} \qquad \text{Eq. (2.6)}$$

One of the primary limitations in elastohydrodynamic mixed-lubrication modeling is achieving the solution to Eqs. 2.4 and 2.5 simultaneously. As seen in Eq. 2.5, film thickness is a primary component of Reynolds equation and according to Eq. 2.4, deformation and

subsequently film thickness are based on fluid pressure. Thus, film thickness is a function of fluid pressure and fluid pressure is a function of film thickness. Therefore, either iterative methods or other methods of solving large sets of non-linear equations need to be utilized in a manner such that Eqs. 2.4 and 2.5 can be solved simultaneously. Under some conditions, it may be difficult to establish stability while solving these equations.

While few attempts have currently been made to implement computational models for shoe-floor-contaminant friction, state-of-the-art models from other fields including chemical mechanical polishing and in elastohydrodynamic lubrication provide insight into techniques that can be applied to shoe-floor-contaminant friction.

2.6 SUMMARY

Currently the methods for measuring shoe-floor-contaminant friction are highly variable and may have varying relevance to actual slip and fall accidents. Computational modeling of the shoe-floor-contaminant interface may provide improved measurements over both slip-testing devices and human-centered measurements because loading conditions identical to a slip can be recreated in the simulation. In addition, computational modeling techniques may provide additional information such as hydrodynamic pressure profile and contact pressure across the surface of the shoe and throughout the slip. Hydrodynamic pressure and contact region information may also be useful in the design of safer shoes and floor surfaces. Therefore, computational models of shoe-floor-contaminant friction may improve evaluation techniques for shoe-floor-contaminant friction, serve as a valuable tool for designing slip-resistant shoe and floor combinations, and provide insight for walking styles that minimize slip risk.

While computational modeling of shoe-floor-contaminant friction provides many benefits as a tool to design safer shoe and floor surfaces as well and to improve understanding of the lubrication that occurs between the shoe-floor-contaminant friction, few researchers have attempted to develop these models. Preliminary models can be developed on the premise that the critical lubrication regime relevant to the transition between safe and slippery surfaces is mixed-lubrication. State-of-the-art modeling techniques for mixed-lubrication from other tribology

specialties such as chemical-mechanical-polishing and elastohydrodynamic lubrication may be useful in developing the first generation shoe-floor-contaminant friction computational models.

3.0 HUMAN FACTORS: IMPACT OF JOINT TORQUES ON HEEL ACCELERATION AT HEEL CONTACT, A CONTRIBUTOR TO SLIPS AND FALLS

This chapter focuses on the relationship between lower body kinetics and heel kinematics to slip and fall accidents. Specifically, heel acceleration at heel contact was determined to be a contributing factor to slips and falls. In addition, lower body joint torques, especially hip flexion/extension torque, was found to be critical to the heel acceleration. Thus the lower body joint torques at and around heel contact are important to the heel kinematics during the initial slip period, which contribute to the outcome of the slip. This chapter is published in *Ergonomics* [76].

3.1 ABSTRACT

Slips/falls are a health burden in the workplace. Previous research has inferred a relationship between foot dynamics at heel contact and slips/falls; however, heel acceleration has received little attention. Heel acceleration as the heel contacts the ground is the result of the combined effort of the leg joint torques to control motion of the foot. This study aims to examine the association of heel acceleration with fall risk, and explore the main joint torque determinant of heel acceleration at contact. Sixteen young and eleven older adults walked on known dry floors and in slippery environments expected to be dry. Heel acceleration at heel contact in the direction of motion, i.e. anterior/posterior, was compared between slip-recovery and slip-fall outcomes. Results showed that subjects that recovered contacted the floor with a greater heel deceleration ($p < 0.05$) than fall subjects. Knee torque alone explained 76% of the heel acceleration variability ($p < 0.01$). These data suggest that walking with reduced knee flexion

torque at heel contact results in a reduced heel deceleration, a potential risk factor for slip-initiated falls.

3.2 INTRODUCTION

The burden of occupational falls is considerable, particularly in older workers. Falls account for over 20% of work-related deaths and for nearly half of the non-fatal injuries in workers over the age of 65 years old [77, 78]. Same level falls, the most common type of work-related falls especially in older adults, are often initiated by slipping [78, 79]. Specifically, answers to the US National Health Interview Survey questionnaire administered in 1997 revealed that 43% of the same-level falls are precipitated by slipping, followed by tripping (18%) and loss of balance (14%) [11]. Injuries attributed to falls can be severe, as more than half of the non-fatal fall-related injuries require emergency department visits [79] and employees sustaining falls-related injuries often take long sick-leave periods [78].

Causes of slip-initiated falls are complex and involve intricate relationships between environmental and human factors [62, 80, 81]. Environmental factors include the shoe-floor interface material and frictional properties, which have yet to be reliably evaluated using biofidelic practical measurement devices and testing parameters relevant to human gait [27, 55, 57, 82-84]. Human factors include neuro-sensorimotor processes [53, 85] and higher cognitive mechanisms [60, 86-90] involved in the detection, perception and anticipation of a perturbation; followed by initiation of appropriate postural responses; and maintenance of dynamic balance. The complex interactions between human and environmental factors contribute to gait biomechanics that are ultimately responsible for failed slip-initiated postural recovery responses and falls.

Gait biomechanics research has identified two broad types of inter-related variables that are likely to have an impact on the risk of slip-initiated falls. The first type of variable is related to postural responses generated after the slip is initiated [62]. The body must generate a quick and effective corrective response to re-establish dynamic balance and to maintain an upright posture while continuing with the locomotion task. Lower extremities, trunk and arms all contribute, in a coordinated manner, to the complex postural response generated in an attempt to

prevent a fall [42, 48-50, 91-93]. Overall, the corrective joint torques generated by the leading/slipping leg, i.e. flexion moment at the knee and hip extension moment, are most consistent and believed to be critical in decelerating the sliding motion of the leading foot and in arresting the vertical descent of the body during a balance loss [48, 62, 93]. The second type of variable, often termed initial conditions, refers to gait factors that can be evaluated prior to the initiation of a slip as a result of normal walking patterns. For example, orientation of the foot at heel contact, step length and cadence are initial condition gait factors that have been implicated in slips and falls [43, 94]. Gait analyses of normal walking patterns can also be used to assess the frictional requirements needed to prevent a slip for a given gait style [18, 19, 23, 40, 95, 96].

Slip events that are most likely to result in a fall occur shortly after contact of the leading foot's heel onto a contaminated floor [62]. Thus, it is somewhat intuitive to hypothesize that heel contact dynamics, which are considered initial condition gait variables, may be potential predictors of slips and falls. Studies that have investigated heel contact dynamics as predictors of slips and falls have, to a large extent, focused on heel contact velocity; which is often viewed as a potential risk factor for slipping despite its weak correlation with falls and with the frictional requirement of a slip-resistant gait [45, 97-99].

Little attention has been dedicated to heel acceleration of the leading foot evaluated at heel contact in the direction of motion, i.e. in the anterior/posterior direction. Heel acceleration reflects the combined effects of joint torques generated by the body [97] and it is a determinant of heel velocity shortly after heel contact. Thus, heel acceleration of the leading foot at heel contact may contribute to slip/fall risk. One study from our group reported no statistically significant differences in heel acceleration at heel contact between fallers and non-fallers [41]. However, in that study, although subjects did not know the specific timing and potential contaminant used to induce the slip, they were exposed to multiple slips. Thus, participants may have modified foot contact kinematics as a result of anticipating a slippery condition [60, 100]. Due to the volume of studies considering heel velocity compared to the relatively few studies that have examined heel acceleration, this paper is focused primarily on heel acceleration at heel contact instead of heel velocity at heel contact.

Heel contact dynamics are one example of variables that can be affected by the complex interaction between environmental and human factors. The determinants of heel contact dynamics have not been disentangled. In this study, we hypothesize that the joint torques

generated by the leading leg play a significant role in controlling heel acceleration at heel contact. Understanding how humans modulate heel contact dynamics, gait factors that have been implicated in slips and falls, may provide insight into the significant variability in these measures reported among participants in recent investigations [94].

Thus, the primary goal of this study was to examine the association of the anterior/ posterior (direction of motion) heel acceleration of the leading foot evaluated at heel contact to slip outcome (fall or recovery) in young and older adults. The second goal was to investigate the relationship between sagittal-plane joint torques generated by the leading leg (ankle, knee and hip) and the anterior/posterior heel acceleration at heel contact.

3.3 METHODS

3.3.1 Subjects, experimental conditions and protocol

Of a total of 31 recruited participants, 27 subjects were analyzed and divided in two age groups, a younger group (n=16 between 20 and 33 years old) and an older group (n=11 between 55 and 67 years old). Four subjects were not analyzed due to technical or testing problems. Written informed consent, approved by the University of Pittsburgh Institutional Review Board, was obtained prior to participation. Exclusion criteria included clinically significant conditions that impede normal walking or affect balance as determined by a neurological examination conducted by a neurologist with expertise in balance disorders. No statistically significant differences in stature and gait speed were found between age groups, however older participants were heavier than their younger counterparts ($p < 0.05$) (Table 3.1).

Table 3.1. Subject population characteristics stratified by age group

Mean (Stand. Dev.) Min - Max	**Age group**	
	Younger	***Older***
N	16 (10 Female, 6 Male)	11 (7 Female, 4 Male)
Age (years)	24 (3.3) 20-33	61 (4.0) 55-67
Stature (cm)	170.2 (8.3) 159.0-194.1	166.2 (8.1) 154.0-179.0
Weight (kg)*	66.8 (10.4) 53.3-89.1	78.2 (10.9) 56.4-92.7

*$p<0.01$

Subjects were exposed to two environmental conditions. First, baseline gait trials (known dry environment) were collected. Second, a slip was induced unexpectedly using a diluted glycerol contaminant (75% glycerol/25% water) applied onto the force platform prior to the slip gait trial. The same researcher applied a consistent amount of contaminant to uniformly and completely cover the surface of the force platform used to measure forces under the leading leg. The dynamic coefficient of friction of the shoe–floor interface was 0.53 and 0.03 for the dry and contaminated conditions, respectively, as measured by English XL VIT Slipmeter1 [101]. The lights were slightly dimmed during the entire experiment to prevent the subject from noticing the glycerol when it was applied onto the floor.

Subjects wore the same brand/model of polyvinyl chloride soled shoes and donned a safety harness. Their body and shoes were instrumented with a set of 79 reflective markers to track gait kinematics at 120 Hz [51]. Next, participants were instructed to walk naturally at a self-selected pace and were allowed to practice walking across the 8.5 m long vinyl-tiled walkway. The walkway was instrumented with two force platforms to collect bilateral ground reaction forces at 1080 Hz. Prior to each gait trial, the participant was asked to face away from the walkway and to listen to music for about 1–2 minutes prior to data collection. In addition to the dimmed environment mentioned previously, these procedures were adopted so that glycerol could be applied in the slippery condition without the subject's knowledge. Data collection during the baseline gait trials began after the subject was told that the first few trials would be dry, thus ensuring natural gait and minimizing any anticipatory effects. After two or three dry

trials, the glycerol was applied to the leading leg force platform without the subject's knowledge and the unexpected slippery gait trial was collected. Only one dry trial (last good trial collected immediately prior to the slippery condition) and the slip trial were considered in the analysis.

3.3.2 Data processing

Heel motion was tracked with a marker placed at the superior posterior aspect of the calcaneous, typically the very back of the heel about 50 mm off the ground. Heel position data in the anterior/posterior direction, i.e. direction of motion, were filtered using a zero-phase second-order Butterworth filter with a cut-off frequency of 10 Hz. From the filtered heel position data, heel velocity and acceleration trajectories were derived using the central difference formula based on three points as shown in Equations (3.1)–(3.2) below:

$$\mathbf{HeelVel_i} = \frac{\mathbf{HeelPos_{i+1} - HeelPos_{i-1}}}{\mathbf{2\Delta t}} \qquad \text{Eq. (3.1)}$$

$$\mathbf{HeelAcc_i} = \frac{\mathbf{HeelPos_{i+1} - 2HeelPos_i + HeelPos_{i-1}}}{\mathbf{\Delta t^2}} \qquad \text{Eq. (3.2)}$$

where $HeelPos_i$ = position of the heel in the anterior-posterior direction at frame i, $HeelVel_i$ = velocity of the heel in the anterior-posterior direction at frame i, $HeelAcc_i$ = acceleration of the heel in the anterior-posterior direction at frame i, and Δt = time step of 1/120s.

At the time of heel contact, *HeelVel* is typically positive (anterior) and *HeelAcc* is typically negative (posterior) meaning that the foot is decelerating (Figure 3.1). In Figure 3.1, the average (black line) +/- standard deviation (gray envelope) of heel velocity (a) and acceleration (b) time series are plotted for baseline dry conditions. Time is normalized by stance time, which represents the period of gait from when the foot initially contacts the floor until the toe lifts off; with 0% representing heel contact and 100% is toe off. Heel contact was characterized initially by a forward moving heel with a large heel deceleration (negative heel acceleration) before, at and after heel contact. The foot has nearly stopped by about 5% stance. The variable HeelAcc, which represents the anterior/posterior heel acceleration, is akin to the variable HeelAccX reported in Cham and Redfern [41].

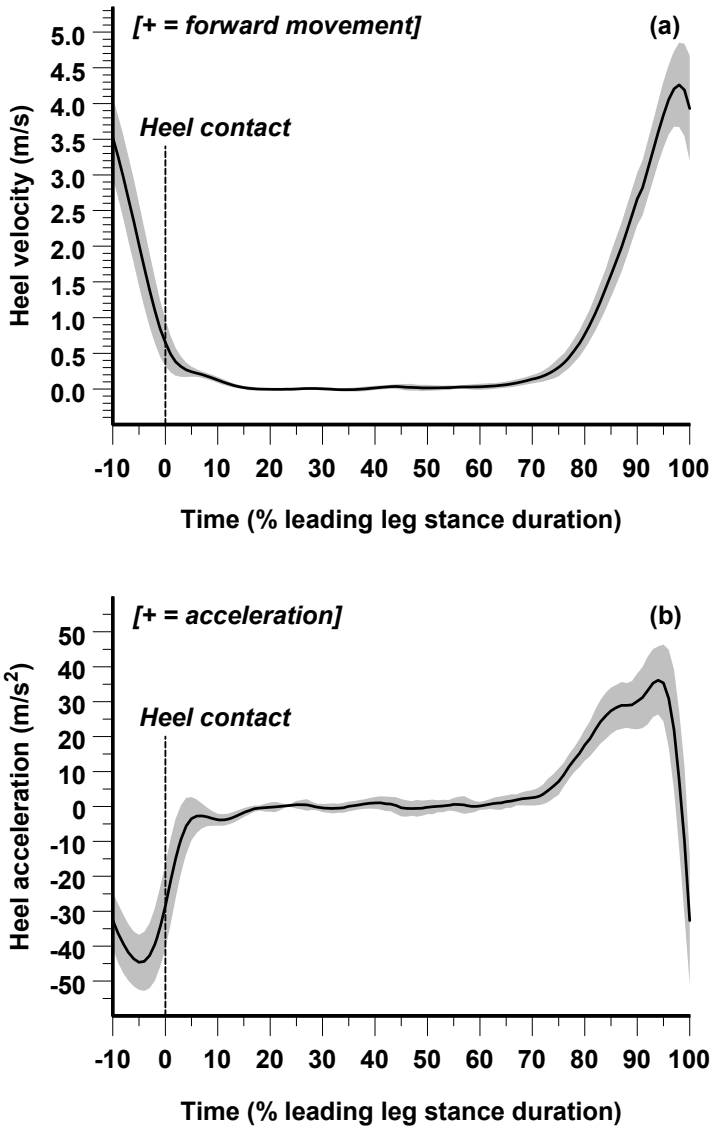

Figure 3.1. Heel velocity and acceleration average time series plots for normal gait

Joint torques were determined using inverse dynamics analyses based on a 15-segment whole-body model developed in our laboratory. This model includes toe, heel, shank, thigh, upper arm, and forearm segments for the right and left sides of the body, as well as pelvis, torso and head segments. Local coordinate systems for each segment were defined using markers from that segment and were, to a considerable extent, based on the work of de Leva [102] with reasonable effort extended to align local coordinate systems with ISB recommendations especially for the pelvis, thigh, shank and foot segments. Gender-specific segmental masses, centre of mass locations, and radii of gyration were adapted from de Leva [102]. Joint moments are reported in the coordinate system of the more proximal segment. The reader is referred to Moyer [51] for more details on the model used in the inverse dynamics analyses. For this study, only sagittal-plane joint torques generated by the ankle, knee and hip of the leading leg were evaluated, i.e. *AnklTorq*, *KneeTorq*, *HipTorq*, respectively. These torques were normalized by dividing by body mass of the subject. The sign convention for the joint torques is positive for ankle plantarflexion, knee flexion and hip extension.

The timing of heel contact, measured from forceplate data, was chosen to parameterize heel acceleration ($HeelAcc_{HC}$), ankle, knee and hip torques (i.e. $AnklTorq_{HC}$, $KneeTorq_{HC}$ and *HipTorqHC*, respectively) as it represents the state of these variables prior to the effects of contact forces between the shoe and floor. Both acceleration and joint torque measures were parameterized at the same time (heel contact) based on the rationale from Newton's equations of motions that force and acceleration patterns are instantaneously coupled. While the three-point differentiation method means that one point after heel contact is used in the calculation of heel acceleration and joint torques, shoe–floor forces within this time range are minimal due to the high sampling rate of the cameras (120 Hz) (Figure 3.2). Therefore, at heel contact, heel acceleration and joint moments are not affected by slip reactions and are only minimally affected by shoe–floor interactions (i.e. contact and tribological effects).

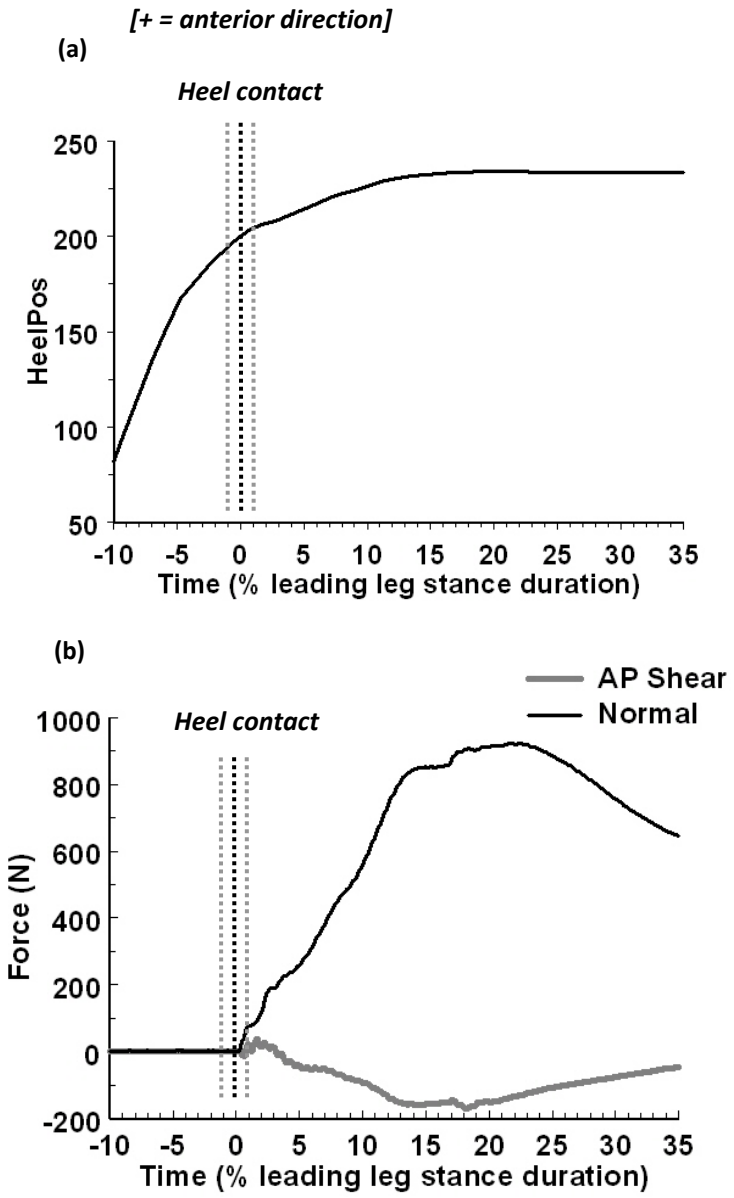

Figure 3.2. Typical heel position (a) and ground reaction forces (b) for baseline and slip trials

The outcome of each slip trial was classified as a fall or recovery. Specifically, a slip trial was classified as a fall if the midpoint between the left and right hip joint centre dropped below 95% of its minimum height measured during normal gait. This fall classification criterion, similar to that of Pai and colleagues [103, 104], was also selected in the light of the presumed objective of slip-initiated postural responses observed in our slip-fall experiments: namely to prevent the vertical descent of the body. Finally, this fall classification criterion also agreed with the visual inspection of recorded trials for all obvious falls and identified trials as falls that were otherwise difficult to visually classify as falls or recoveries. Enough slack was left in the harness so that it did not catch subjects before they reached this fall threshold.

Gait speed, cadence and step length normalized to leg length (termed step length ratio) were recorded to characterize the walking style of the subjects. Step length and cadence were calculated using the heel marker and gait velocity was calculated as the average centre of mass velocity. These variables were derived both in the known dry environment and in the contaminated condition prior to slip onset.

3.4 RESULTS

Heel velocity and acceleration trajectories in the anterior-posterior direction (*HeelVel* and *HeelAcc*, respectively) during the dry conditions were consistent across subjects, as reflected by the relatively small standard deviation magnitude (Figure 3.1). The horizontal heel dynamics are characterized by a rapid deceleration before, at, and soon after heel contact bringing the foot nearly to a stop by about 5% of stance time. The heel does not start to move again until later in the stance as the subject prepares for the unloading/swing phase. Joint torque trajectories were found to be similar to previously published results [41, 48]. In particular, at heel contact, the ankle, knee and hip joints of the leading leg generate a plantarflexion, flexion and extension torque, respectively. Specifically, the mean (standard deviation) values for $AnklTorq_{HC}$, $KneeTorq_{HC}$ and $HipTorq_{HC}$ were 0.12 (0.05), 0.37 (0.09) and 0.47 (0.17) N*m/kg, respectively. No age group differences in joint torques at heel contact were found ($p > 0.05$).

There were no significant within-subject differences in gait speed, step length ratio, cadence, heel dynamics ($HeelAcc_{HC}$) or joint torques ($AnklTorq_{HC}$, $KneeTorq_{HC}$, $HipTorq_{HC}$)

between baseline and slippery conditions ($p > 0.05$). These findings imply that subjects did not anticipate the slippery floor during the contaminated conditions and that shoe-floor interaction minimally affected the measured parameters. Thus, within-subject means of these variables were computed across conditions and used in subsequent analyses.

3.4.1 Overview of general gait differences between recoveries and falls

The slip outcome classification yielded 10 falls and 17 recoveries (Table 3.2). Subjects classified as falls slipped with a greater anterior heel velocity and acceleration throughout the slip (Figure 3.3). Overall, older subjects experienced a slightly greater rate of falls than younger participants, specifically 45% (5 out of 11) versus 31% (5 out of 16). Statistical analyses regressing general gait variables of interest on age group, slip outcome and age group x slip outcome revealed significant differences only in cadence between recoveries and falls (Table 3.2). Specifically, a faster cadence characterized the gait patterns of subjects who recovered from the slip compared to participants who fell ($p < 0.05$, Table 3.2). Only age-group differences in step length ratio were statistically significant, with older adults taking shorter steps than their younger counterparts ($p < 0.05$, Table 3.2). Gait speed was similar between age groups and slip outcomes, i.e. about 1.4 m/s ($p > 0.1$, Table 3.2).

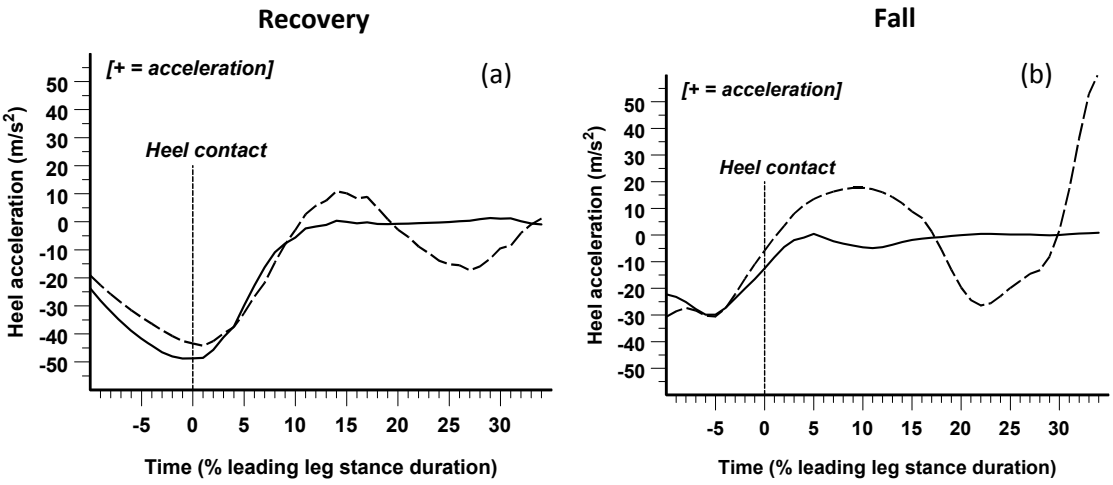

Figure 3.3. Typical heel acceleration time series plots from dry (solid) and slip (dashed) trials

Table 3.2. General gait characteristics stratified by slip outcome and age group

Slip Outcome	**Fall**		**Recovery**	
Age group	***Older***	***Younger***	***Older***	***Younger***
N (% fall / recovery events within age group)	5 (45%)	5 (31%)	6 (55%)	11 (69%)
Required coefficient of friction	0.21 (0.05)	0.19 (0.02)	0.19 (0.02)	0.20 (0.02)
Gait speed (m/s)	1.4 (0.1)	1.4 (0.1)	1.4 (0.1)	1.5 (0.1)
Step length ratio [$p_{age} < 0.05$]	0.79 (0.04)	0.84 (0.02)	0.77 (0.06)	0.83 (0.07)
Cadence (steps/min) [$p_{outcome} < 0.01$]	115 (9)	109 (9)	126 (10)	120 (8)

Continuous gait variables of interest were each regressed on *slip outcome*, *age group*, and *slip outcome x age group*. Statistically significant effects are indicated in brackets in the first column.

3.4.2 Contribution of heel acceleration at heel contact to slip outcome

To test differences in heel contact dynamics between slip outcomes in young and older participants, a regression analysis was conducted with age group, slip outcome and their interaction used as predictors and with $HeelAcc_{HC}$ as the dependent variable. This analysis revealed that subjects who recovered had a greater heel deceleration (greater negative acceleration) at heel contact than subjects who fell (Figure 3.4, $p < 0.05$). The regression analyses reflected no statistically significant age group and slip outcome x age group effects.

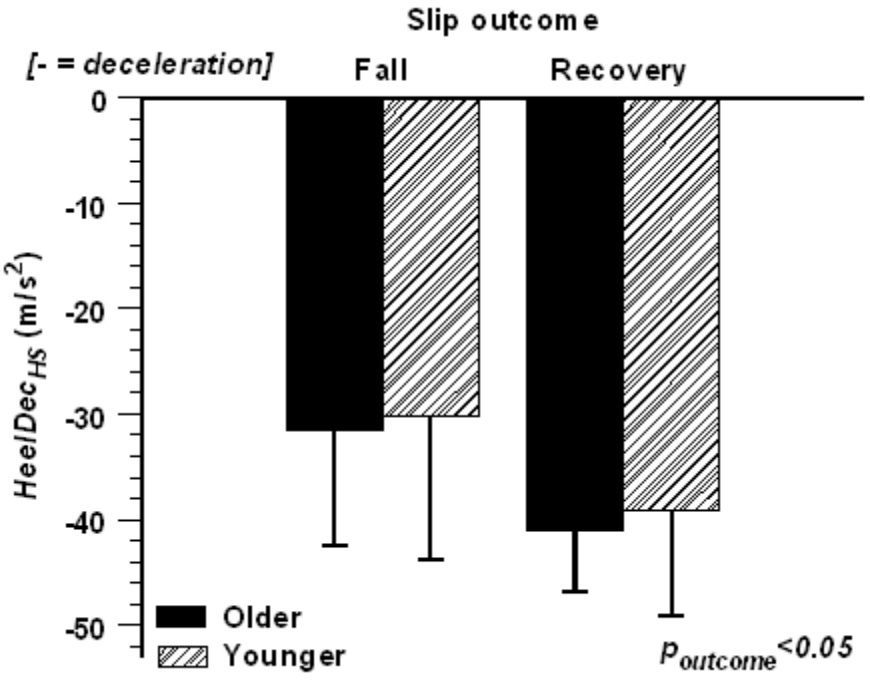

Figure 3.4. Heel acceleration stratified by slip outcome and age group

3.4.3 Heel contact heel acceleration determined by joint torques

All three joint torques at heel contact were found to strongly correlate with heel acceleration at heel contact ($|r|$*~0.6-0.9*, Table 3.3). Specifically, increasing ankle plantarflexion, knee flexion and hip extension moment resulted in greater heel deceleration (negative acceleration) at heel contact ($p<0.01$). Because ankle, knee and hip torques are interdependent, as shown by the Pearson correlation coefficients (Table 3.3), further regression analyses were conducted to determine the main joint contributor to heel acceleration at heel contact. Specifically, $HeelAcc_{HC}$ was regressed on $AnklTorq_{HC}$, $KneeTorq_{HC}$ and $HipTorq_{HC}$ both individually and simultaneously in different models and the behavior of model R^2 was examined (Table 3.4). In order to determine driving determinants of heel contact heel acceleration, special attention was paid to the additional contribution of a specific joint torque to explaining $HeelAcc_{HC}$ variability above and beyond that explained by other joint torques (reflected by ΔR^2 between models in Table 3.4). Findings of this analysis indicate that a greater proportion of the variability in $HeelAcc_{HC}$ is explained by knee torque than by ankle or hip torques (Table 3.4). For example, 76% of the variability in $HeelAcc_{HC}$ is explained by $KneeTorq_{HC}$ alone, compared to 38 and 56% by $AnklTorq_{HC}$ and $HipTorq_{HC}$ alone, respectively. Furthermore, the added contribution to R^2 by the combination of any two or all three joint torques explained no more than 1% of the variability in $HeelAcc_{HC}$ above and beyond the contribution by $KneeTorq_{HC}$ alone. In summary, knee kinetics are the main determinant of heel acceleration at heel contact, with increasing knee flexion torque being positively correlated with heel contact heel deceleration (Figure 3.5, $p<0.01$).

Table 3.3. Pearson correlation coefficients relating gait variables of interest

$\boldsymbol{HeelAcc_{HC}}$	-0.48*	0.09	-0.62**	-0.62**	-0.87**	-0.75**
	Gait speed	0.31	0.65**	0.27	0.52**	0.55**
		Step length ratio	-0.15	0.11	-0.10	-0.25
			Cadence	-0.02	0.53**	0.81**
				$\boldsymbol{AnklTorq_{HC}}$	0.72**	0.32
					$\boldsymbol{KneeTorq_{HC}}$	0.83**
						$\boldsymbol{HipTorq_{HC}}$

Significant correlation (*$p<0.05$, **$p<0.01$).

Table 3.4 R^2 values of $HeelAcc_{HC}$ regressed on each joint torque individually and simultaneously

Independent variables	**Model 1** $AnklTorq_{HC}$	**Model 2** $KneeTorq_{HC}$	**Model 3** $HipTorq_{HC}$	**Model 4** $AnklTorq_{HC}$ *and* $KneeTorq_{HC}$	**Model 5** $AnklTorq_{HC}$ *and* $HipTorq_{HC}$	**Model 6** $KneeTorq_{HC}$ *and* $HipTorq_{HC}$	**Model 7** $AnklTorq_{HC,}$ $KneeTorq_{HC}$ *and* $HipTorq_{HC}$
	0.38	0.76	0.56	0.76	0.72	0.77	0.77
Statistical significant effects							
$AnklTorq_{HC}$	p=0.001	N/A	N/A	p=0.863	p<0.002	N/A	p=0.881
$KneeTorq_{HC}$	N/A	p<0.001	N/A	p<0.001	N/A	p<0.001	p=0.054
$HipTorq_{HC}$	N/A	N/A	p<0.001	N/A	p<0.001	p=0.694	p=0.707

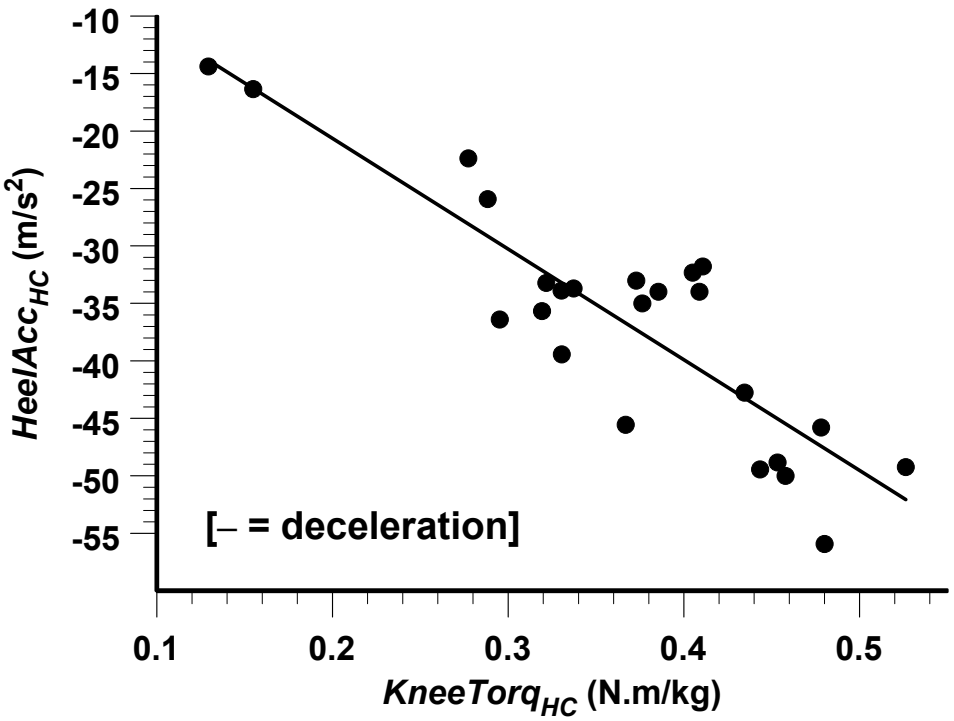

Figure 3.5. Regression plot of $HeelAcc_{HC}$ against $KneeTorq_{HC}$

3.4.4 Relationship between heel acceleration at heel contact and general gait variables

A multivariate regression analysis was performed among $HeelAcc_{HC}$, joint torques at heel contact ($AnklTorq_{HC}$, $KneeTorq_{HC}$ and $HipTorq_{HC}$) and spatiotemporal gait variables to gain a general understanding of the relationship among all of these variables (Table 3.3). $HeelAcc_{HC}$ was found to significantly correlate with gait speed and cadence: specifically a higher gait speed and cadence were correlated with more negative $HeelAcc_{HC}$ (higher heel deceleration). Some interrelation between joint torques was found: $AnklTorq_{HC}$ was positively correlated with $KneeTorq_{HC}$ and $KneeTorq_{HC}$ was positively correlated with $HipTorq_{HC}$. In addition, $KneeTorq_{HC}$ and $HipTorq_{HC}$ were both positively correlated with cadence and gait speed. Step length ratio was not correlated with any other variable measured.

3.5 DISCUSSION

Anterior heel acceleration at heel contact was found to be a significant contributor to slip outcome. Specifically, greater deceleration (negative acceleration) at heel contact was associated with an improved chance of slip recovery. Additionally, knee flexion torque of the leading leg appears to be the major determinant of heel acceleration at heel contact. Heel acceleration at heel contact correlates with gait variables previously identified as potential contributors to hazardous slips, e.g. cadence. Finally, no statistically significant age group effects were found.

Findings of this study suggest that leading leg kinetics at heel contact, particularly knee flexion torque coupled with hip extension torque, play a significant role in reducing the risk of slips and falls by increasing heel acceleration. Although leg kinetics have not been previously linked with heel dynamics, the beneficial effects of increased knee flexion and hip extension torques have been reported in studies examining both reactive and proactive slip-related responses. Indeed, once a slip is initiated, reactive strategies consist of increasing knee flexion and hip extension torques in an attempt to slow the slipping leg down and to move the center of mass over the leading leg [48]. Similarly, proactive strategies, often generated when anticipating a slip, also consist of increased hip extensor and knee flexor muscle activity, particularly in muscles such as the biceps femoris [93] and medial hamstring [54]. Therefore healthy subjects anticipating a slip, and thus presumably adopting a safer walking style, are shown to further activate muscles that generate joint torques found in this study to correlate with heel acceleration. In summary, having greater knee flexion and hip extension torques occurring naturally in the gait cycle especially at heel contact may be important in successfully decelerating the heel, decreasing the extent of the individual's reliance on shoe-floor friction or reactive responses to recover balance, and can potentially be perceived as a safer walking pattern.

The importance of heel acceleration at heel contact may contribute to the lack of consistent evidence studies that investigated associations between heel velocity and fall risk. For example, Lockhart, Woldstad et al. [45] associated a higher fall rate among older adults due to an

increased heel velocity at heel contact while Lockhart and Kim [97] found that older adults, whom also fell at a higher rate than their young counter parts, had a smaller heel velocity at heel contact. Heel acceleration at heel contact, a result of leading leg joint torques, rapidly decreases heel velocity shortly after heel contact. The combined effect of heel velocity and acceleration at heel contact may explain a greater proportion of the variability in initial conditions of the heel and subsequently fall risk than heel velocity alone. Intuitively, subjects with higher anterior heel velocity at heel contact can compensate with increased heel deceleration (rearward acceleration) at heel contact.

The findings correlating heel acceleration at heel contact with slip outcome may be of particular interest in identifying individuals at greater risk of slipping and falling. Heel acceleration at heel contact can be easily and inexpensively measured with accelerometers and pressure sensors or footswitches to determine the timing of heel contact. In fact, quality of data acquired with accelerometers may be improved beyond this study because accelerometers do not require that data be twice differentiated when acquiring acceleration from marker data. Additionally, this research has shown that heel acceleration at heel contact is correlated with cadence. Specifically, increasing cadence may be one way to increase heel contact heel deceleration. More research is needed to determine if imposing changes in cadence actually affects heel contact heel dynamics and whether this change will lead to improved slip/fall risk. While heel acceleration reflects the kinetics of the leading leg at heel contact, it is not completely deterministic of the outcome of a slip as post-slip reactions also play a vital role in determining the outcome of a slip [48, 49, 62, 105].

No age group effects were found. These findings imply that the older adults in this study had similar relationships between heel dynamics and slip risk/outcome as the younger adults. These results may be due to the fact that our group of older participants was very healthy (rigorous screening) and perhaps not old enough to reflect age group differences. Older adults over the age of 70 years old were not enrolled in this study due to safety constraints related to the slippery conditions included in the protocol. Thus, age and health characteristics of the subjects used in this study may have somewhat restricted the implication of the findings in other populations. For example, in frail older adults, particularly those with deficiencies in lower leg strength, the relationships between heel acceleration, joint torques and fall risk may be different than the results reported in this study.

In conclusion, a reduced deceleration of the heel at heel contact may be a risk factor for slip-initiated falls. The torque generated by the knee of the leading leg is a significant determinant of heel contact heel acceleration. While an intervention study is needed to determine the effectivity of manipulating heel acceleration to reduce fall risk, the results of this research are promising for identification and improvement of high risk walking styles.

4.0 EXPERIMENTAL STUDIES

This chapter covers experimental testing that were conducted as part of an exploratory effort to determine the lubrication effects that are critical to slip and fall accidents. The first section in this chapter measures the effects of different slip testing parameters, mainly normal force, sliding speed and shoe angle, on coefficient of friction for an entire shoe against a floor surface within the range of conditions that are relevant to slip and fall accidents. Inferences about the lubrication effects that are relevant to slip and fall accidents are then made by examining the coefficient of friction response to these different slip testing parameters. This study was published in [57]. The second section of this chapter uses a pin-on-disk apparatus to precisely vary normal pressure and sliding speed in order to determine fundamental tribological mechanisms that occur between shoe and floor materials in the presence of a contaminant. The pin-on-disk research serves a secondary purpose of showing that the critical lubrication effects relevant to human slip and fall accidents, as determined in the first section, can be recreated with a pin-on-disk apparatus. Therefore, modeling the lubrication effect of shoe and floor materials applied to a pin-on-disk apparatus, which is conducted in Chapter 5, is relevant to the lubrication effect experienced by shoes during slip and fall accidents.

4.1 EFFECTS OF SLIP TESTING PARAMETERS ON MEASURED COFFICIENT OF FRICTION

The first section in this chapter was focused on the effects of slip testing parameters (i.e. normal force, shoe angle and sliding speed) on the overall friction coefficient between a shoe heel and floor surface. The slip testing parameters were selected to cover the range of conditions considered that could be considered biomechanically relevant or “biofidellic”. This study serves

two major purposes: (1) inferences can be made about the lubrication regime experienced in the shoe-floor-contaminant interface from the experimental data and (2) the limitations of measuring friction coefficient under a single set of testing conditions is realized. This work was published as a journal article in [57].

4.1.1 Abstract

Slips and falls are a major cause of injuries in the workplace. Devices that measure coefficient of friction (COF) of the shoe-floor-contaminant interface are used to evaluate slip resistance in various environments. Testing conditions (e.g. loading rate, timing, normal force, speed, shoe angle) are believed to affect COF measurements; however the nature of that relationship is not well understood. This study examines the effects of normal force, speed, and shoe angle on COF within physiologically relevant ranges. A polyvinyl chloride shoe was tested using a modified industrial robot that could attain high vertical loads and relatively high speeds. Ground reaction forces were measured with a loadcell to compute COF. Experiment #1 measured COF over a range of normal forces (~100-500N) for two shoe angles (10°, 20°), four speeds (0.05, 0,20, 0.35, and 0.50 m/sec), and two contaminants (diluted detergent and diluted glycerol). Experiment #2 further explored speed effect by testing 7 speeds (0.01, 0.05, 0.20, 0.35, 0.50, 0.75, 1.00 m/sec) at a given normal force (350 N) and shoe angle (20°) using the same two contaminants. Experiment #1 showed that faster speeds significantly decreased COF, and that a complex interaction existed between normal force and shoe angle. Experiment #2 showed that increasing speed decreased COF asymptotically. The results imply that COF is dependent on film thickness separating the shoe and the heel, which is dependent on speed, shoe angle, and NF, consistent with tribological theory.

4.1.2 Introduction

Slippery surfaces are a major cause of injuries from falls in the workplace. Slip, trip, and fall events were the estimated cause of between 20% and 40% of disabling injuries in the developed world [11]. Slips, trips, and falls are a major source of hospital visits in many sectors including services, manufacturing, retail, and construction [79]. Floor contaminants were the reported

cause of same-level falls in industry 19% of the time for females and 32% of the time for males [79]. Thus the prevention of slips is an important public and occupational health issue.

Evaluating the slip potential of different shoe floor interfaces is one tool used to design shoes and floors that are more resistant to slips and falls. Experts have stated the need for a device that is biomechanically representative of the conditions that are present during a slip [106]. Existing slip testers range from small portable devices for field use [28] to large laboratory devices that are capable of testing over a wide range of parameters including high forces and fast speeds. Lab devices usually test an entire shoe and apply a normal force, shoe angle, and speed and then determine the shear force. Coefficient of Friction (COF) is then measured as the ratio of shear force to normal force (NF). The levels of NF, shoe angle, and speed are highly variable across devices, potentially resulting in different COF measurements for the same floor/shoe/contaminant conditions.

Most whole shoe testers operate similarly by measuring COF during a phase when NF, speed, and angle are constant. The most common whole shoe devices are the LABINRS [107], BST 2000 [58], Stevenson devices [108, 109], Slip Simulator [56], Programmable Slip Resistance Tester [25], Slip Resistance Tester (STM603) [26], and the Portable Slip Simulator [110]. These devices typically differ in their choice of NF, speed, and angle as seen in Table 4.1 [55]. In addition, the Slip Simulator and the Portable Slip Simulator differ from the rest of the slip testers because they record COF within the first 250 msec after heel strike, while other testers record COF much later after heel strike.

Table 4.1. List of whole shoe slip-testing devices and their testing conditions

Device:	Foot Floor Angle	Horizontal Speed	Vertical Load
LABINRS	0-20 deg	0.2m/s*	600 N*
PSRT	5-15 deg	0.01-0.2 m/s	40-80 N
Stevenson (1989)	10 deg	~0.4m/sec*	350 N
Stevenson (1997)	5 deg	0.25 m/sec	490 N
STM603	5 deg*	0.1 m/s*	400 N*
BST 2000	-15deg - +15 deg	0.2 m/sec	500 N*
Slip Simulator	5 deg*	0.4 m/sec*	700 N*
Portable Slip Simulator**	5 deg*	0.2 m/sec*	500 N*

Adapted primarily from [55]; *Typical values; **[110]

The parameters chosen to test friction (i.e. NF, speed, shoe angle, and dwell time) are generally intended to represent conditions endured by the shoe at the critical point during a slip event. The time between shoe down and COF measurement is an important parameter when testing with liquid contaminants because dwell time affects the film thickness and subsequently the lubrication regime [82]. Transitional friction, occurring in the first 250 msec of a slip, and steady state friction, occurring later in the slip, have both been found to be relevant to a slip, although transitional friction is more important [27, 29]. The critical NF for a slip has been cited as being between 35% and 90% of body weight thus testing with a wide range of NF would seem appropriate [111]. An appropriate range of sliding speeds based on slip studies has been determined to be between 0 and 1m/sec [41, 45, 82]; clearly a large range of sliding speeds could be defended as being biomechanically relevant. Shoe angle at heel contact was found to be over 20° at heel contact although variation is high across and within subjects [60, 64] and decreases rapidly to about 12° at the time of forward slip [64]. Because of the wide range of timing, shoe speed, NF, and shoe angles that are considered biomechanically relevant and the wide range of

parameters that slip testers typically test with (Table 4.1), it is important to understand how these parameters affect the measurement of COF.

There is a paucity of research examining how testing parameters affect measurements of COF. Redfern and Bidanda found that speed had an effect on COF under certain shoe-floor-contaminant conditions and that NF and angle had either unsubstantial or insignificant effect [25]. This study used relatively small loads (40-80 N) and speeds (0.01-0.15 m/sec). Wilson found that for most rubber soles on steel and vinyl floor combinations, COF was smaller for high speed (1.5 m/sec) than medium speed (0.1 m/sec) trials [26]. Similarly, Leclercq et al. showed that while measuring friction with a braked wheel, larger wheel speeds decreased friction for liquid contaminated surface [24]. Other research, conducted with shoe material samples attached to a pneumatic wheel, has shown that NF between 100N and 200N and speed between 0.15 m/sec and 0.30 m/sec significantly affect COF measurement [112]. Proctor and Coleman have used fluid dynamic theory to describe the effects of viscosity, speed, contact area, and NF on film thickness, which is a major contributor to friction [68]. Research has shown significant parameter effects, however little is known about the trends of this effect.

The purpose of this study was to systematically examine the effects of NF, speed, shoe angle, and their interactions on measured COF. We chose high vertical forces, relative to a previous similar study [25], for two different contaminant conditions and a single shoe-floor combination as a demonstration of the potential effects of these parameters on COF. The device with which these tests were performed operates in the steady state friction region in order to mimic the majority of the devices in existence.

4.1.3 Methods

4.1.3.1 Equipment

The device consists of a high payload robot, load cell, and end-effector (Figure 4.1). The robot that drives the slip tester is a six axis serial articulated manipulator (Kuka KR210 Series 2000), which is ordinarily used as a manufacturing robot. The manipulator can move about each of its 6 axes at speeds of at least 85 degrees $\sec^{-1}$ while exerting over 2000N of force with a position repeatability of 0.12mm [113]. A six-degree of freedom load cell (ATI Theta-350-2100) with an

accuracy of 1N for each of the shear axes and 2N for the compression/tension axis was attached to the end of the robotic arm to measure shear force and NF during the tests. An end-effector secured the shoe to the device and consisted of a metal plate, a four inch spacer, and a solid resin foot for attachment of the shoe. The spacer was used to roughly resemble the bottom of the shank such that boots and larger shoes could be attached.

Figure 4.1. Slip-testing device

A polyvinyl chloride (PVC) soled work shoe was tested on a vinyl tiled floor, which was cleaned before the beginning of a testing session. The shoe sole was partially worn, with some tread (1.5mm depth) still on the heel. The floor section was surrounded by a barrier to minimize contaminant leakage. Contaminants used were a high viscosity 75% glycerol - 25% water mixture (viscosity = 41.6 mPa-sec) and a relatively low viscosity 2% detergent - 98% water mixture (viscosity = 1.28 mPa-sec).

4.1.3.2 General protocol and data processing

The shoe height to achieve the desired NF for each trial was initially obtained using the robot in position control mode. The end-effector was manually moved along an axis normal to the floor until the desired NF was achieved by visually monitoring the output from the load cell. An axis of the loadcell that was nearly aligned perpendicular to the floor was used to approximate the NF within 5N of the target normal force (NF_T). The coordinates of the end-effector at this position were saved by the robot controller. The shoe was then raised from the floor until a gap (0.10 m) existed between the floor and shoe.

Five trials were then performed to assess the COF for each floor condition and speed. For each trial, the shoe was moved through a set of positions in a closed loop manner by the robot. Initially the shoe was moved downward to the shoe height determined previously for achieving the desired NF at 0.10 m/sec. The shoe was then moved forward, or along an axis parallel to the surface of the floor at the desired speed for 0.40 m for Experiment #1 and 1.00 m for Experiment #2. During this motion, the shoe experienced three phases: 1) positive acceleration; 2) zero acceleration (or constant speed); and 3) negative acceleration. The shoe was subsequently lifted from the floor along a normal axis to the floor and return to its starting position. Finally, the shoe was moved laterally 4 cm before the process was repeated for the next trial. These motions were performed automatically by the robot in position control mode and the three dimensional forces from the loadcell (NF) were collected at 100 Hz for the entire loop.

To calculate the COF, a transformation was applied to the collected forces to align the forces to the floor (i.e. parallel and perpendicular to the floor). The transformed NF and shear force time series were then filtered using a first order low-pass Butterworth filter with a cutoff frequency of 10 Hz. The COF time series were calculated by dividing the collected NF value into the shear force value at each time sample.

4.1.3.3 Experiment #1

A full-factorial experimental design was used to investigate the impact of NF, speed, and shoe angle on COF for two different contaminant conditions. Levels of the fixed effects were: speed (0.05m/sec, 0.20m/sec, 0.35m/sec, 0.50m/sec), and shoe angle (10 degrees, 20 degrees) for both contaminants. Normal force was initially set at three levels (NF_T = 180, 360, or 540 N). The variability in NF because of position control rather than force control allowed COF measures over a continuous range of NF, making the recorded NF (NF_R) random within a range determined by the NF_T. Therefore, NF_R was treated as a random effects independent variable. Five repeated trials within condition were performed. COF and NF were averaged over a 20 cm path on the floor during steady shear forces to determine the COF that corresponded with the recorded NF (NF_R). The tested parameters were chosen because they were in the range of biomechanically relevant parameters previously discussed. This resulted in a total of 3 contaminants x 4 speeds x 2 shoe angles x 3 NF_T x 5 trials = 360 trials. Within a 5 trial set, contaminants were not reapplied; however, contaminants were reapplied between trial sets. The 4cm lateral movement ensured that contaminant was underneath the shoe for each trial.
Two statistical analyses were performed. For each contaminant condition, a separate mixed-model ANOVA was run to determine the effects of NF_R, shoe angle, speed, and their interactions on COF. Shoe angle and speed were analyzed as fixed effects, while NF_R was a random effect variable. A second analysis to further describe the interaction of NF_R, speed, and shoe angle, was performed using a second order polynomial regression model to each contaminant, shoe angle, and speed condition:

$$\mathbf{COF = a * NF_R^2 + b * NF_R + c} \qquad \text{Eq. (4.1)}$$

If the coefficient of the second order component, a, was found to be non-significantly different from zero ($\alpha>0.05$), then a linear model was used. If b, the first order component, was not significantly different from zero ($\alpha>0.05$), the COF was considered a constant. Plots of these regressions were used to demonstrate the effects of speed, foot angle, and contaminant as well as their interactions.

4.1.3.4 Experiment #2

A second experiment was conducted to determine the impact of velocity over a greater range of speeds. This data was used to compare to the theoretical speed effects described by Proctor and Coleman [68]. NF_R and angle were held at 350 N and 20°, using previously described contaminants (detergent and glycerol). Seven speeds were tested: a very low speed (0.01 m/sec), the four speeds tested in Experiment #1 (0.05 m/sec, 0.20 m/sec, 0.35 m/sec, 0.50 m/sec), and two faster speeds (0.75 m/sec and 1.0 m/sec). The amount of distance that was required to accelerate the shoe to its steady state velocity was dependent on this steady state velocity. In order to accommodate the larger velocities in this experiment, a distance of 1.00 m was used for this experiment. The shoe was not moved laterally between trials; however, the contaminant was reapplied between each trial. While NF was still not controlled, at some point during constant velocity of each trial the NF became 350 N; COF was recorded over 0.1 seconds when NF was between 350-355 N therefore all trials had a NF_R between 350 and 355N.

Results of Experiment #2 were analyzed by creating confidence intervals for each speed-contaminant condition based on the five repeated trials. The effect of speed on COF was determined by comparing subsequent speeds using a t-test with $\alpha<0.05$.

4.1.4 Results

4.1.4.1 Force and COF profiles

The general shapes of the force and COF profiles during a test are demonstrated in Figure 4.2. The time series consisted of a loading phase, acceleration phase, a constant speed phase, a deceleration phase, and an unloading phase. During loading (1) and unloading (5) phases, the shoe was being moved vertically to the target position corresponding to NF_T, which lasted for about 0.1 sec. The shoe was then accelerated forward for about 0.5 sec to its steady state speed, referred to as the acceleration phase (2). The constant speed (3) phase duration was between 0.75 sec and 8 sec for Experiment #1 and between 0.9 sec and 99 sec for Experiment #2, depending upon the testing speed, and was characterized by a steady region of the shear forces. The deceleration phase (4), where the shoe was slowed to a stop, lasted about 0.4 seconds. Trials at

slower speeds had a long steady region whereas trials with a higher speed covered the fixed distance quicker and therefore had a shorter steady region (Figures 4.2). Vibration during the constant speed phase occurred in some of the trials. Although the amount of vibration varied from trial to trial, generally the trials at lower speeds had larger vibrations.

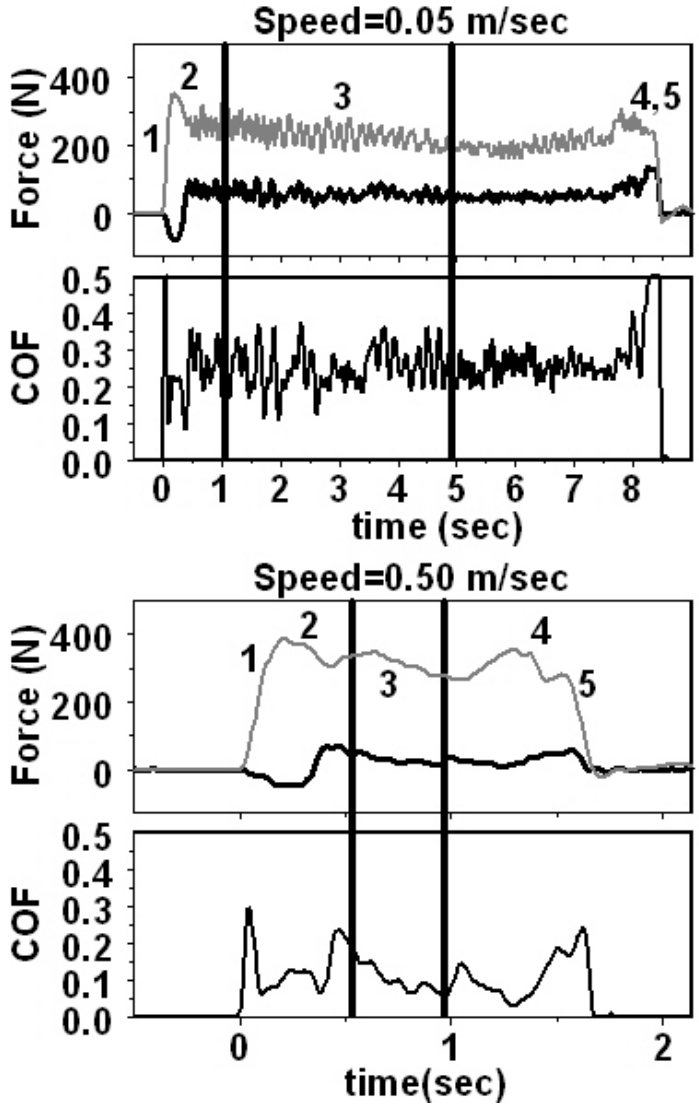

Figure 4.2. Normal and shear force profiles for slow speed (a) and fast speed (b)

4.1.4.2 Experiment #1

The ANOVA analysis showed that for the detergent condition, NF_R ($F_{1,104}$=63.2, $p<0.001$), speed ($F_{3,104}$=118.0, $p<0.001$), shoe angle ($F_{1,104}$=137.6, $p<0.001$) and the interactions between NF_R and angle ($F_{1,104}$=95.9, $p<0.001$) affect COF. The glycerol condition showed the same contribution from NF_R ($F_{1, 104}$ $p<0.001$), speed ($F_{3,104}$= 223.7, $p<0.001$), shoe angle ($F_{1,104}$=562.0, $p<0.001$) and NF_R-angle interaction ($F_{1,104}$=27.0, $p<0.001$), but also found a significant speed-angle interaction ($F_{3,104}$=17.2, $p<0.001$) and speed- NF_R interaction ($F_{3,104}$=3.07, $p<0.05$).

To further demonstrate the effects of the independent variables on COF, regression analyses were performed. The strength of the regressions varied, with the coefficient of determination ranging from 0.39 to 0.95 (Table 4.2, Figure 4.3). Regression of COF to NF_R for different speeds, shoe angle, and contaminant conditions had very different outcomes (Figure 4.4). Increased shoe angle (20° versus 10°) reduced COF for both contaminants. Shoe angle affected the relationship between NF_R and COF. For the detergent condition, COF was dependent on NF_R at a shoe angle of 10° (Figure 4.4a) but not at a shoe angle of 20° (Figure 4.4c). For the glycerol condition, a 20° shoe angle (Figure 4.4d) reduced the NF_R effect compared to the 10° angle (Figure 4.4b). Thus, the impact of shoe angle on COF responses to NF_R was not the same across the two contaminants, indicating the complexity of the interaction. Speed also had a very pronounced effect on COF. Faster speeds decreased COF for all contaminant-angle conditions. This effect appears to be approaching an asymptote as speeds continue to increase (Figures 4.4b-d).

Table 4.2. Correlation coefficients for regression analyses

Contaminant	Speed (m/s)	Coefficient of Determination (r^2) 10°	20°
Detergent	0.05	0.73	---*
	0.20	0.95	---*
	0.35	0.82	---*
	0.50	0.94	---*
Glycerol	0.05	0.52	0.62
	0.20	0.40	---*
	0.35	0.69	0.90
	0.50	0.61	0.39

* No model was applied (a=0; b=0)

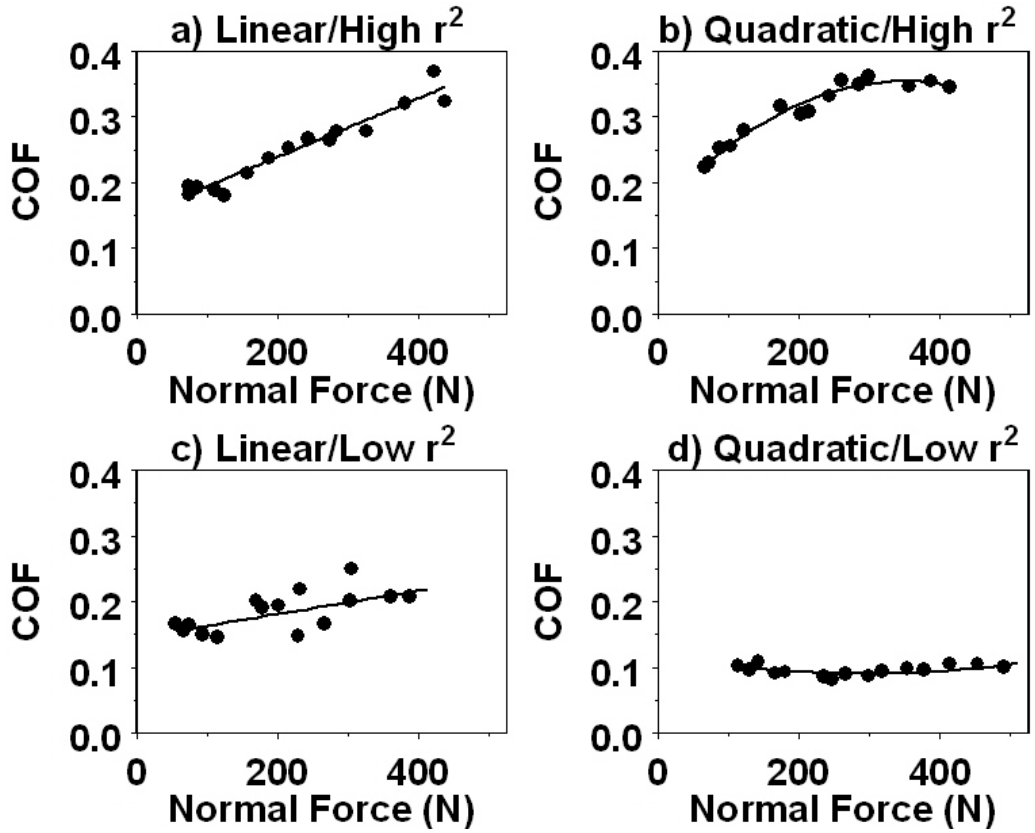

Figure 4.3. Examples of linear and quadratic correlations with low and high r^2 values

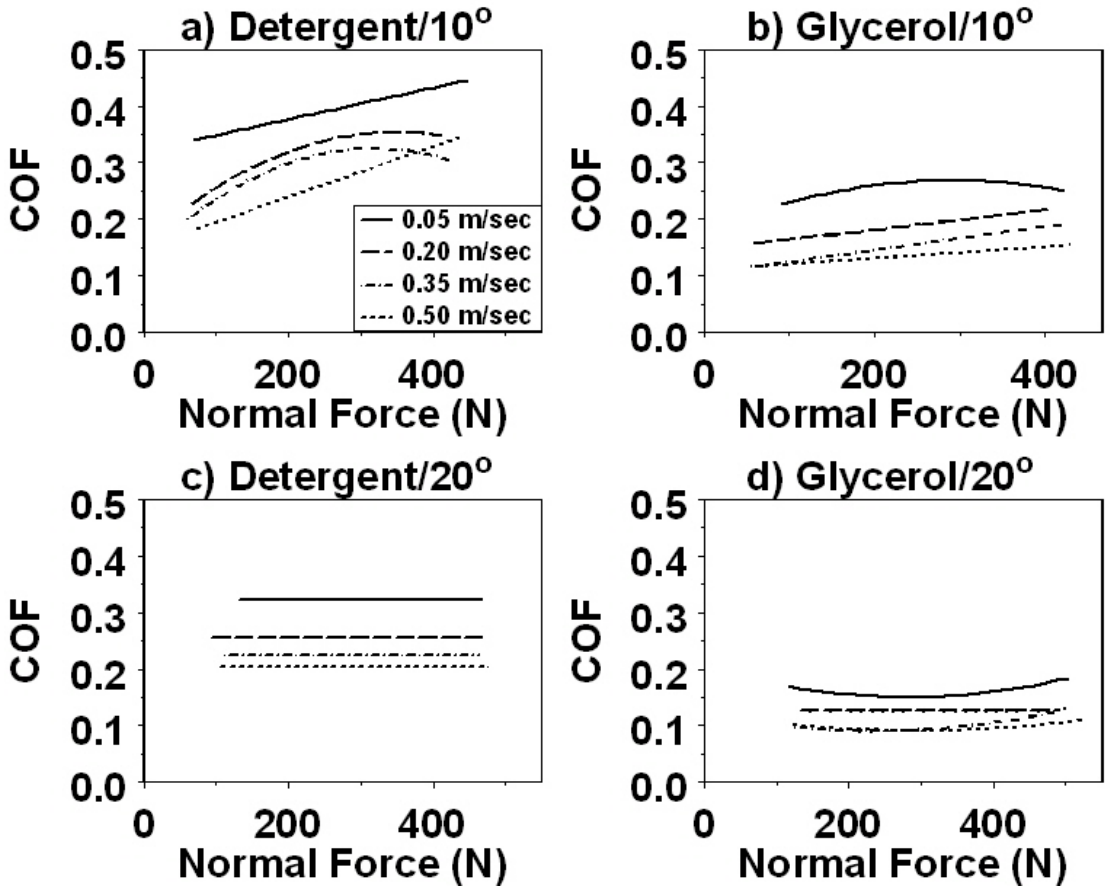

Figure 4.4 COF-normal force regression plots stratified by fluid contaminant and shoe angle across a range of testing speeds

4.1.4.3 Experiment #2

The speed test (Experiment #2) indicated speed had an effect on COF outside the range conducted in Experiment #1 (Figure 4.5). As speed increased from slow to fast, COF continually decreased until a threshold was reached and speed no longer affected COF. Varying speed no longer significantly affected COF above 0.75 m/sec and 0.35 m/sec for detergent and glycerol, respectively. Although COF differed in the glycerol condition significantly between 0.20 and 0.35 m/sec, the difference was only 0.0041 and therefore insubstantial. After these threshold speeds were reached, there was no statistical difference in COF found for subsequent speeds.

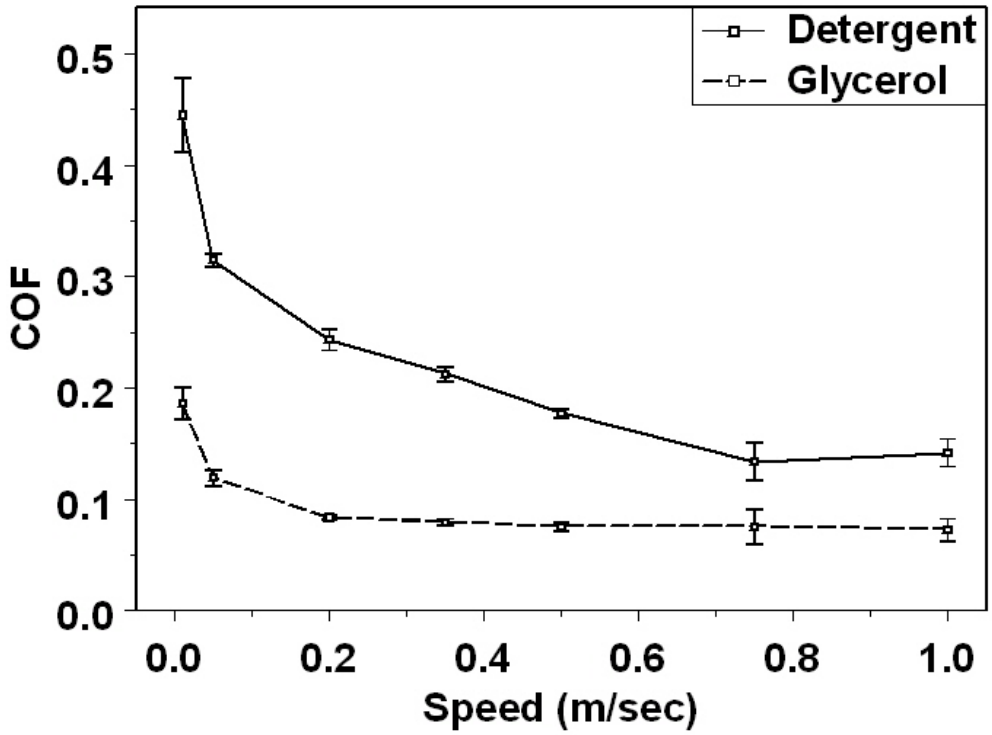

Figure 4.5. Effect of speed on COF for two contaminants

4.1.5 Discussion

This study demonstrates the complex effects of speed, shoe angle, and NF on measurements of steady-state friction. Faster speeds generally lowered COF while a more complex relationship occurred between the angle and NF_R contribution. Redfern and Bidanda also found that speed affected friction as part of an interaction with both contaminant and shoe over smaller ranges of NF and speed [25]. Their results found a NF-shoe material and speed-shoe material interaction, which implies that the results may be dependent on shoe material. The effect of speed on COF is consistent with results of other studies who also found that faster speeds lowered COF [26, 112].

The results of experiment #2 showed large changes in COF with speed that resemble the theoretical Stribeck curve [114], which relates speed and friction (Figure 4.6). The relationship

between speed, fluid thickness, and COF in the Stribeck curve results from different regimes of material interactions at various speeds. Faster speeds increase film thickness, which decreases COF, until the surfaces are fully separated. This theory is consistent with the general shape of the speed-COF results in Figure 4.5 as increasing speed increased fluid thickness until the surfaces were fully separated at which point speed no longer had a substantial effect. The mathematical relationship describing the film thickness separating two surfaces (sometimes called the wedge term) is defined as:

$$\mathbf{h^2 = \frac{0.066ul^3v}{NF}} \qquad \text{Eq. (4.2)}$$

where *u* is the viscosity, *l* is based on contact area, *v* is the speed, and *NF* is the normal force [68]. The difference in the speed at which the COF leveled off for the two contaminant conditions (Figure 4.5) is predicted to be due to the relatively different viscosities (i.e. a larger viscosity requires smaller speeds to achieve a certain film thickness). The results show that COF testing at high normal force levels are consistent with theory.

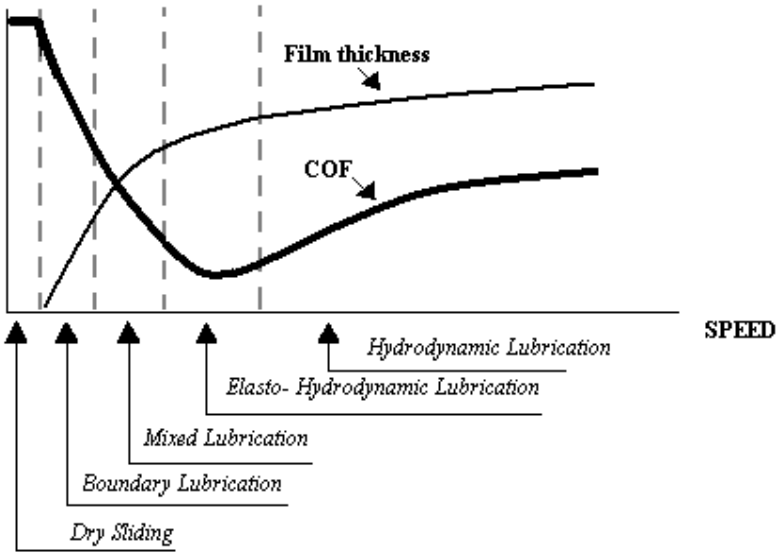

Figure 4.6. Theoretical Stribeck curve

There are complexities that are not included in the fundamental models of friction which result in discrepancies between predictions and actual measurements. Fundamental theory usually assumes a constant contact area, does not include tread design, and does not focus on a particular shoe material used. This limits the specificity of the general theory. The deformable nature of the shoe results in a contact area that would be dependent on NF and direction of loading (shoe angle). This variable contact area during loading may explain the complex relationship seen in our results among COF, shoe angle, and NF. Another effect that cannot be explained by fundamental theory is the quadratic nature of the speed dependence of the relationship between COF and NF_R for detergent and glycerol at 10°. The high coefficients of determination for the detergent, 10° shoe angle condition, a significant quadratic relationship) suggest that this effect is not merely statistical artifact. Theory based on the work of Proctor and Coleman and the Stribeck curve does not provide a simple explanation for this effect. These two theories are merely approximations of a complex interaction between a shoe, contaminant and floor surface; which do not include shoe shape, material properties or fluid drainage via tread in the shoe. Including these factors in future models may improve the ability to predict COF based upon theory.

Because slip testers operate at different NF, shoe angle, and speed, the COF values will be dependent on the slip tester used. The complex interactions of NF and shoe angle imply that comparisons between different slip testers will be non-linear. The current study, however, measures steady-state friction, and therefore the results may be different than transitional friction devices like the slip simulator and portable slip simulator [56, 110]. Furthermore, the high variance in walking styles and limited understanding of critical parameters imply that a single value for COF may be insufficient in order to describe the slip resistance nature of a shoe-floor combination.

4.1.6 Conclusion

This study showed that changing NF, speed, and shoe angle, within the range considered biomechanically relevant can affect friction measurement. Because the complex nonlinear fashion in which these parameters affect COF, values across slip testers operating under different

conditions may give different results that are difficult to compare. The similarity between the COF measures using high normal forces and theory demonstrates the importance of testing at levels nearing those found in walking. The discrepancies found between theoretical models and the measured COF values suggests that including other complexities into the models, such as variable contact area and tread, is warranted.

4.2 SHOE-FLOOR FRICTIONAL PROPERTIES FOR VARYING SLIDING SPEED, PRESSURE AND CONTAMINANT

4.2.1 Abstract

Injuries resulting from slips and falls are a major health concern. Current devices to measure slip resistance of shoe-floor-contaminant interfaces attempt to mimic biomechanical conditions (shoe angle, sliding speed, and normal force); however, the results are variable, depending upon the measurement methods used. Thus, an understanding of shoe-floor interaction from a theoretical view could provide insights into coefficient of friction (COF) of the shoe-floor interface. The purpose of this work was to determine the effects of normal pressure, sliding speed and contaminant on coefficient of friction of shoe and floor samples to shed light on the fundamental tribological behavior of these interactions. This work also serves a secondary purpose of ensuring the mixed-lubrication effects, which are critical to human slips, can be recreated using a pin-on-disk apparatus. Experiments were conducted using a pin-on-disk apparatus where the pin was one of 2 different samples of shoe material and the disk was a sample of flooring material. Two different loading levels, 5 different speeds and 3 different contaminants were evaluated with a full factorial design. Stribeck curves were then generated where COF was plotted against service parameter, which combined viscosity, speed and normal load. Stribeck curves were generated for both shoe materials with higher variation occurring at low service parameter values. An ANOVA analysis revealed that all variables (material, normal force, fluid and speed) had an effect on COF as well as numerous interaction effects. The results indicated that understanding shoe-floor-contaminant friction across a range of conditions may be more informative than using a single friction value.

4.2.2 Introduction

Injuries occurring directly from a slip, trip and fall incident account for between 20-40% of disabling injuries [11]. Floor contaminants are the primary cause for between 19 and 32% of these falls [79]. Therefore, understanding slipping events and reducing the number of these falls is an important health issue. The amount of friction between the shoe-floor surface in the presence of a contaminant is critical to whether a person slips or not during gait [19]. Numerous methods have been developed to determine shoe-floor-contaminant friction under conditions (i.e. shoe speed, shoe angle and normal force) experienced by the shoe during a slip event [55]. Unfortunately, shoe speed, shoe angle and normal force vary across and within people, which makes identifying the set of conditions to test a shoe-floor-contaminant friction difficult. Therefore, it is important to study shoe-floor-friction from a tribology perspective to improve understanding of shoe-floor conditions effects on coefficient of friction (COF). Normal force, speed and shoe angle are known to affect the amount of friction between a whole shoe and floor surface in the presence and absence of a contaminant [25, 57]. Previous studies, however, tested a whole shoe and the results are thus dependent on deformation of the shoe and tread patterns. In order to understand the shoe-floor-contaminant system at a more fundamental level, it is important to first understand how normal pressure and speed effect COF between shoe and floor surfaces. In addition, by replicating the mixed-lubrication effect, which is relevant to human slip and fall accidents because it represents the transition from safe high friction conditions to dangerous low friction conditions, is useful to showing that the pin-on-disk apparatus is relevant to shoe-floor-contaminant friction. Showing that the pin-on-disk apparatus is relevant to human slips and falls is important because the simplified loading conditions and geometry of the pin-on-disk apparatus provides an opportunity for a simple, first-generation shoe-floor-contaminant friction model as developed in Chapter 5. The purpose of this study is to examine the effects of normal pressure, sliding speed and contaminant on the friction coefficient and lubrication regime between two commonly used shoe materials (polyurethane and polyvinyl chloride) and a commonly used floor material (vinyl tile).

4.2.3 Methods

All experiments were conducted with a standard pin-on-disk device where the pin was a sample of shoe material, which rested on a spinning disk of floor material (Figure 4.7). The device allows for the normal force to be adjusted by placing different sized hanging masses on a balanced lever arm that attaches to the pin. A load cell, also attached to this balanced lever arm records shear force. A custom program developed in Labview collected shear forces and controlled the speed of the spinning disk.

The two shoe materials used in this study were cut directly from the heels of commercially available shoes. One of the specimens was made of polyurethane (PU) and had a roughness of 14.4µm while the other specimen was made of polyvinyl chloride (PVC) and had a RMS roughness of 3.4µm. The PU material was softer than the PVC material. The flooring material was commercially available vinyl tile.

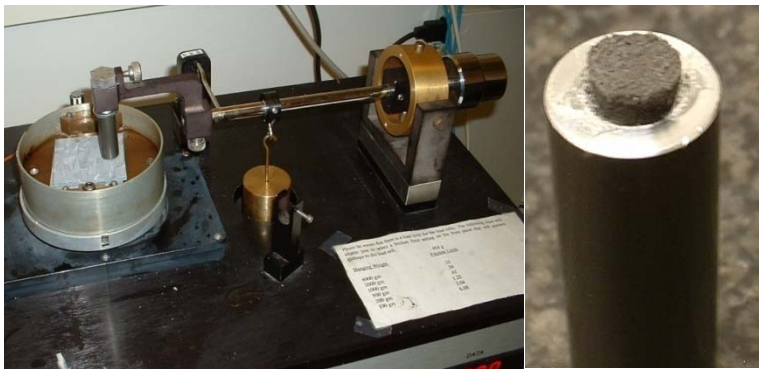

Figure 4.7. Pin-on-disk apparatus

The shoe and floor samples were tested across a range of conditions including 2 levels of normal pressure (26 kPa and 70kPa), 5 levels of sliding speeds (10, 20, 50, 100 and 200 mm/s), and 3 levels of fluid contaminant (75% glycerol, 50% glycerol and 25% glycerol). A full

factorial testing design was used to test all combinations of these conditions. Five trials for each set of conditions were collected. Each trial lasted approximately 1 minute with COF being averaged across a 5 second period. The shoe material was prepared before each trial to ensure that the surface roughness was consistent throughout the testing process. The shoe material was cleaned, abraded with 240 grit sandpaper and dried between each of the trials.

The analysis of the data was conducted on two levels. Stribeck curves were generated for each of the shoe materials. For these plots, COF was plotted against service parameter, which is defined as viscosity * speed / normal force. In addition, an ANOVA analysis was performed to determine the effects of shoe material, contaminant, normal pressure and sliding speed as well as the first order interactions on COF.

4.2.4 Results

Stribeck curves were successfully generated for each of the two materials. For PU (Figure 4.8), COF values ranged between 0.5 and 0.7 at low service parameter conditions and between 0.2 and 0.3 for high service parameter conditions. In general, there was greater variability at low service parameter conditions with lower pressures were associated with higher coefficient of friction. For PVC (Figure 4.9), COF values ranged between 0.8 and 1.2 for low service parameter conditions and between 0.1 and 0.2 for high service parameter conditions. Once again, COF was more variable at low to mid levels of service parameter with the low normal pressure conditions consistently having larger COF values than high pressure conditions.

The results of the ANOVA analysis indicated that most of the testing conditions affected shoe-floor-contaminant friction. Shoe material ($p<0.01$), contaminant ($p<0.01$), force ($p<0.01$) and speed ($p<0.01$) all had an effect on shoe-floor-contaminant friction. In addition, the interactions between material and fluid ($p<0.05$); material and force ($p<0.05$); material and speed ($p<0.01$); fluid and speed ($p<0.01$); and force and speed ($p<0.01$) all were determined to significantly contribute to shoe-floor-contaminant friction.

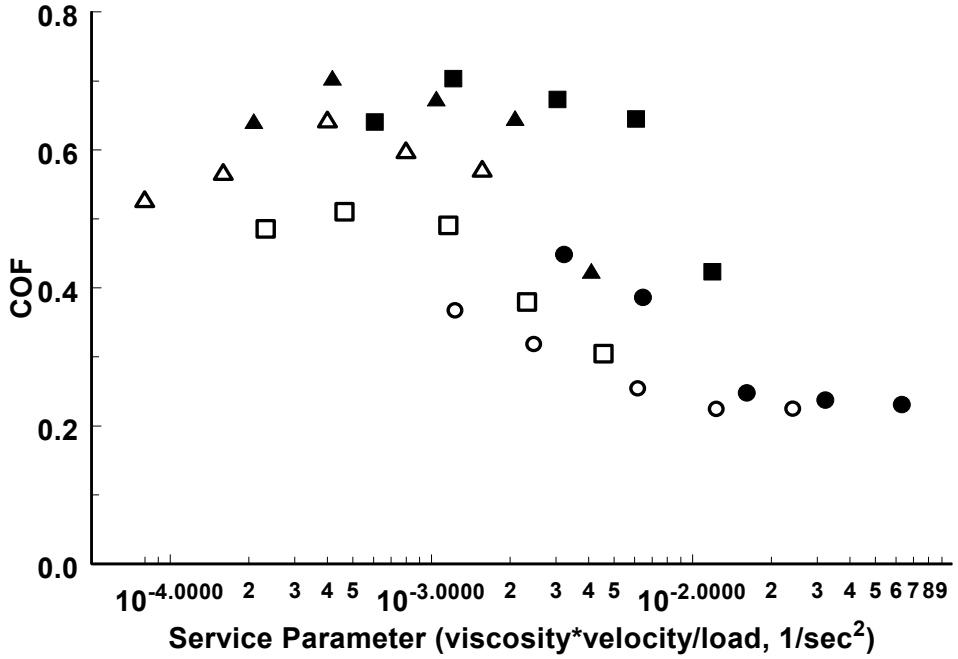

Figure 4.8. Stribeck curve for polyurethane. Low and high pressures represented as solid and hollow symbols. High, medium and slow speeds are circles, squares and triangles, respectively.

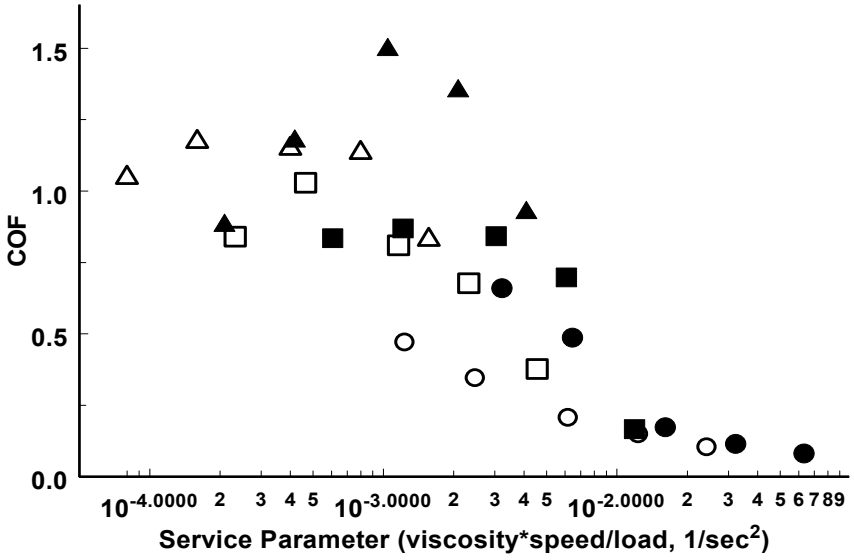

Figure 4.9. Stribeck curve for polyvinyl chloride Low and high pressures represented as solid and hollow symbols. High, medium and slow speeds are circles, squares and triangles.

4.2.5 Discussion and Conclusions

The testing conditions were shown to affect shoe-floor-contaminant friction consistent with the Stribeck effect. Greater variability was seen at lower service parameter values, indicating that the friction is dominated by the asperity interaction between the materials. This COF value for these interacting asperities may vary according to normal pressure and sliding speed. COF values were more consistent at high service parameter values indicating that shoe-floor-contaminant friction may be dominated by hydrodynamic effects in this region. The results of the ANOVA analysis indicate that all testing parameters (shoe material, fluid, normal force and sliding speed) have an effect on COF friction. Another interesting finding is that the COF values of the PVC are higher than the PU at low service parameter values while the COF values of the PU was higher than the PVC at high service parameter values. This highlights the importance of understanding how COF varies across a range of conditions rather than evaluating shoe-floor-contaminant friction under a single set of testing conditions.

4.3 SUMMARY

These experimental studies resulted in the conclusion that shoe-floor-contaminant friction is dependent on the testing parameters in a way that is consistent with the Stribeck effect. The lubrication regime that is most relevant to slip and fall accidents is mixed-lubrication because this represents the transition between safe high friction conditions and dangerous low friction conditions. The Stribeck effect that was observed in experiments with a whole shoe against floor surfaces was reproduced for a pin-on-disk setup. Therefore, the next chapter will focus on generating a mixed-lubrication model applied to the pin-on-disk setup.

5.0 SHOE-FLOOR FRICTION MICRO-MODEL

This chapter describes the primary efforts in this dissertation to model lubrication of the shoe-floor-contaminant interface applied to a pin-on-disk apparatus. For this first-generation shoe-floor-contaminant friction model, the pin-on-disk apparatus is used so that the model can be developed under quasi-static conditions without the complexities of complex tread patterns or transient loading pattern. In the first section, a model is introduced which simulates hydrodynamic and contact pressures across the shoe (pin) surface. The shoe-floor-contaminant friction model yields output that shows good agreement with experimental data. The second section in this chapter is the derivation of polar Reynolds equation using the assumptions that are relevant to the pin-on-disk apparatus. Typically, the polar form of Reynolds equation makes the unstated assumptions that radial and tangential entrainment velocities, the velocities of the surfaces that are separated by the fluid, are independent of the radial and angular coordinates, respectively. These assumptions in the typically stated form of polar Reynolds equation are shown to generate large differences with the derived form of polar Reynolds equation. Thus, this work, which was published as a technical note [115], is critical to the hydrodynamic modeling of shoe-floor-contaminant friction. This chapter provides preliminary modeling efforts of shoe-floor-contaminant friction. Because the lubrication effects of pin-on-disk are similar to those experienced by whole shoes against floor surfaces as described in Chapter 4, the model generated in this chapter provides a framework upon which future models for an entire shoe against a floor surface can be created.

5.1 MODELING MIXED-LUBRICATION OF A SHOE-FLOOR INTERFACE APPLIED TO A PIN-ON-DISK APPARATUS

5.1.1 Abstract

While slip and fall accidents are a serious health concern, few attempts have been made to tribologically model the shoe-floor-contaminant interface. To this end, modeling techniques are introduced here for shoe and floor materials operating in mixed lubrication. The proposed analytical model results are compared with experimental data in order to assess the validity of the developed model. Coefficient of friction (COF) values are generated using a pin-on-disk apparatus across a range of sliding speeds with two different shoe materials operating in the mixed-lubrication regime. The model solves for the contact condition using Hertzian contact mechanics theory and the hydrodynamic pressure condition using the Reynolds equation. The amount of contact deformation is adjusted iteratively such that the summed force from the fluid and contacting asperities is equivalent to the total normal force. The model predicts friction values based on the proportion of the load supported by the fluid versus the proportion of the load supported by contacting asperities. The model-generated COF-velocity plots showed close agreement with experimental values for both shoe materials studied. In addition, the model predicts that as the speed between the surfaces increases, hydrodynamic lift increases. This in turn decreases the contact area and the load borne by the contacting surfaces. Hence, the model presented serves as an initial step towards developing shoe-floor-contaminant models.

5.1.2 Introduction

Slip and fall accidents are a serious health concern that create an economic burden on society and cause injuries resulting in a reduced quality of life or even death. The annual direct costs of fall accidents are estimated to be around US$6 billion [11]. In 2006, fall accidents accounted for 16% of non-fatal injuries requiring days away from work and 14% of fatal injuries [116, 117]. Slipperiness contributes to an estimated 40-50% of falls [11].

In response to the severity of the slip and fall issue, numerous studies have been conducted to improve understanding of slip and fall accidents. A special symposium, held in

2001, which included members from our research group provides a review of literature of slip and fall accidents as of that time [118]. Several research groups have studied slip and fall accidents from a biomechanical perspective to identify safer walking styles and to quantify the post-slip postural responses that attempt to regain stability [48, 62, 119]. In addition, numerous slip-testing devices have been developed with the goal of quantifying the slipperiness of the shoe-floor-contaminant interface [55]. The contribution of shoe and floor surface features such as roughness and waviness to shoe-floor-contaminant friction has also been a topic of much research [38, 65]. Despite the prevalence of studies that improve understanding of the biomechanics of slip and fall accidents, develop devices to quantify slipperiness, and determine the contribution of shoe and floor topographical features to friction, few efforts have been attempted to model the lubrication of the shoe-floor-contaminant interface.

Slip-testing devices are often used to measure slipperiness of the shoe-floor-contaminant surface in order to identify high risk combinations. The choice of methodology and slip-testing device is a contentious issue as indicated by the large number of devices in existence. An overview of many different slip testing devices is offered by Chang et al. [55]. One caveat in the current methodology is that no protocol has been developed for testing shoe-floor-contaminant friction across a range of conditions and therefore, most measurements are based on coefficient of friction measurements taken using a single normal force, sliding speed and contaminant. However, it is well known that normal force and sliding speed vary throughout a slip event and across different subjects [62]. In addition, friction has been shown to be sensitive to sliding speed and normal force as described by the mixed lubrication regime of the Stribeck curve within limits relevant to walking [57]. Therefore, it is not surprising that coefficient of friction measurements have been found to vary greatly according to the choice of testing parameters. In addition, the available friction during walking may be highly variable throughout a step and between different people. An understanding of the friction mechanisms that dominate the shoe-floor-contaminant interface is needed to develop devices and testing protocols that adequately capture the effect of shoe-floor-contaminant friction relevant to the walking styles of a wide range of people.

A few studies have discussed the lubrication of the shoe-floor-contaminant interface from a theoretical perspective. Chang et al. provides an overview of current lubrication theory applied to shoe-floor-contaminant interface and identifies the Reynolds equation as being critical to

understanding this lubrication effect [82]. Despite this, the Reynolds equation has only been solved for simplified circumstances as academic exercises that bear little relevance to the complexities of a shoe. For example, Strandberg demonstrated the effect of the squeeze-film term using the solution of Reynolds equation for two square parallel plates squeezing fluid under a constant force to show film thickness as a function of viscosity, contact area, normal force and time [119]. Proctor and Coleman used the solution of the Reynolds equation for a slider bearing to demonstrate the effects of viscosity, contact area, sliding speed and normal force on the film thickness [68]. In addition to the efforts to describe role of a lubricant in shoe-floor-contaminant friction, Kim and Nagata have proposed a model for contacting asperities and have demonstrated the effect of wear on coefficient of friction between dry shoe and floor surfaces [120].

The mixed lubrication regime represents the transition from boundary lubrication, where friction is high and a slip is unlikely to full film lubrication where friction is low and a slip is likely. Therefore, modeling this region is of great interest to slips and falls as it represents the transition from a safe to dangerous shoe-floor-contaminant friction values. Mixed lubrication models solve hydrodynamic lubrication and surface contact simultaneously, and subsequently predict hydrodynamic pressure, contact stress and the load borne by the fluid and the contacting asperities. Therefore, the application of these models to the shoe-floor interface may provide tremendous insight into the tribophysics of slips and falls.

The mixed lubrication effect has been studied extensively using both stochastic and deterministic modeling efforts. One example applied to chemical-mechanical polishing (CMP) by Shan et al. determined interfacial fluid pressure between a silicon wafer and a rough polyurethane pad [71]. In this approach, Reynolds equation is solved while implementing the Greenwood and Williamson method to determine film thickness from contact stress, material properties and information about the surface topography [72]. Other studies have performed elastohydrodynamic lubrication (EHL) analyses to determine solid contact pressure and hydrodynamic pressure, applied to roller bearings using both deterministic [75] and stochastic methods [121].

The purpose of this study is to apply physics-based modeling techniques to the mixed lubrication regime of a pin-on-disk setup with shoe and floor materials. Regions of the shoe material to be supported by hydrodynamic fluid pressure and regions to be in contact with the floor are modeled. Model results are validated by pin-on-disk experiments.

5.1.3 Analytical Model

The mixed lubrication model consists of a contact mechanics model and a fluid flow model. The hydrodynamic and contact pressures of the surfaces were modeled separately (see for example [122]). The inputs to the model are the shape of the pin (shoe sample), the roughness of the shoe and floor samples, the normal load, the contaminant viscosity, the shoe material properties and the sliding speed. The model outputs are the amount of the total normal load that is supported by the contacting asperities and the fluid. In addition, the model also outputs the contact and hydrodynamic pressures across the surface. As shown in Figure 5.1, the model is solved iteratively by changing the radius of the contact region, a, until the summed force of the fluid and contact region totals the experimental normal force. Convergence of the model is achieved using a method similar to [123].

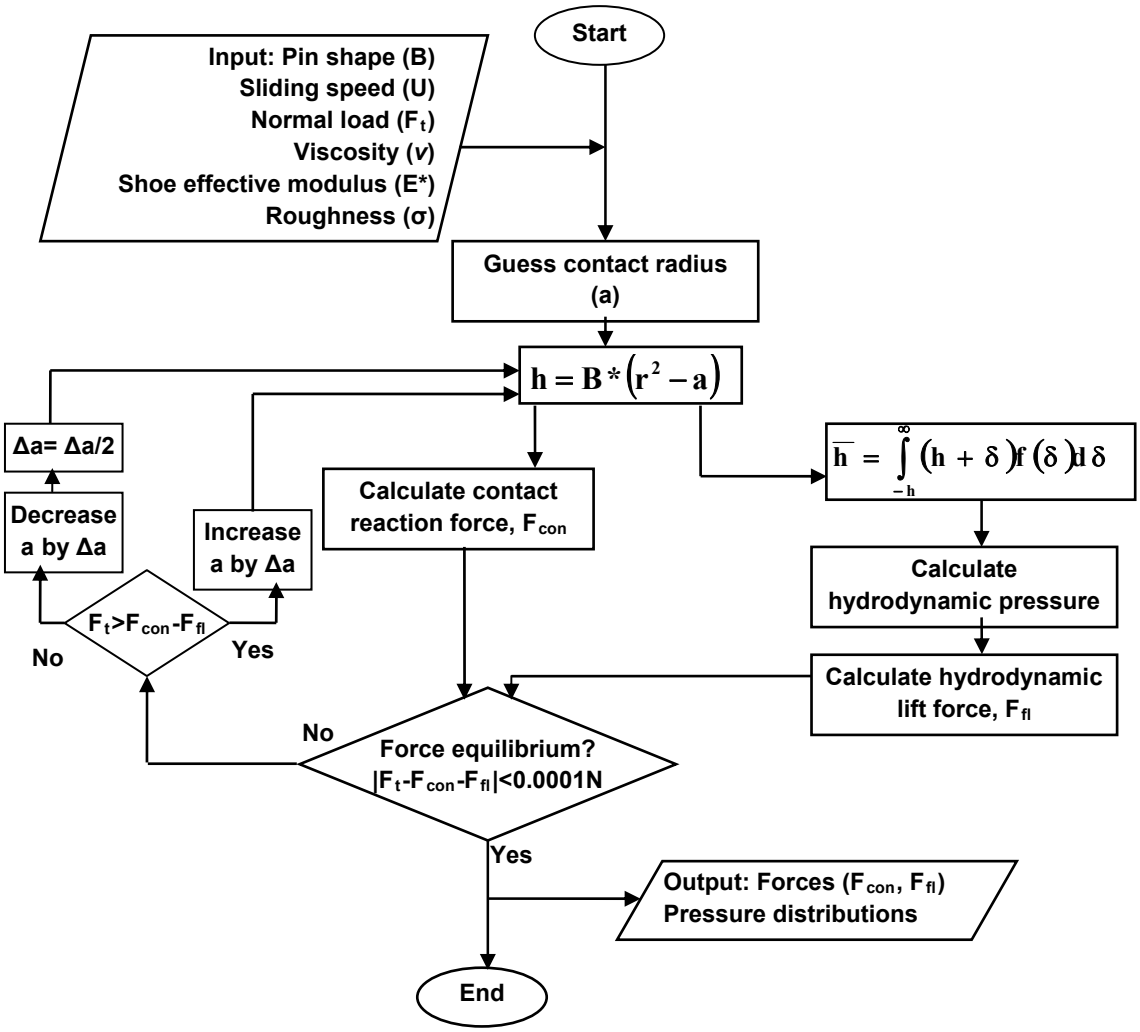

Figure 5.1. Iterative method for determining fluid and contact forces on pin

The shape of the pin (shoe sample) for the model was measured using a contact profilometer (Taylor-Hobson Talysurf 2.0). Initial examination of profiles revealed a quadratic shape across the surface. Therefore, second order polynomials were fit to profiles taken at 4 random orientations (Fig. 5.2). The surface of the pin was modeled with the form of Equation (5.1), where B is the second-order coefficient attained from fitting the polynomials to the profiles and inversely proportional to the radius of curvature.

$$\mathbf{h(r,\theta)=B*r^2} \qquad \text{Eq. (5.1)}$$

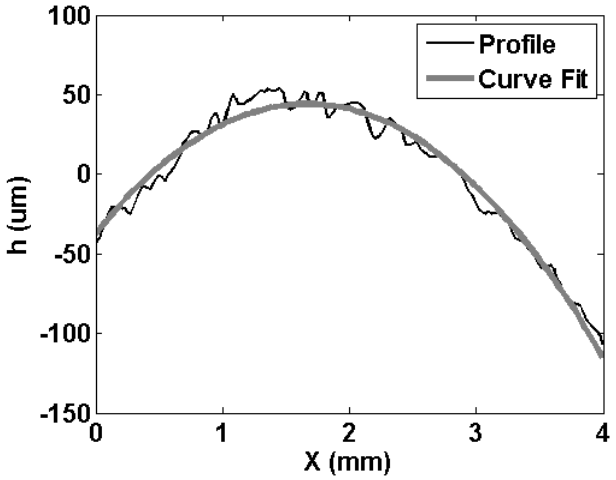

Figure 5.2. Profile of pin surface with polynomial curve fit

5.1.3.1 Contact Modeling

The contact force F_{con} from the pin on to the disk was determined from Hertzian contact mechanics [124] based on a sphere contacting a perfectly flat surface:

$$\mathbf{F_{con} = \frac{4E^* a^3}{3R}} \qquad \text{Eq. (5.2)}$$

where E^* is the effective modulus, a is the radius of the contact region and R is the radius of curvature of the pin. The radius of curvature for the pin was found using the approximation:

$$\mathbf{R} = \frac{\mathbf{1}}{\mathbf{2 * B}} \qquad \text{Eq. (5.3)}$$

5.1.3.2 Hydrodynamic Modeling

The hydrodynamic pressure distribution across the surface was determined by implementing numerical methods to solve Reynolds equation in cylindrical coordinates. Reynolds equation was reduced to Eq. (5.4) using the assumptions [125]: (i) the squeeze term can be ignored because measurements are taken at steady state; (ii) h is a function of r and not θ; (iii) viscosity and density are constant spatially and temporally (fluids are Newtonian); and (iv) both the radial and tangential velocities, v_r and v_θ respectively, are a function of only θ. Given the above assumptions, the Reynolds equation as derived in Section 5.2 becomes [115]:

$$\frac{\partial}{\partial r}\left(r\frac{\bar{h}^3}{12\nu}\frac{\partial p}{\partial r}\right)+\frac{1}{r}\frac{\partial}{\partial \theta}\left(\frac{\bar{h}^3}{12\nu}\frac{\partial p}{\partial \theta}\right)=v_r\frac{\partial}{\partial r}\left(r\frac{\bar{h}}{2}\right)+\frac{\bar{h}}{2}\frac{\partial}{\partial \theta}(v_\theta) \qquad \text{Eq. (5.4)}$$

The relative speed, U, of the disk to the pin was determined for the center of the pin as the product of the angular velocity of the disk, ω, and the distance of the center of the pin from the center of the disk, D (Figure 5.3). The coordinate system was established such that the origin was at the center of the pin and θ=0 was in the direction of the vector pointing from the center of the disk to the center of the pin. The radial and tangential components of the velocity are thus given as:

$$v_r = -U\sin(\theta) \qquad \text{Eq. (5.5a)}$$

$$v_\theta = -U\cos(\theta) \qquad \text{Eq. (5.5b)}$$

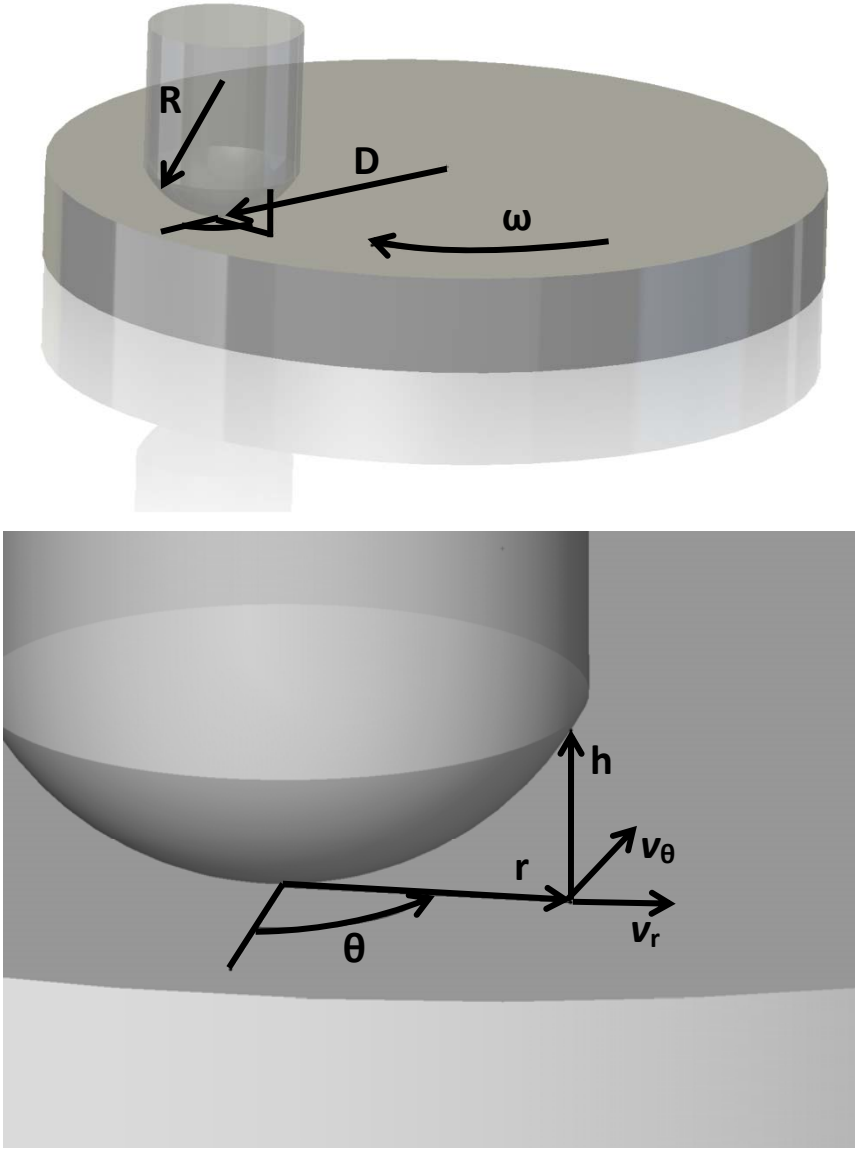

Figure 5.3: Pin-on-disk setup with coordinate system labeled

The film thickness h in the pin/disk interface was determined as the average gap between the smooth floor surface and the rough shoe surface. The nominal film thickness was identified as:

$$h = B * \left(r^2 - a^2\right) \qquad \text{Eq. (5.6)}$$

From the nominal film thickness, the average gap was determined as:

$$\bar{h} = \int_{-h}^{\infty} (h + \delta) f(\delta) d\delta \qquad \text{Eq. (5.7)}$$

The distribution was assumed to be an exponential distribution such that:

$$f(\delta) = \frac{1}{\sigma} \exp\left(\frac{-\delta}{\sigma}\right) \qquad \text{Eq. (5.8)}$$

RMS roughness values were taken from surface profilometry measurements. The RMS roughness of the shoe (σ_{shoe}) was combined with that of the floor (σ_{floor}) to get a composite roughness (σ):

$$\sigma = \sqrt{\sigma_{floor}^2 + \sigma_{shoe}^2} \qquad \text{Eq. (5.9)}$$

For the numerical solution of the Reynolds equation, the film thickness was meshed with a grid of 100 increments in the radial direction and 60 increments in the angular direction (6000 total nodes).

To numerically solve for the hydrodynamic pressures, the difference equation form of Eq. (5.4) can be written as:

$$\left(\bar{h}_{i,j}^3 + 3r_{i,j}\bar{h}_{i,j}^2 \frac{\partial h}{\partial r}_{i,j}\right) \frac{p_{i+1,j} - p_{i-1,j}}{2\Delta r} + r_{i,j}\bar{h}_{i,j}^3 \frac{p_{i+1,j} - 2p_{i,j} + p_{i-1,j}}{\Delta r^2} + \frac{\bar{h}_{i,j}^3}{r_{i,j}} \frac{p_{i,j+1} - 2p_{i,j} + p_{i,j-1}}{\Delta\theta^2} = 6\nu\left(-U * \sin(\theta)\right) r_{i,j} \frac{\partial \bar{h}}{\partial r}_{i,j} \qquad \text{Eq. (5.10)}$$

where (i) represents the radial nodal position and (j) represents the angular nodal position. Equation (5.10) was developed for all internal nodes and the system was solved simultaneously as a linear set of equations. One limitation of the Reynolds equation is that when the film thickness approaches 0, the hydrodynamic pressure approaches infinity. Yet, as the average gap film thickness becomes smaller, more of the asperities become in contact and prevent the ability of the fluid to maintain hydrodynamic pressures. Therefore, when more than 75% of the

asperities were in contact, the Reynolds equation was no longer considered valid. Boundary conditions were established such that:

$$\mathbf{p = 0} \text{ at } \mathbf{r = d/2} \qquad \text{Eq. (5.11a)}$$

$$\mathbf{q_r = -\frac{\bar{h}^3}{12\eta}\frac{\partial p}{\partial r} + \frac{\nu_r}{2}\bar{h} = 0} \text{ at } \mathbf{\bar{h} = \bar{h}_{0.75}} \qquad \text{Eq. (5.11b)}$$

The first boundary condition (5.11a) assumes that the pin experiences ambient pressure at the boundary of the pin. The second boundary condition (5.11b) is established to prevent fluid from entering the contact region, where Reynolds equation is no longer valid. Using the assumption that cavitation occurs (i.e. half-Sommerfeld), fluid is restricted from supporting sub-ambient pressures:

$$\mathbf{p \geq 0} \qquad \text{Eq. (5.12)}$$

5.1.3.3 Friction Model

The overall coefficient of friction was determined as the sum of the fluid and contact friction forces region divided by the total normal force:

$$\mu = \frac{F_{fl(shear)} + F_{con(shear)}}{F_{tot}} \qquad \text{Eq. (5.13a)}$$

The friction force from the fluid region was determined as the force required to shear the fluid:

$$F_{fl} = \int\int_A \tau dxdy = -\int\int_A \eta \frac{\nu_r * \sin\theta + \nu_\theta * \cos\theta}{h} dxdy = \int\int_A \eta \frac{U}{h} dxdy \qquad \text{Eq. (5.13b)}$$

The friction due to the contacting asperities is simply the contact normal force multiplied by the COF for the contacting asperities.

$$F_{con(shear)} = F_{con}\mu_{con} \qquad \text{Eq. (5.13c)}$$

The contact friction coefficient was determined by regressing the model outputs of the contact forces, fluid shear forces and the experimental COF values.

5.1.4 Experimental Testing

For measuring friction between sliding surfaces, a standard pin on disk apparatus (Figure 5.4) was used to collect friction data for two shoe materials in contact with a common floor material. The apparatus allowed friction testing in the presence of a contaminant and across a range of speeds that are similar to those experienced during walking. The model was tested against experimental data for a range of testing conditions using different shoe samples and fluids. Shoe materials were cut directly from shoe heels made of polyurethane (PU) and polyvinyl chloride (PVC). The shoe sample was 6.2mm in diameter and 1.2 mm thick for the PU and 6.6 mm in diameter and 2.0 mm thick for PVC. The vinyl tile floor material sample was 5x5cm and taken from commercially available tile and had a roughness of 4.1μm. Glycerol was used as the lubricating fluid because it is water soluble and can be diluted to different viscosities. The exact concentrations were determined so that the COF decreased across the range of speeds consistent with mixed lubrication. While altering the range of sliding speeds or the applied normal force could have also ensured that mixed-lubrication was being tested, previous experience by this research group have shown that the asperity friction may be dependent on sliding speed and normal force [126]. Therefore, it was determined that changing the fluid viscosity rather than normal force or range of speeds was the best way to maintain comparable conditions across the two conditions. A normal force of 2.5N was applied to the shoe material resulting in a mean normal pressure of 65 kPa. Sliding speeds were recorded at several levels between 10 and 200 mm/sec. The exact operating conditions for each material can be found in Table 5.1. Between each trial, the shoe material was prepared by removing the contaminant and abrading the surface with 240 grit sandpaper to maintain constant roughness. The roughness of the shoe samples as measured with a contact profilometer is provided in Table 5.1. Between each trial, the surface was dried using compressed air. The floor surface was then completely covered with sufficient fluid to simulate a fully flooded condition. Trials were taken for 40 to 60 seconds until steady state friction had been achieved. COF values were averaged over a 5 second period and the mean and standard deviation of 5 trials were taken.

The ability of the model to fit the data was examined by comparing model with experimental data. Initially, the ability of the model to match the general trends of the experimental data was qualitatively assessed. In addition, the average absolute difference and the

root mean square (RMS) difference between the experimental and the model data were calculated across the different speeds that were tested for each of the two shoe materials.

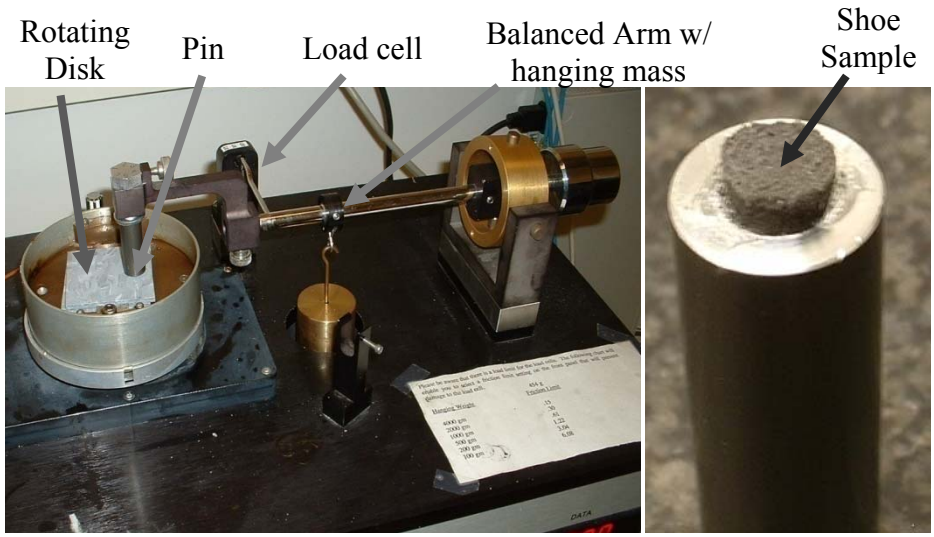

Figure 5.4. Tribometer Device

Table 5.1. Testing Conditions

	Polyurethane	Polyvinyl Chloride
Diameter (mm)	6.6	6.2
Shoe Bulk Modulus (MPa)	2.0	5.2
Roughness (μm)	14.4	4.1
Curvature Parameter, B (mm^{-1})	0.019	0.011
Fluid Contaminant (viscosity)	50% glycerol/50% water (7.2 mPa-s)	60% glycerol/40% water (10.7 mPa-s)

5.1.5 Results

5.1.5.1 Experimental Results

The experimental COF values were found to decrease with increasing speed, which is consistent with the mixed-lubrication regime predicted by the Stribeck curve (Figure 5.5). For both materials, the figures show that the mean values were approximately the same at the lowest speeds and then began non-linearly decreasing with increasing speed. Since the COF appears to be inversely proportional to speed even at the highest sliding speeds it is clear that full film lubrication was not reached for either material and the system was operating in the mixed lubrication regime.

5.1.5.2 Analytical Model Results

As illustrated in Figure 5.5, the mixed lubrication model results demonstrate strong agreement with the experimental data. In fact, the non-linear decrease in COF found in the experimental results is nearly replicated by the model. The average absolute value of the difference between the model and the experimental data for the PU material was 0.024 and the RMS difference was found to be 0.028. The average absolute value of the difference between the model and the experimental data for the PVC material was slightly higher at 0.048 and the RMS difference was 0.051. The friction values for the contacting shoe-floor asperities were reasonable at levels of 0.60 for PU and 0.83 for PVC. The reduction in μ is primarily due to load support transferred from the shoe sample to the fluid. Overall, as shown in Figure 5.5, the model fits experimental data better at higher speeds than lower speeds.

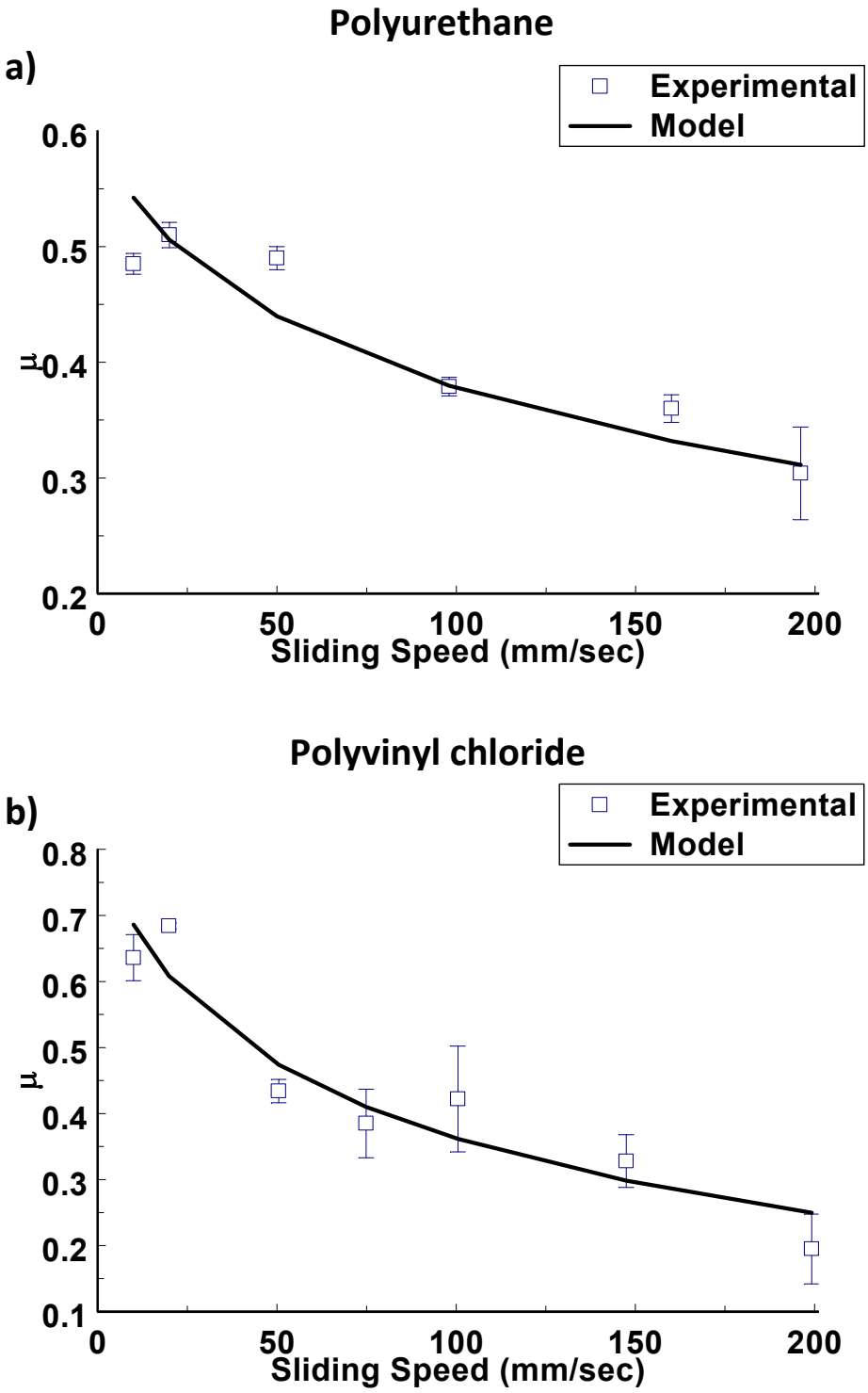

Figure 5.5. Model COF plotted against experimental COF values for PU (a) and PVC (b)

Hydrodynamic pressure profiles across the surface of the pin predicted by the model all have a similar shape for the simulated velocities and thus Figure 5.6 is representative. As predicted by the Reynolds equation, the hydrodynamic pressure reaches a maximum just outside the contact region and then decreases as the radius increases. The contact stress is localized at the center of the pin due to higher deformation in this region consistent with Hertzian contact (Figure 5.6b). As predicted by the Stribeck effect, the percentage of the apparent area actually in contact with the disk surface decreases with increasing sliding speed (Figure 5.7).

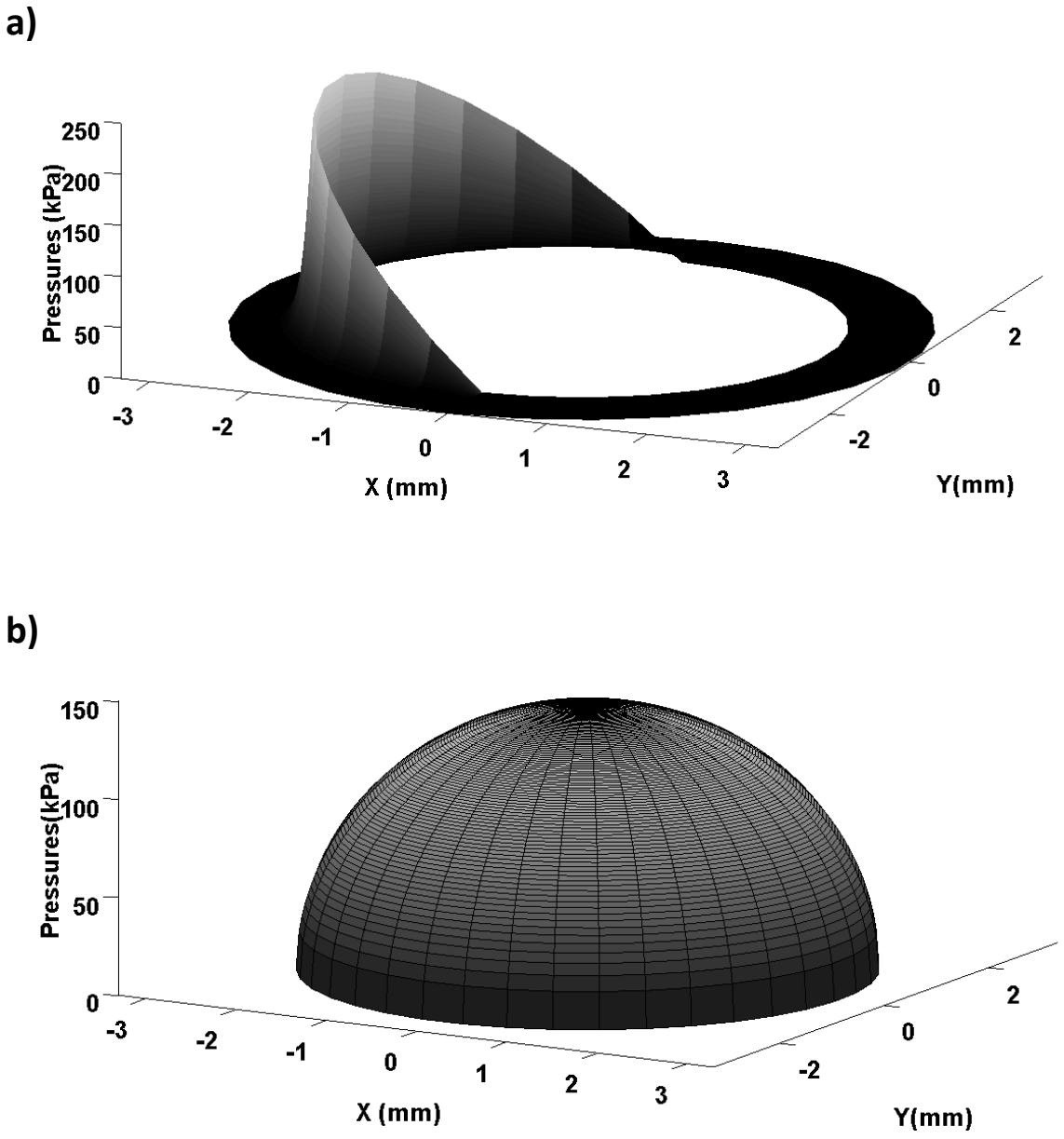

Figure 5.6. Representative hydrodynamic (a) and contact pressures (b) across the pin surface as predicted by Reynolds equation and Hertzian contact mechanics. The motion of the disk relative to the pin is in the +X direction.

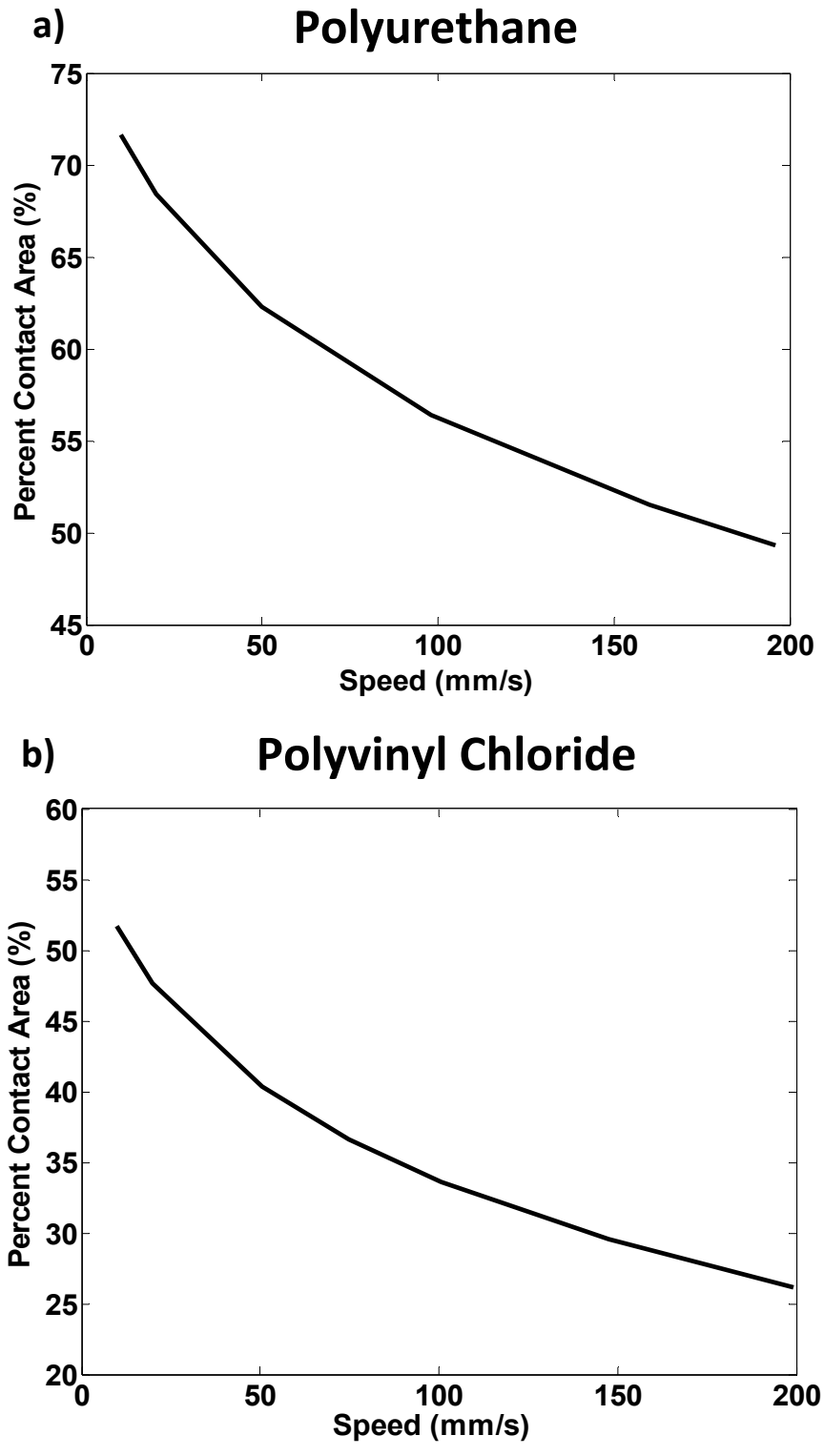

Figure 5.7. Model estimates for percent contact area plotted across speed for PU (a) and PVC (b)

5.1.6 Discussion

Examining the analytical results, the model was found to provide realistic results under the conditions examined where most of the primary inputs were measurable. The model predicted the shoe material to be in mixed lubrication and the shape of the COF-velocity curve matched up well with experimental data. In addition, the model predicts the transfer of load from the shoe material to fluid with increasing sliding speed.

The agreement between model and experimental data for both of the different shoe materials demonstrates that the model may effectively captured the effects of roughness, elastic modulus and geometric differences of shoe tread. The PVC material had a higher dry COF, a larger bulk modulus, had less curvature, and was slightly smoother than the PU material. As a result of these differences, the PVC had a much more severe COF drop-off than the PU material. This strengthens the argument that evaluating shoe-floor friction cannot be performed under a single testing condition. For example, if tests were conducted at low sliding speeds, the PVC material would have a much higher COF than the PU material. At higher speeds, however, the PU has a larger COF than the PVC material. This finding demonstrates the potential for computational modeling to be used as a tool to predict how friction changes across a range of walking parameters without extensive experiments.

Other advantages offered by the modeling technique presented herein are the ability to capture complex geometrical effects and widely vary lubrication and loading conditions. An advantage of using numerical methods is that complex geometries can be considered specific to environmental conditions (i.e. shoe geometry, surface characteristics, material properties and fluid viscosity) and to biomechanical conditions (i.e. normal force and sliding speed). Furthermore, the developed analytical model can be used to perform parametric analyses in order to isolate variables (normal force, roughness, elastic modulus) to which friction is most sensitive. The developed computational model allows for a user to quickly calculate friction coefficients across many different conditions, which may give a range of COF values that are more relevant to the variability encountered during gait. The model shows best agreement with experimental data when hydrodynamic forces are large, which is particularly encouraging because the transition between low and high probability of slipping tends to occur at COF values between 0.15 and 0.30 [18, 19].

In order to prevent hydrodynamic pressures from approaching excessive levels as the average gap film thickness approached 0, a limit was imposed such that Reynolds equation was not evaluated when more than a certain percentage of the asperities were in contact. For the conditions considered in this manuscript, the threshold for solid/fluid boundary was when 75% of asperities were in contact. While the same threshold appears to produce good replication between the model and experimental data for the two shoe samples evaluated here, it is possible that this may not universally be the case. Other studies have instead selected the threshold for this boundary to be tied directly to the film thickness instead of to the roughness profiles [74, 75]. One potential reason for this difference is that other models often superimpose roughness on the surface and apply deterministic modeling. These models, therefore, are already taking roughness into consideration. Because the roughness profile is modeled stochastically in this study, it is reasonable to use real to apparent contact area (i.e. percent of asperities in contact) to determine the threshold for which Reynolds equation is valid.

While the model was able to reproduce experimental results under two different sets of testing conditions, improvements to the model may make the model more physically accurate. Currently, deformation due to hydrodynamic pressure is not considered. It is likely that significant deformation may occur near the fluid/solid boundary where the hydrodynamic pressures were at their highest levels. Future versions of this model will be improved by including deformation from fluid pressure into the film thickness equations and thus adding an EHL component to the analysis. In addition, the effect of roughness on shoe-floor-contaminant friction has previously been shown to be a complex one. The use of roughness merely in the gap equation and to determine the fluid/solid boundary may not completely capture the effect of surface roughness. Floor roughness has been determined to be critical to the shoe-floor-contaminant friction [35, 38], therefore, future models may need to include flow factors as developed by Patir and Cheng into the Reynolds equation [73]. In addition, the friction coefficient for the contacting asperities was considered to be constant across all testing conditions for each of the shoe materials. Previous research by this group has implied that asperity (i.e. dry) friction may vary with normal pressure and sliding speed [126]. While the modeling technique presented in this manuscript showed good agreement with the experimental data, certain improvements, particularly EHL, may make the model more physically representative of the shoe-floor-contaminant interface.

5.1.7 Conclusions

The model presented here represents a first step towards the development of a computational model of shoe-floor-contaminant friction. While challenges remain to modeling an entire shoe under conditions relevant to walking, this model offers a framework towards achieving that goal.

Certain challenges still exist before the developed model can be used as an evaluative or design tool for shoe and floor surfaces. The primary improvement of the model to achieve this goal is including features of the heel of a shoe including the shape of the contact area and tread. Other important improvements to the model would be to add an EHL component and time-dependency (i.e. squeeze film effect) to the Reynolds equation. Because of the rapidly changing conditions during gait, the squeeze-film effect has been identified as a critical phenomenon to capture for slip-testing devices [55]. A shoe-floor-contaminant friction model based on the framework of this manuscript coupled with these improvements would be a valuable tool in the design and evaluation of shoe and floor surfaces as well as an improved understanding of shoe-floor-contaminant interface.

5.2 SOLUTION OF REYNOLDS EQUATION IN POLAR COORDINATES APPLICABLE TO NON-SYMMETRIC ENTRAINMENT VELOCITIES

5.2.1 Abstract

Reynolds equation in polar cylindrical (polar) coordinates is used for numerous tribological applications that feature thin fluid films in sliding contacts, such as chemical mechanical polishing (CMP) and pin-on-disk testing. Although unstated, tribology textbooks and literary resources that present Reynolds equation in polar coordinates often make assumptions that the radial and tangential entrainment velocities are independent of the radial and tangential directions, respectively. The form of polar Reynolds equation is thus typically presented while neglecting additional terms crucial to obtaining accurate solutions when these assumptions are not met. In the present investigation, the polar Reynolds equation is derived from the cylindrical

Navier-Stokes equations without the aforementioned assumptions and the resulting form is compared with results obtained from more traditionally used forms of the polar Reynolds equation. The polar form of Reynolds equation derived in this manuscript shows results that agree with the commonly used Cartesian form of Reynolds equation but are drastically different from the typically published form of the polar Reynolds equation. It is therefore suggested that the polar form of Reynolds equation proposed in this technical note be utilized when entrainment velocities are known to vary with either radial or angular position.

5.2.2 Introduction

The Reynolds equation, which is derived from the Navier-Stokes equations using thin-film assumptions, is commonly used in tribological applications. The Reynolds equation in polar cylindrical (or polar) form can be easily found in multiple textbooks; few if any of these sources, however, derive the polar Reynolds equation directly from the cylindrical Navier-Stokes equation [127-129]. The polar Reynolds equation is often derived from the Cartesian form without a thorough analysis of how changing coordinate systems might affect the assumptions made during the original derivation. One such assumption typically made in deriving the Cartesian form of Reynolds equation is that the entrainment velocities cannot vary across the surfaces because "this means a rubber-like stretching of the bearing material" [129]. While this may be typically true in Cartesian coordinates, entrainment velocities in polar form may vary across the radial and angular directions without any such stretching. A consequence of improperly transferring this assumption to the polar form of Reynolds equation is that different results may be obtained when solving the same problem with the Cartesian and polar forms of Reynolds equation. In this brief article, the Reynolds equation from the polar Navier-Stokes equations is derived, without making assumptions about the entrainment velocities. Case studies related to pin-on-disk and chemical mechanical polishing (CMP) are presented to emphasize the impact of using a form of Reynolds equation that is based on improper assumptions.

5.2.3 Methodology

Reynolds equation is derived from the Navier-Stokes equations by combining its continuity and momentum equations. The continuity and momentum equations in cylindrical form assuming constant density (ρ) and viscosity (η) are [128]:

$$\frac{1}{r}\frac{\partial}{\partial r}\left(r v_r\right) + \frac{1}{r}\frac{\partial}{\partial \theta}\left(v_\theta\right) + \frac{\partial}{\partial z}\left(v_z\right) = 0 \qquad \text{Eq. (5.14)}$$

r-momentum

$$0 = \rho\left(\frac{\partial v_r}{\partial t} + v_r\frac{\partial v_r}{\partial r} + \frac{v_\theta}{r}\frac{\partial v_r}{\partial \theta} + v_z\frac{\partial v_r}{\partial z} + \frac{v_\theta^2}{r}\right) + \frac{\partial p}{\partial r} - \eta\left(\nabla^2 v_r - \frac{v_r}{r^2} - \frac{2}{r^2}\frac{\partial v_\theta}{\partial \theta}\right) \qquad \text{Eq. (5.15)}$$

θ-momentum

$$0 = \rho\left(\frac{\partial v_\theta}{\partial t} + v_r\frac{\partial v_\theta}{\partial r} + \frac{v_\theta}{r}\frac{\partial v_\theta}{\partial \theta} + v_z\frac{\partial v_\theta}{\partial z} + \frac{v_r v_\theta}{r}\right) + \frac{1}{r}\frac{\partial p}{\partial \theta} - \eta\left(\nabla^2 v_\theta - \frac{v_\theta}{r^2} + \frac{2}{r^2}\frac{\partial v_r}{\partial \theta}\right) \qquad \text{Eq. (5.16)}$$

z-momentum

$$0 = \rho\left(\frac{\partial v_z}{\partial t} + v_r\frac{\partial v_z}{\partial r} + \frac{v_\theta}{r}\frac{\partial v_z}{\partial \theta} + v_z\frac{\partial v_z}{\partial z}\right) + \frac{\partial p}{\partial z} - \eta\left(\nabla^2 v_z\right) \qquad \text{Eq. (5.17)}$$

$$\nabla^2 = \frac{\partial^2}{\partial r^2} + \frac{1}{r}\frac{\partial}{\partial r} + \frac{1}{r^2}\frac{\partial}{\partial \theta^2} + \frac{\partial}{\partial \theta^2} \qquad \text{Eq. (5.18)}$$

Reynolds equation can be obtained through the solution of the continuity equation and the momentum equations. As deduced by Meyer [125], the following assumptions can be made:

1. No property variation across the film (constant density)
2. Viscous forces are much larger than inertia forces and body forces can be ignored.
3. The thin film assumption is adopted such that velocity gradients are much larger across the film in the z-dimension than the r and θ dimensions. In addition, velocity flow in the z-direction is negligible.

4. The fluid is Newtonian.

5. The system is in steady state ($\partial/\partial t=0$)

After multiplying both sides of Eq. (5.14) by r*dz and integrating from 0 to h, the continuity equation becomes:

$$\int_0^h \frac{\partial}{\partial r}(r v_r)dz + \int_0^h \frac{\partial}{\partial \theta}(v_\theta)dz = 0 \qquad \text{Eq. (5.19)}$$

Using the stated assumptions and the Leibniz integration rule:

$$\int_0^h \frac{\partial}{\partial x}[f(x,y,z)dz = -f(x,y,h)\frac{\partial h}{\partial x} + \frac{\partial}{\partial x}\left[\int_0^h f(x,y,z)dz\right] \qquad \text{Eq. (5.20)}$$

Equation (5.15) can be rewritten as:

$$-(r v_r)_{z=h}\frac{\partial h}{\partial r} + \frac{\partial}{\partial r}\int_0^h (r v_r)dz - (v_\theta)_{z=h}\frac{\partial h}{\partial \theta} + \frac{\partial}{\partial \theta}\int_0^h (v_\theta)dz = 0 \qquad \text{Eq. (5.21a)}$$

And by grouping the integral terms on one side of the equation, we obtain Equation (5.21b).

$$\frac{\partial}{\partial r}\int_0^h (r v_r)dz + \frac{\partial}{\partial \theta}\int_0^h (v_\theta)dz = (r v_r)_{z=h}\frac{\partial h}{\partial r} + (v_\theta)_{z=h}\frac{\partial h}{\partial \theta} \qquad \text{Eq. (5.21b)}$$

Because of no-slip criteria, the velocity at z=0 is the velocity of the bottom surface (a) and the velocity at z=h is the velocity of the top surface (b). Applying the stated assumptions to Equations. (5.15) and (5.16) yields the following relationships:

$$\frac{\partial p}{\partial r} = \eta\frac{\partial}{\partial z}\left(\frac{\partial v_r}{\partial z}\right) \qquad \text{Eq. (5.22a)}$$

$$\frac{1}{r}\frac{\partial p}{\partial \theta} = \eta\frac{\partial}{\partial z}\left(\frac{\partial v_\theta}{\partial z}\right) \qquad \text{Eq. (5.22b)}$$

Equations (5.22a) and (5.22b) can be solved to determine the fluid velocity profile in the r and θ directions as:

$$v_r = -z\frac{h-z}{2\eta}\frac{\partial p}{\partial r} + v_{r(a)}\frac{h-z}{h} + v_{r(b)}\frac{z}{h} \qquad \text{Eq. (5.23a)}$$

$$v_\theta = -z\frac{h-z}{2\eta r}\frac{\partial p}{\partial \theta} + v_{\theta(a)}\frac{h-z}{h} + v_{\theta(b)}\frac{z}{h} \qquad \text{Eq. (5.23b)}$$

where $\nu_{r(a)}$ and $\nu_{r(b)}$ are the radial velocities of the bottom and top surfaces, respectively and $\nu_{\theta(a)}$ and $\nu_{\theta(b)}$ are the tangential velocities of the bottom and top surfaces, respectively. Equation (5.23) is now integrated across z from 0 to h to obtain:

$$\int_0^h \nu_r dz = -\frac{h^3}{12\eta}\frac{\partial p}{\partial r} + \frac{\nu_{r(a)} + \nu_{r(b)}}{2} h \qquad \text{Eq. (5.24a)}$$

$$\int_0^h \nu_\theta dz = -\frac{h^3}{12\eta r}\frac{\partial p}{\partial \theta} + \frac{\nu_{\theta(a)} + \nu_{\theta(b)}}{2} h \qquad \text{Eq. (5.24b)}$$

Equation (5.24) can then be substituted back into Equation (5.21) to get the general form of Reynolds equation in Polar Coordinates:

$$\frac{1}{12\eta}\frac{\partial}{\partial r}\left(-h^3\frac{\partial p}{\partial r}\right) + \frac{\partial}{\partial r}\left(\frac{\nu_{r(a)} + \nu_{r(b)}}{2}\right) + \frac{1}{12\eta r}\frac{\partial}{\partial \theta}\left(-h^3\frac{\partial p}{\partial \theta}\right) + \frac{\partial}{\partial \theta}\left(\frac{\nu_{\theta(a)} + \nu_{\theta(b)}}{2}\right) = (r\upsilon_r)_{z=h}\frac{\partial h}{\partial r} + (\upsilon_\theta)_{z=h}\frac{\partial h}{\partial \theta} \qquad \text{Eq. (5.25a)}$$

The terms of Equation (5.25a) can be rearranged to obtain Reynolds equation in its typical form:

$$\frac{1}{12\eta}\frac{\partial}{\partial r}\left[rh^3\frac{\partial p}{\partial r}\right] + \frac{1}{12\eta r}\frac{\partial}{\partial \theta}\left(h^3\frac{\partial p}{\partial \theta}\right) = -\nu_{r(b)} r\frac{\partial h}{\partial r} - \nu_{\theta(b)}\frac{\partial h}{\partial \theta} + + \frac{\partial}{\partial r}\left(\frac{\nu_{r(a)} + \nu_{r(b)}}{2} rh\right) + \frac{\partial}{\partial \theta}\left(\frac{\nu_{\theta(a)} + \nu_{\theta(b)}}{2} h\right) \qquad \text{Eq. (5.25b)}$$

Equation (5.25b) can also be written in dimensionless form as:

$$\frac{\partial}{\partial r^*}\left[r^* H^3\frac{\partial p^*}{\partial r^*}\right] + \frac{1}{r^*}\frac{\partial}{\partial \theta}\left(H^3\frac{\partial p^*}{\partial \theta}\right) = \lambda\left[-2\bar{\nu}_{r(b)} r^*\frac{\partial H}{\partial r^*} - 2\bar{\nu}_{\theta(b)}\frac{\partial H}{\partial \theta} + + \frac{\partial}{\partial r^*}\left[\left(\bar{\nu}_{r(a)} + \bar{\nu}_{r(b)}\right) r^* H\right] + \frac{\partial}{\partial \theta}\left[\left(\bar{\nu}_{\theta(a)} + \bar{\nu}_{\theta(b)}\right) H\right]\right] \qquad \text{Eq. (5.25c)}$$

Such that the following dimensionless terms are defined as:

$$r^* = \frac{r}{R};\ H = \frac{h}{h_m};\ p^* = \frac{p}{p_{atm}};\ \bar{\nu}_r = \frac{\nu_{r(a)}}{V};\ \bar{\nu}_\theta = \frac{\nu_{\theta(a)}}{V};\ \lambda = \frac{6\eta RV}{h_m^2 p_{atm}} \qquad \text{Eq. (5.25d)}$$

In Equation (5.25d), R represents the maximum radius and is the equivalent of a characteristic length; h_m is either the minimum or mean fluid thickness; V is the characteristic velocity; and p_{atm} is atmospheric pressure. It is important to note that the velocity terms inside the derivatives of Equation (5.25a-c) can only be pulled out under the circumstance that ν_r is independent of r and that ν_θ is independent of θ. As a main theme of this work, this rule is shown to be critical in

the next section with respect to a simulation relevant to CMP and pin-on-disk processes. Case studies are presented in this work to compare the results from the general form of polar Reynolds equation (5.25) to the form of Reynolds equation typically provided in tribology textbooks, Equation (5.26) [127, 128]:

$$\frac{\partial}{\partial r}\left[r\frac{h^3}{12\eta}\frac{\partial p}{\partial r}\right]+\frac{1}{r}\frac{\partial}{\partial \theta}\left(\frac{h^3}{12\eta}\frac{\partial p}{\partial \theta}\right)= \frac{v_{r(a)}+v_{r(b)}}{2}\frac{\partial}{\partial r}(rh)+\frac{v_{\theta(a)}+v_{\theta(b)}}{2}\frac{\partial h}{\partial \theta} \quad \text{Eq. (5.26a)}$$

Equation (5.26a) can be written in dimensionless form similar to Equation (5.25c):

$$\frac{\partial}{\partial r^*}\left[r^* H^3\frac{\partial p^*}{\partial r^*}\right]+\frac{1}{r^*}\frac{\partial}{\partial \theta}\left(H^3\frac{\partial p^*}{\partial \theta}\right)= \lambda\left[\left(\bar{v}_{r(a)}+\bar{v}_{r(b)}\right)\frac{\partial}{\partial r^*}\left(r^* h\right)+\left(\bar{v}_{\theta(a)}+\bar{v}_{\theta(b)}\right)\frac{\partial H}{\partial \theta}\right] \quad \text{Eq. (5.26b)}$$

5.2.4 Case Study I: Pin-on-Disk

In this section, the hydrodynamic lift from a pin-on-disk in full film lubrication is modeled using Reynolds equation. In a pin-on-disk setup, the pin is placed away from the center of the disk such that the pin slides across the surface of the disk with an approximately linear velocity (Fig. 5.8). When considering the perspective of the pin, the tangential velocity (v_θ) is not independent of the angle since the pin is eccentrically displaced from the center of the disk. Therefore the problem will be solved with the appropriate set of assumptions and Equation (5.25). In addition, the problem will also be solved using the more traditional form of polar Reynolds equation (5.26) to describe the difference in results between the two equations. For the sake of this simulation, we assume that the pin is sufficiently far away from the center of the disk such that the velocity fields for the pin surface are defined as:

$$v_{r(a)} = -U\sin(\theta) \quad \text{Eq. (5.27a)}$$

$$v_{\theta(a)} = -U\cos(\theta) \qquad \text{Eq. (5.27b)}$$

The velocity of the pin surface (b) is assumed to be zero and the disk surface is assumed to be moving. The simulation is done where the film thickness is defined by the geometry of the pin and the minimum film thickness as:

$$h(r) = B * r^2 + h_0 \qquad \text{Eq. (5.28)}$$

where B is a constant representing the curvature of the pin and h_0 is the minimum film thickness. It is important to note that only the leading half of the pin is modeled due to the half-Sommerfeld assumption that the fluid cannot support a negative pressure region. All of the parameters used for this simulation are listed in Table 5.2. The non-dimensional form of Reynolds equations (5.25c) are used by normalizing the radius term by the radius of the pin, R; the film thickness by the minimum film thickness, h_0; pressure by atmospheric pressure, p_{atm}; and velocity terms by the average sliding speed, U.

Table 5.2. Simulation parameters for pin-on-disk

Radius (mm)	Curvature, B (mm^{-1})	h_0 (mm)	Viscosity, η (cP)	Sliding speed, U ($mm*s^{-1}$)
3.3	0.011	0.02	10.7	50

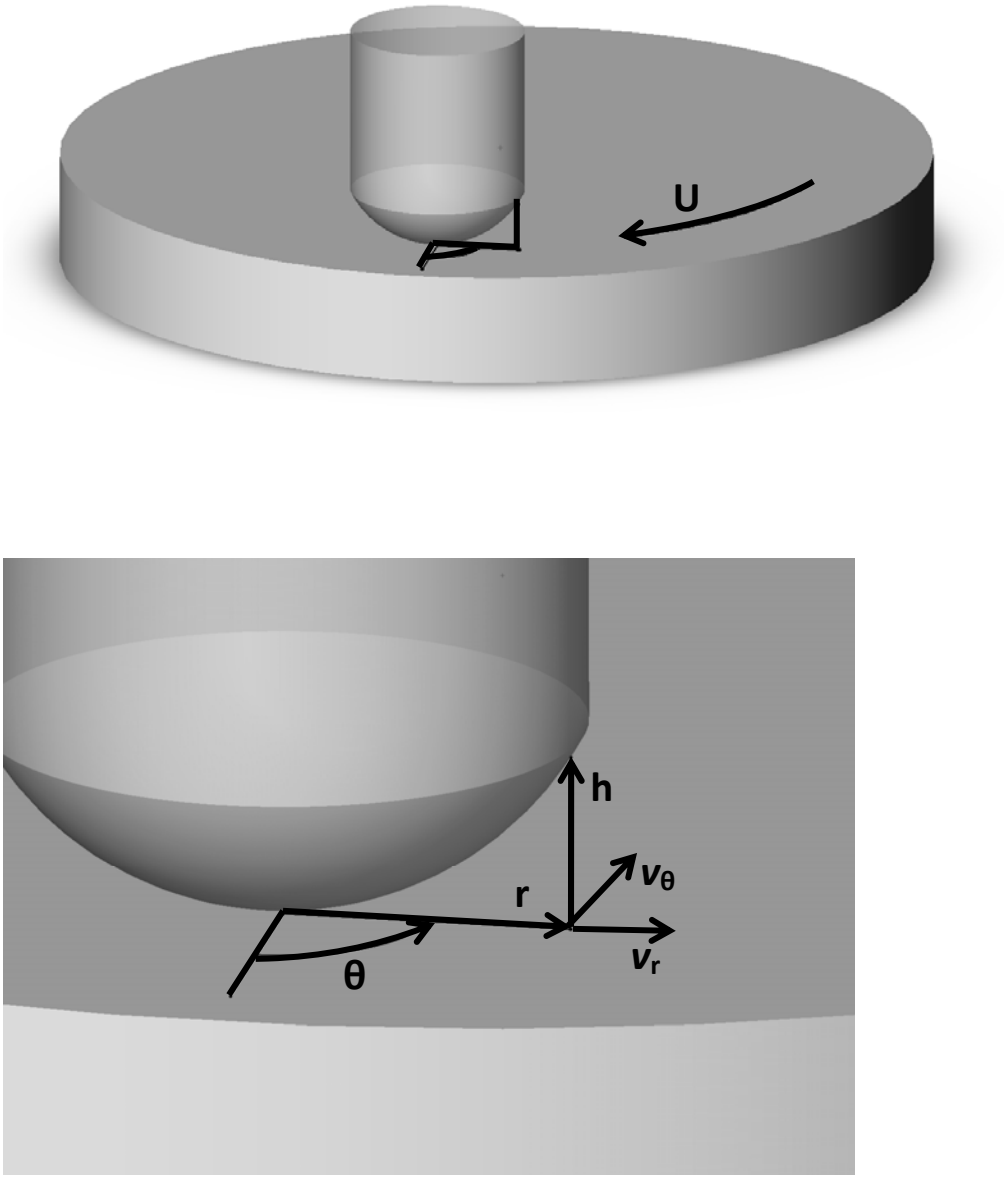

Figure 5.8. Diagram of pin-on-disk with the polar coordinate system labeled

As a point of reference, the problem is first solved in Cartesian coordinates to verify the consistency of the results. In Cartesian coordinates, the velocity profiles become:

$$\nu_{x(a)} = U \qquad \text{Eq. (5.29a)}$$

$$\nu_{y(a)} = 0 \qquad \text{Eq. (5.29b)}$$

Once again, the velocity profile of surface (b) is assumed to be 0. The film thickness similarly becomes:

$$h(x,y) = B * \left(x^2 + y^2\right) + h_0 \qquad \text{Eq. (5.30)}$$

The Reynolds equation in Cartesian form using the previously listed assumptions and information about the velocity profiles becomes:

$$\frac{\partial}{\partial x^*}\left(H^3 \frac{\partial p^*}{\partial x^*}\right) + \frac{\partial}{\partial y^*}\left(H^3 \frac{\partial p^*}{\partial y^*}\right) = \frac{6\eta RU}{h_0^2 p_{atm}} \frac{\partial H}{\partial x^*} \qquad \text{Eq. (5.31)}$$

Upon solving the problem posed, substantial differences are found when using the traditional version of polar Reynolds equation versus the form that does not make assumptions that the tangential velocity is independent of angle. The results from the non-traditional form of polar Reynolds equation (5.25) shown in Fig. 5.9a are found to be consistent with the results of Reynolds equation (5.31) in Cartesian form shown in Fig. 5.9b. When comparing the results of the derived polar Reynolds equation (5.25) and the Cartesian Reynolds equation (5.31), the percent difference was less than 3% for all cases except where r = 3mm (Table 5.3). The absolute difference between the solutions at r = 3 mm was merely 5.94E-5 but the percent error was higher (17%) due to the relatively small absolute pressures (~3.5E-4). The small amount of differences between the results of the Cartesian equation and the polar equation is likely due to the numerical errors introduced by the different meshing schemes. The traditional version of polar Reynolds equation (5.26), however, yields a peak pressure of 2.13E-2, which is more than 3 times as large as the peak pressure of the solution with the more appropriate polar Reynolds equation (5.25). The traditional form of polar Reynolds equation also has a slightly different shape to its pressure profile (Fig. 5.9c). Therefore, implementing the proper set of assumptions when considering a pin-on-disk setup is imperative to achieving the correct quantitative solution.

This case study also can be applied to non-rotating CMP wafer experiments, where the origin is set at the center of the wafer.

Table 5.3. Comparison of Cartesian (Eq. 5.25c) and polar (Eq. 5.31) Reynolds equation results

Position	Cartesian	Polar	% Difference
Peak Pressure	6.51E-3	6.39E-3	1.9
r = 1mm	6.11E-3	5.95E-3	2.6
r = 2mm	2.23E-3	2.22E-3	1.1
r = 3mm	3.17E-4	3.76E-4	17.2

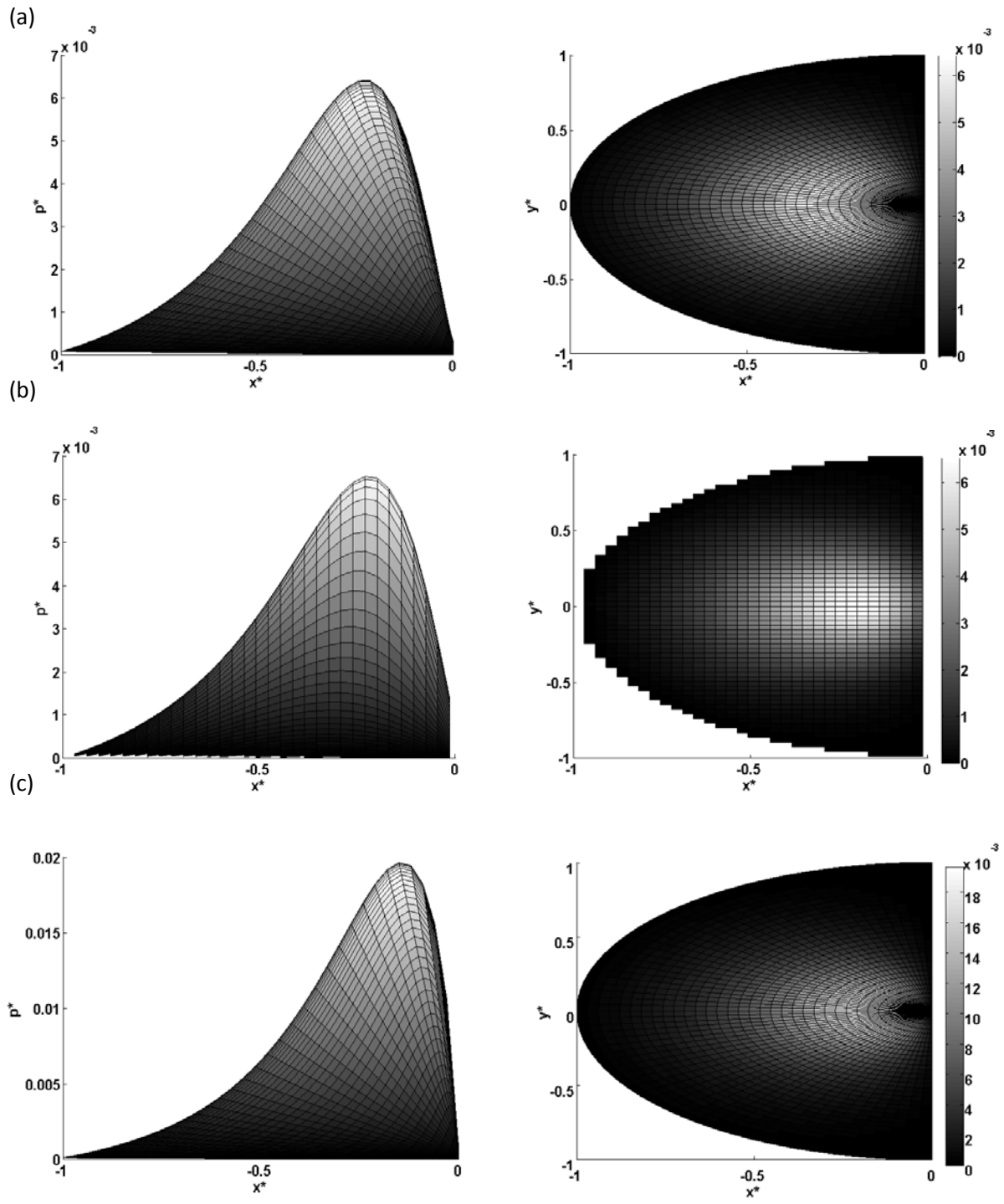

Figure 5.9. Pressure profile from side (left) and top view (right) for pin on disk for three forms of Reynolds equation (a-c)

5.2.5. Case Study II: Chemical-Mechanical Polishing (CMP)

Chemical mechanical polishing (CMP) involves a tribosystem of a circular wafer being loaded on top of a larger spinning circular pad that is flooded with a thin film of liquid slurry. In CMP, the polar form of Reynolds equation is often used because the entrainment velocities and film thickness are simpler in polar form [70, 130]. For example, Higgs et al. made the pad the origin since only their pad was spinning, which caused the tangential velocity v_θ to not be a function of θ. Thus the tangential velocity was $v_\theta = \omega_p r$ = constant. However, when both the wafer and pad are spinning (Figure 5.10) as they do in industry-scale CMP machines, Park et al. expresses the entrainment velocities for the pad (surface (a)) and the wafer (surface (b)) as [130]:

$$v_{r(a)} = d\sin(\theta)\omega_p \quad \text{Eq. (5.32a)}$$

$$v_{\theta(a)} = (r + d\cos(\theta)) * \omega_p \quad \text{Eq. (5.32b)}$$

$$v_{r(b)} = 0 \quad \text{Eq. (5.32c)}$$

$$v_{\theta(b)} = r\omega_w \quad \text{Eq. (5.32d)}$$

In the above text and Equation (5.32), d represents the distance of the center of the wafer from the center of the pad, ω_p is the rotational speed of the pad and ω_w is the rotational speed of the wafer. The film thickness across the surface of the wafer can be expressed as:

$$h(r,\theta) = h_M - r\sin\alpha * \cos\theta - r\sin\beta * \sin\theta \quad \text{Eq. (5.33)}$$

In Equation (5.33), h_M represents the mean film thickness while α and β are tilt angles in the wafer that lead to the wedge term. The values used for this simulation can be found in Table 5.4. When evaluating this CMP example in non-dimensional terms (Equation (5.25)), the radial term is normalized by the radius of the wafer, R; film thickness is normalized by the mean film thickness, h_M; pressure is normalized by atmospheric pressure, p_{atm}; and the velocity terms are normalized by the maximum velocity of the wafer, ω_w*R.

Table 5.4. Simulation conditions for CMP

Wafer Radius, R (mm)	d (mm)	ω_p (RPM)	ω_w (RPM)	h_M (μm)	α (°)	β (°)
100	150	100	50	100	0.015	0.015

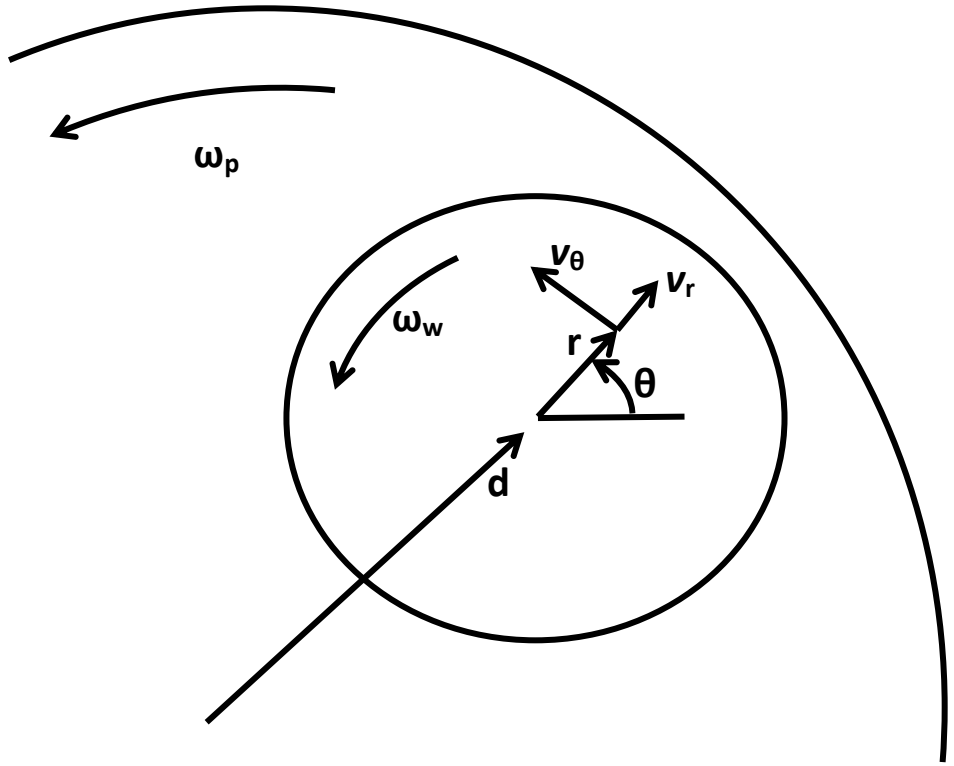

Figure 5.10 Orientation of wafer on pad with polar coordinate system labeled

When the above conditions are solved using the new Equation (5.25), the resulting pressure profile, as shown in Figure 5.11a, has all positive pressures and a peak normalized pressure of around 1.75. When tangential velocity is assumed to be independent of angle and Equation (5.26) is used as shown in Figure 5.11b, a peak pressure of around 4 is reached and a sub-ambient pressure region is generated. For this CMP example, using the traditional assumptions not only drastically changes the magnitudes of pressure but also generates a completely different sub-ambient effect. While sub-ambient pressure effects have been found in both spinning and stationary CMP wafer experiments [71, 131], they would not be predicted using the new Equation (5.25) for the modeling conditions specified in this case study. As was found for the pin-on-disk example, using the proper set of assumptions is necessary for achieving the correct solution when evaluating Reynolds equation for CMP.

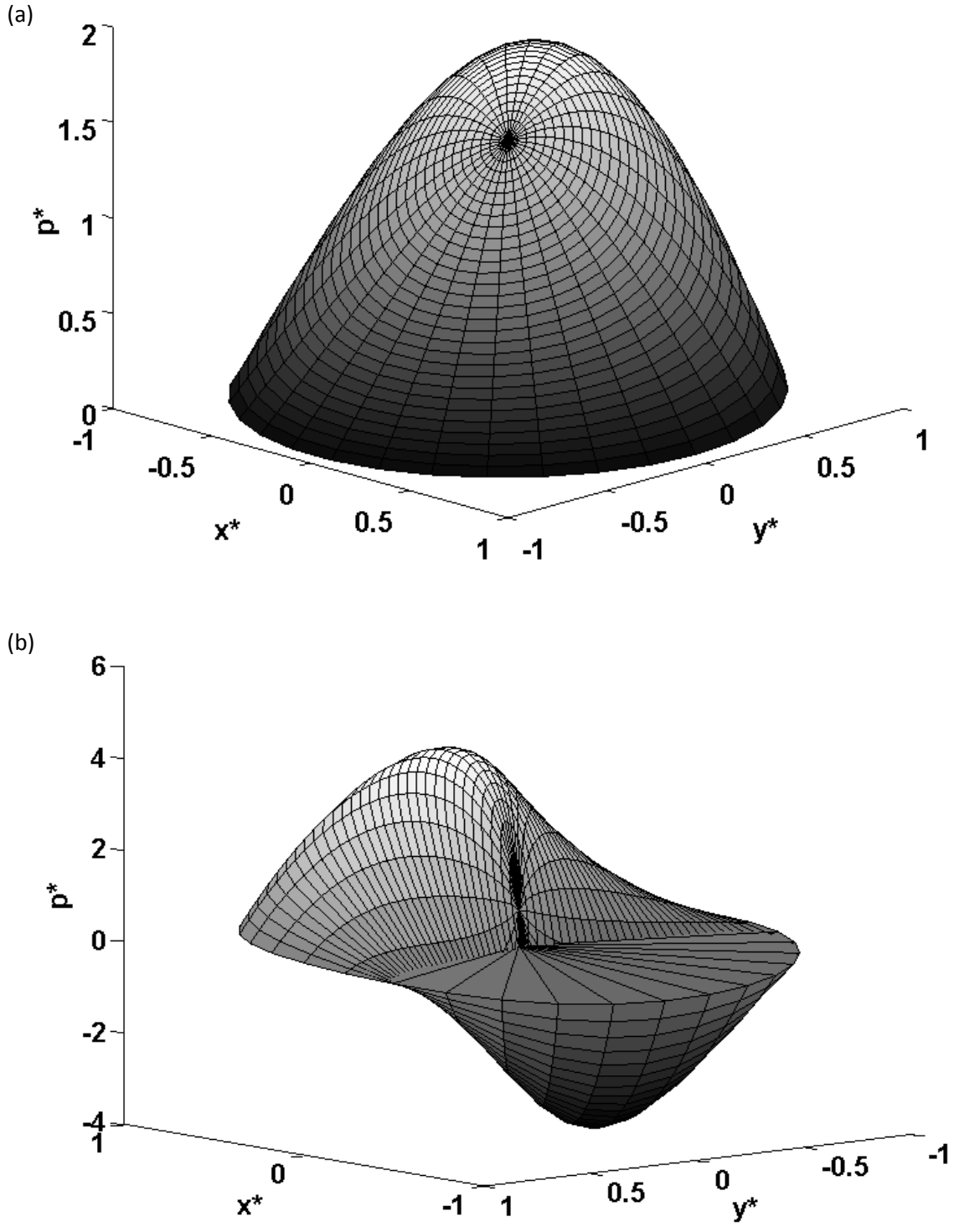

Figure 5.11. Solution to developed (a) and traditional (b) polar Reynolds equation applied to CMP

5.2.6 Conclusions

The Reynolds equation in polar form is derived from the cylindrical form of Navier-Stokes equations with the allowance that v_r may be a function of r and v_θ may be a function θ. This derived equation is especially useful in pin-on-disk and in CMP applications where v_θ is known to vary with θ [130]. In cases where inappropriate assumptions are made to the contrary, one may attain incorrect and misleading results.

5.3 SUMMARY

A shoe-floor-contaminant friction model was created and applied to a pin-on-disk apparatus. Model output showed good agreement with the experimental data. The hydrodynamic portion of the modeling utilized a form of polar Reynolds equation that was derived with a set of assumptions appropriate to pin-on-disk conditions. While the developed model performed well against experimental data, improvements to the model are recommended such as including deformation effects due to the hydrodynamic pressure and adjusting the hydrodynamic modeling to account for roughness. In addition, numerous challenges remain to apply the framework of the developed model towards modeling an entire shoe against a floor surface. Some of these challenges are described in Chapter 6.

6.0 SHOE-FLOOR FRICTION MACRO-MODEL

The development of a computational model capable of predicting friction between an entire shoe and floor surface separated by a fluid would be a valuable tool in understanding slip and fall accidents from a tribological perspective. Directly applying the modeling efforts that were developed in Chapter 5 to an entire shoe may be difficult, especially when considering the contact pressures of complex tread patterns, transient loading effects and non-linear material properties. Therefore, finite element analysis (FEA) software packages are an attractive option for obtaining solutions that include all of these different complex behaviors. This chapter outlines some preliminary efforts to model shoe-floor-contaminant friction using one of the most common FEA software packages, ANSYS. This chapter describes the attempts to model shoe-floor-contaminant friction using a commercial software package and problems that were encountered during these efforts. Finally, a hybrid model that combines the power of FEA along with the versatility of custom modeling is proposed.

6.1 PRELIMINARY SHOE-FLOOR-CONTAMINANT FINITE ELEMENT MODELING

In this section, efforts to create FEA models of shoe-floor-contaminant interface are discussed. These efforts used both implicit and explicit solution techniques with the software package, ANSYS (version 11.0) due to the strengths and limitations of each. Both implicit and explicit solution techniques use numerical integration techniques to solve for nodal displacements over time. Implicit analyses are typically stable across most time intervals and require a matrix inversion, which is often computationally expensive, while explicit analyses are efficient but often require small time steps to ensure stability. Therefore, explicit analyses may require more time steps to obtain a solution, which may result in a longer solution time. While there is no rule

for which solution type to use, explicit analyses tend to be better equipped for highly transient and short duration simulations. In the ANSYS software package, different element types are used for each of the two analysis techniques. Thus, differences in functionality may be experienced when using the two types of solution techniques. The primary goal of this section was to determine the ability of both implicit and explicit solving techniques in ANSYS to simulate the contact and lubrication between the shoe and floor surfaces. A secondary goal of this section was to establish a methodology for implementing the boundary conditions so that shoe-floor angle, normal force and heel velocity could all be controlled independently.

6.1.1 Methodology

Both implicit and explicit solving algorithms within ANSYS and ANSYS/LS-Dyna, respectively, are explored for their ability to simulate the solid contact and fluid effect of the shoe-floor-contaminant interface. Separate models are developed for both the implicit and explicit solvers because each solver uses different element types and contact algorithms. The simulations are generated by writing computer code in ANSYS Parametric Design Language that is input into ANSYS. This code performs all the tasks related to generating, solving and analyzing the results of the FEA model including creating the geometry of the shoe heel, fluid and floor surface; meshing the surfaces with the specified element types and material properties; initiating the appropriate contact options; applying the loading conditions; solving the problem with an appropriate set of solution options; and exporting the desired output into a text file.

6.1.1.1 Implicit analysis

In this analysis, a simple treadless shoe is evaluated against a flat floor surface. The shoe heel geometry is defined as a half disk and the floor surface is modeled as a flat planar surface (Figure 6.1). A linear elastic material is applied to the shoe heel and is meshed with 10 node tetrahedral elements, which provides maximum accuracy for meshing the curved heel volume. The SOLID187 element type is used because of its ability to retain accuracy during non-linear analyses. The floor material for the implicit analysis is meshed using a PLANE182 element type with square elements. Contact elements are superimposed over the shoe and floor surfaces using

the CONTA174 and TARGE170 element types, respectively. A rigid-flexible contact is implemented with the floor material being rigid and the shoe material being flexible. The coefficient of friction value was set to 0.8.

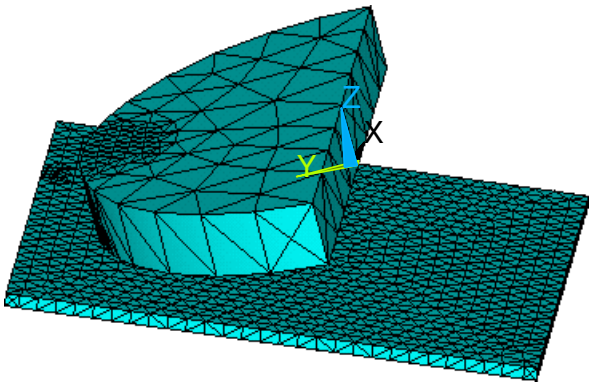

Figure 6.1. Geometry and meshing of the shoe heel, floor surface and fluid for implicit analysis

The implicit model was also evaluated for its ability to generate viscous hydrodynamic pressures between the shoe and floor surfaces. The fluid is modeled with a thin rectangular volume modeled with FLUID136 element types. The FLUID136 elements are designed to model viscous and squeeze film effects of thin fluids. The FLUID136 element type has options that allow the user to input the gap (i.e. film thickness) and the entrainment velocity (i.e. velocity of the adjacent solid surface). Neither of these options are used, however, because neither film thickness nor the shoe heel velocity are expected to be constant throughout simulations of the shoe heel during slipping. The ANSYS documentation is unclear how to create an interaction between the fluid and the contacting surfaces; therefore initial efforts attempted to apply the contact elements, described previously as CONTA174 and TARGE170, between the fluid and shoe material. These contact algorithms caused the fluid elements to become highly distorted and unstable. Therefore, the implicit analysis simulations described in this section do not use any contact algorithm between the shoe heel and the thin film fluid.

The secondary purpose of this section is to describe methodology for applying boundary conditions so that shoe-floor angle, normal force and heel velocity can all be controlled independently. Initial efforts attempted to control shoe angle by applying rotational constraints and subsequently controlling the rotation of all the nodes on the top surface of the shoe heel. These efforts did not work because rotation angle is not an active degree of freedom for nodes on SOLID187 element types. Therefore, boundary conditions could only be applied to control displacement of nodes or forces applied to nodes:

BC1. Shoe angle was controlled using displacement constraints.

BC2. Normal force was controlled by applying force loads.

BC3. Heel velocity was controlled using displacement constraints.

As seen in Figure 6.2, shoe-floor angle (BC1) is controlled by specifying the displacement in the z-direction of a single line of nodes, which are far from the contact region. The normal force (BC2) is specified by applying force loads in the z-direction on the top surface of the shoe, approximately above the contact region. By placing the normal force loads (BC2) over the contact region and the shoe-floor angle displacement constraints (BC1) far from the contact region, shoe-floor angle and normal force are mostly independent and very little of the normal force (BC2) is transmitted to the displacement constraints (BC1). Heel velocity (BC3) is controlled by specifying the y-displacement over time of the nodes located on the surface highlighted in Figure 6.2.

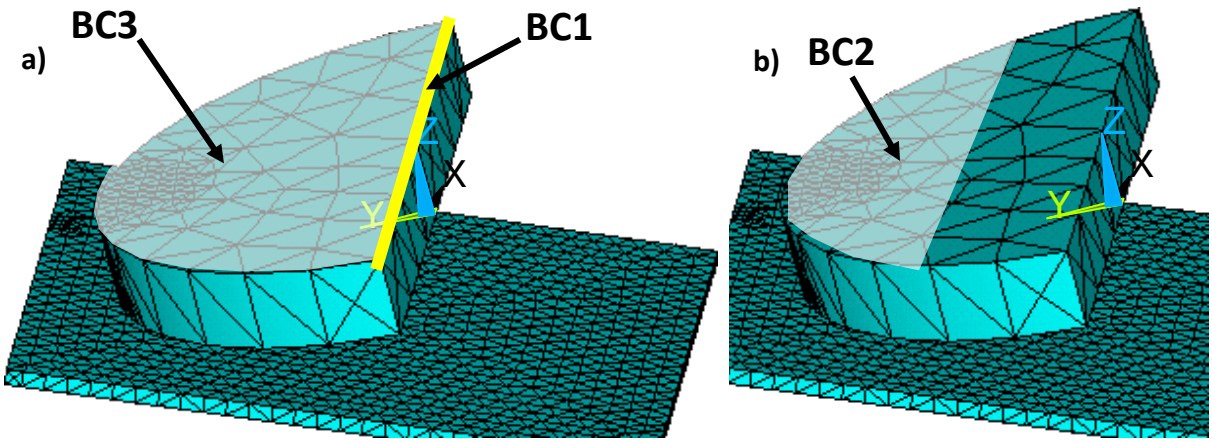

Figure 6.2. Geometry of shoe heel and applied boundary conditions

In an effort to model the transient effects of the shoe during slipping, multiple loading steps were implemented for the implicit analysis model so that shoe angle, normal force and heel velocity were varied in a way relevant to slipping accidents. An initial load step was also implemented in order to establish stable contact between the shoe and floor surfaces. These loading steps can be found in Table 6.1.

Table 6.1. Loading conditions for the implicit analysis simulation

Load Step	Time (ms)	Normal Force (N)	Velocity (m/s)	Shoe Angle (°)
1	10	7	0	20
2	20	157	0	20
3	50	320	0.417	15
4	100	765	0.020	7
5	200	644	0.100	5

6.1.1.2 Explicit Analysis

Similar to the implicit analysis, a simple treadless heel geometry is considered in the explicit analysis. While the half-disk shape, used in the implicit analysis, bears a stronger resemblance to the heel of a shoe than a block, the curved geometries of a half-disk require smaller element types that can drastically increase the computational time of the explicit analysis. Thus the shoe heel is modeled as a block (Figure 6.3) in the explicit analysis with the understanding that if preliminary simulations were successful, more complex geometries could be considered at the cost of greater computational time. The floor surface is also modeled as a block. Modeling the floor as a 3D volume instead of a 2D surface, while requiring more elements and increasing computational time, is necessary for the explicit analysis model because the explicit analysis contact algorithms prevent contact between a 2D and 3D object. A linear elastic material is applied to both the shoe and floor material although the elastic modulus for the floor was much larger than the shoe so that the floor was effectively rigid. Both the shoe and floor materials are meshed with a SOLID164 element type, which is an element type that is specifically made for explicit analyses. The shoe and floor volumes are meshed with block shaped elements because of their high accuracy and computational efficiency. The Automatic General contact option is used, which automatically detects and initiates contact between solid surfaces. Coefficient of friction was set to 0.8. For the explicit analysis, there is no fluid element type available but fluid properties can be applied to solid element types like SOLID164. The only material property that is available, however, is bulk modulus, which is only capable of describing the relationship between deformation and hydrostatic pressures. Therefore, no options were available in the explicit analysis for modeling the viscous effects of the fluid and the fluid was not included in this model.

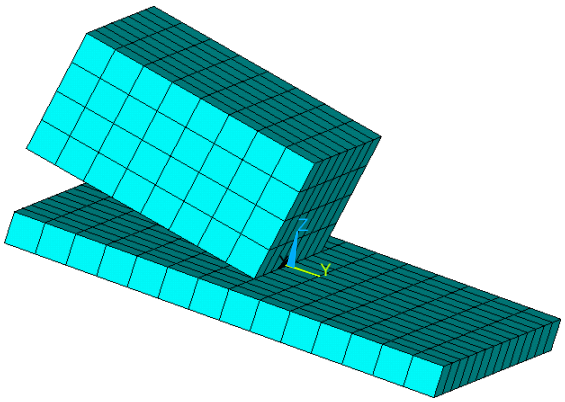

Figure 6.3. Geometry and meshing of shoe-floor model for explicit analysis

6.1.2 Results

For the implicit analysis, the FEA model successfully converged to a solution in approximately 5 hours using a standard PC. The contact methods that were used did not cause the model to become unstable and successfully prevented the shoe volume from penetrating the floor surface. The applied loads resulted in a relatively uniform stress throughout the shoe heel with some higher stress levels near the posterior region of the heel (Figure 6.4). The normal force, which was applied over the contact region, caused deformation at the posterior section of the shoe, which resulted in an increased contact region. In addition, contact stresses were at their highest level in the center of the contact region (Figure 6.4b). No hydrodynamic pressures were found in the fluid indicating that it did not participate in the interaction of the shoe and floor surfaces.

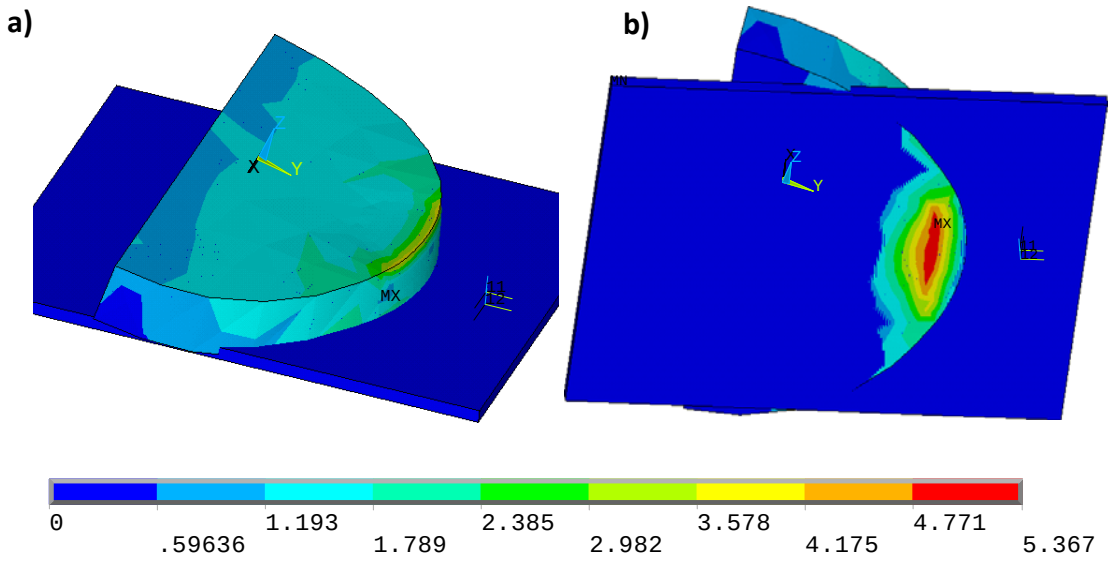

Figure 6.4. Stresses in the heel material (left) and of the contact (right) from implicit analysis simulations

The applied boundary conditions in the implicit analysis resulted in the model reproducing the desired values of shoe-floor angle, normal force and heel velocity. Throughout each of the load steps, normal force and shoe angle changed in a linear fashion. Heel velocity remained constant during each load step and then discontinuously changed between load steps. Therefore, more load steps may be necessary in order to prevent the large discontinuities in heel velocity. Figure 6.5 shows how COF varied as shoe angle, heel velocity and normal force varied. COF values stayed at the dry COF level of 0.8 when relative motion between the shoe and floor surfaces occurred (i.e. during positive heel velocity). This finding further supports the argument that there was no hydrodynamic lift effect from the fluid.

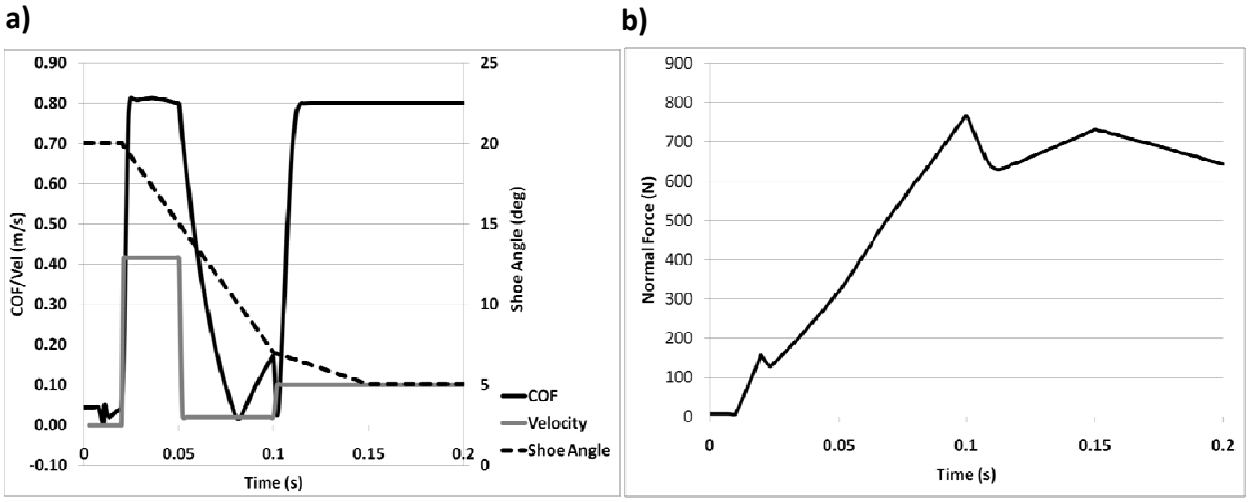

Figure 6.5. Plots of utilized COF, velocity, shoe angle and normal force across the simulation

The explicit FEA models also successfully converged to a solution but did so in a much shorter time of approximately 5 minutes using a PC. The contact method, Automatic General, did not cause the model to become unstable and successfully prevented the shoe volume from penetrating the floor volume. The highest stresses occurred near the contact region and the stress values rapidly decreased moving away from the contact region (Figure 6.6).

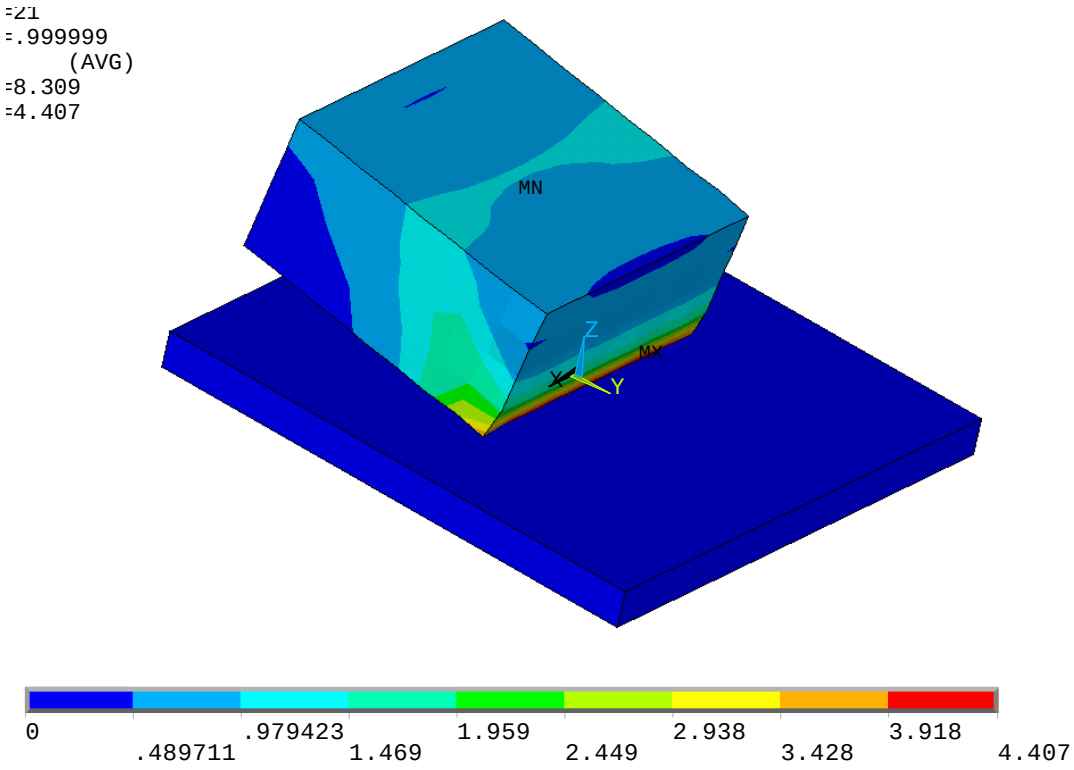

Figure 6.6. Material stresses of shoe-floor contact simulation using explicit solution techniques

6.1.3 Limitations of Current FEA Modeling Approaches

The primary limitation in the modeling of shoe-floor-contaminant interaction using FEA analyses in ANSYS was the inability of the fluid models to simulate viscous effects. Therefore, neither implicit nor explicit analysis model is useful for evaluating shoe-floor-contaminant friction. The documentation on the fluid element, FLUID136 (used in the implicit analysis model), indicates that this element type may perform best when information such as gap distance (or film thickness) and fluid velocity are input into the model for each of the elements [132]. In the case of shoe-floor-contaminant interaction, however, these variables are constantly changing based on the varying number of shoe nodes interacting with the fluid throughout the slip. The varying shoe-floor angle causes portions of the shoe to transition from being above the fluid to coming into contact with the fluid. In addition, as fluid is pressed out from underneath the shoe

due to the normal force, sections of the shoe-floor interface to transition from being separated by the fluid to being in direct contact. Therefore, gap distance and entrainment velocity cannot be input into the model for the case of shoe-floor-contaminant friction modeling. For the explicit analysis, no element types are available for developing viscous forces. Therefore, ANSYS/LS-Dyna may be poorly equipped in its current state from evaluating shoe-floor-contaminant friction. Another potential avenue to simulate fluid-contaminated shoe-floor interactions is discussed in Section 6.2.

6.1.4 Using Finite Element Analysis for Modeling Shoe-Floor-Contaminant Friction

The attempts to use commercial finite element analysis software to simulate shoe-floor-contaminant friction demonstrate the current limitations of the software packages, ANSYS and ANSYS/LS-Dyna, to model lubrication effects under conditions relevant to slips and falls. The interaction between shoe and floor surfaces was simulated using both implicit and explicit analysis techniques yet neither effort was able to capture viscous hydrodynamic pressures. The explicit analysis (Section 6.1.2) achieved solutions much faster than the implicit analysis yet the implicit analysis solver in ANSYS has access to more element types including a fluid element that is capable of generating viscous forces. The current recommendations made by the ANSYS software for coupling this fluid to the shoe heel and floor surfaces are not practical for capturing the transient loading effects of the interacting shoe and floor surfaces. The modeling techniques that are established in this section, however, provide a framework for how to apply the boundary conditions if improvements are made in the software package, ANSYS and ANSYS/LS-Dyna, to improve the interactions between fluid and solid surfaces. In addition, a hybrid model is proposed in the next section that intends to utilize the power of FEA software and the versatility of custom software.

6.2 PROPOSED HYBRID SHOE-FLOOR-CONTAMINANT FRICTION MODEL: CUSTOM MODELING UTILIZING FINITE ELEMENT ANALYSIS

The purpose of this section is to propose a hybrid model that is able to take advantage of the versatility of custom modeling while utilizing the power of finite element analysis software. This custom model has not been implemented successfully, but is believed to have the potential to overcome the limitations of FEA. Thus, the goal of this section is to lay out the principles of the hybrid model for future development.

The concept in the hybrid model is to use customized computer code to evaluate the viscous hydrodynamic pressures at each step, and then allow the FEA to solve the shoe-floor contact forces and deformation of the shoe material. In addition, the hybrid model would include an algorithm to integrate results from both components and employ iterative methods to achieve a solution (similar to Figure 5.1). The custom code of this hybrid model will address the limitations of current finite element analysis software.

The structure of the hybrid model would be similar to that of the micro-model (Section 5.1) in which iterative methods are employed to alter the amount of deformation until the sum of the hydrodynamic and contacting forces are equal to the total normal force (Figure 6.7). The primary outputs of this modeling effort are the amount of normal force supported by the fluid and by the contacting asperities, while the inputs are the geometry of the shoe heel, shoe and floor roughness, shoe and floor material properties, fluid viscosity, fluid film thickness, normal force profile, shoe angle profile and sliding speed profile. The amount of force supported by the contacting regions is determined by the FEA simulations while the amount of force supported by the fluid region is determined from custom modeling approach. The iterative process is performed for each time step with shoe angle, normal force and heel velocity being updated for each subsequent time step. Once the iterative process determines the amount of the load supported by the contact region and fluid region, coefficient of friction can be determined with Equations 5.13(a-c). The results of this hybrid model will provide valuable information about the under-shoe conditions during slipping such as coefficient of friction, contact and hydrodynamic pressures and the deformed shape of the shoe material.

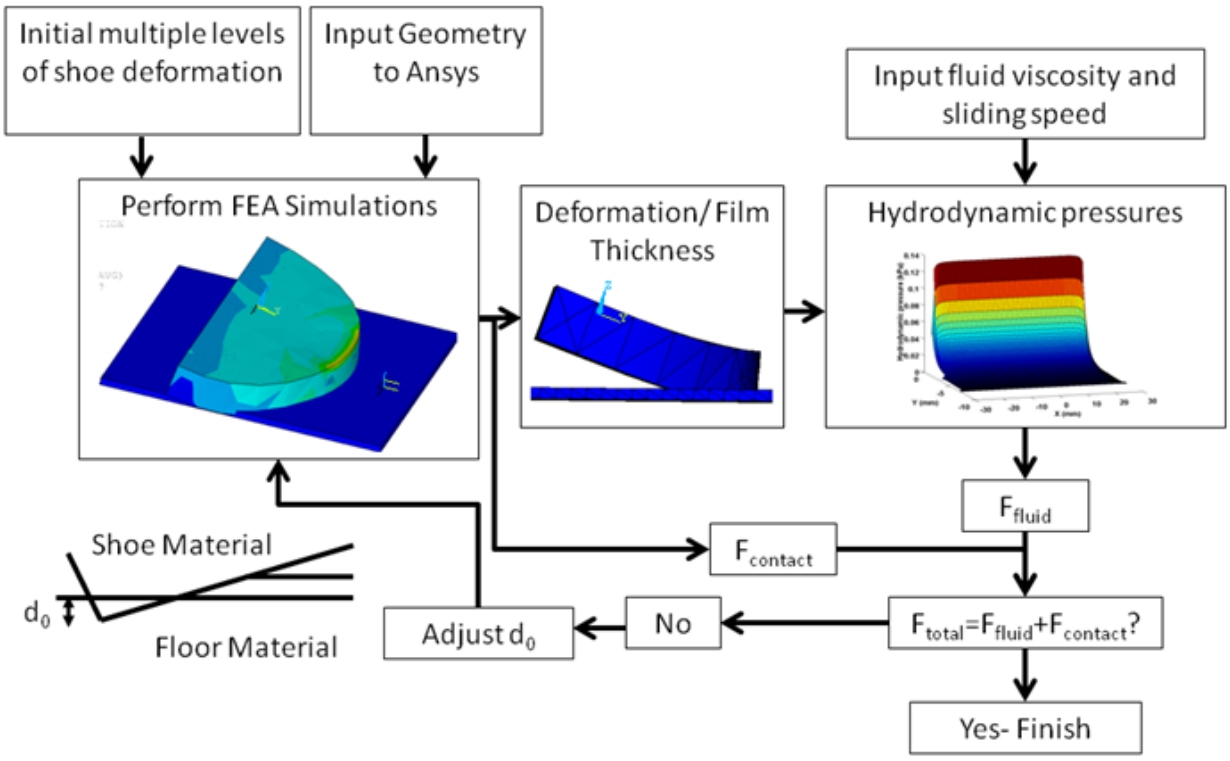

Figure 6.7. Iterative scheme for determining force supported by contact and fluid regions

The hybrid model will rely on FEA to analyze the contacting regions of the shoe against the floor surface. Due to the iterative approach which varies deformation to solve for contacting and hydrodynamic forces, a large number of FEA simulations at different deformation levels will be conducted. In addition, these simulations will be conducted across the range of shoe angles that are found in a slipping accident. For each timestep, the shoe-floor angle is applied and levels of deformation are evaluated that range between 0 and 100% of the total normal force. The loading will be applied as shown in Section 6.1.1. The FEA model will then output the normal force supported by the contact regions and the deformed geometry of the shoe heel for each level of deformation. One limitation with this approach is that the time-history of the loading is not known therefore dynamic effects including inertia and time-dependent material effects of the shoe material are not considered.

The custom modeling portion of a developed hybrid model will be used to solve for the hydrodynamic pressures across the regions of the shoe that are separated by a thin film of fluid. In addition, the custom modeling algorithm will be responsible for integrating information from the FEA results and the hydrodynamic modeling algorithm. The hydrodynamic component of the hybrid model will be based on the framework of the micro-model as described in Section 5.1. As described previously (Sections 5.1 and 5.2), numerical methods have been developed to solve Reynolds equation in both the polar and Cartesian coordinate systems. Similar algorithms will be used to solve Reynolds equation in this hybrid modeling approach. The methodology for evaluating the transition between full film lubrication and full contact between the surfaces will be similar to those found in Section 5.1.3.2 (Equation 5.11). As described in Section 5.1.3.2, the interacting shoe and floor surfaces were considered in full contact when at least 75% of the asperities are in contact as determined using stochastic methods. Boundary conditions were established at this border to prevent flow of fluid inside the contact region. The transition between full fluid and full contact will be treated similarly for the hybrid model except the exact threshold of 75% may be adjusted as needed to acquire good agreement between the model and experimental results. Film thickness, a required component to solve Reynolds equation, will be determined based on the deformed shape of the shoe material from the solution of the FEA analysis. In addition, Reynolds equation will be adapted to include squeeze-film effects so that the Reynolds equation will become:

$$\frac{\partial}{\partial \mathbf{x}}\left(\mathbf{h}^3 \frac{\partial \mathbf{p}}{\partial \mathbf{x}}\right)+\frac{\partial}{\partial \mathbf{y}}\left(\mathbf{h}^3 \frac{\partial \mathbf{p}}{\partial \mathbf{y}}\right)=12\eta \mathbf{U}\left(\frac{\partial \mathbf{h}}{\partial \mathbf{x}}+\frac{\partial \mathbf{h}}{\partial \mathbf{t}}\right) \qquad \text{Equation 6.1}$$

A time history of film thickness will be maintained such that for each iteration, the squeeze film effect ($\partial \mathbf{h}/\partial \mathbf{t}$) can be determined based on the current film thickness and the film thickness from the solution of the previous timestep. The film thickness profile for each iteration, **h(x,y),** will be determined based on output from the FEA solutions. Interpolation schemes will be used to determine the deformed shape of the heel when the deformation level of the current timestep is between different levels of deformation that are input from the FEA analysis.

The proposed hybrid modeling approach may be able to supplement the limitations of the other modeling attempts in this dissertation such as the custom modeling approaches as

described in Section 5.1.6 or the FEA analysis as described in Section 6.1.1. The hybrid modeling relies on FEA for determining the deformation and normal forces of contacting regions between the shoe and floor surfaces while utilizing the developed custom modeling approaches to determine hydrodynamic pressures based on Reynolds equation. In addition, the proposed hybrid modeling approach introduces the squeeze film effect as described by Equation 6.1. A developed hybrid model will be useful for determining how friction varies throughout a slipping accident, how biomechanical factors (normal force, shoe angle and sliding speeds) affect friction and how design factors (floor roughness, tread pattern and shoe material properties) affect friction. This hybrid model may provide critical information of shoe-floor-contaminant friction until better methods are designed in ANSYS that are able to properly evaluate the lubrication effect under the transient conditions relevant to slipping accidents.

6.3 SUMMARY

In this chapter, simulations were performed using the both implicit and explicit solution techniques of the FEA software packages, ANSYS and ANSYS/LS-Dyna. There were limitations in the current software packages that prevented modeling of shoe-floor-contaminant friction, primarily the inability to capture the viscous hydrodynamic effect of the fluid under the transient conditions relevant to slipping. To this end, a hybrid modeling approach is proposed that combines the ability of FEA software to simulate contact between two surfaces while using custom computational modeling to simulate hydrodynamic pressures and to integrate the results of the contact and hydrodynamic models. The hybrid model was described, but has not yet been successfully implemented. It is hoped that the concepts will assist in future development of a model that can more accurately describe true shoe-floor-contaminant friction.

7.0 DISCUSSION AND CONCLUSIONS

This dissertation aimed to improve the understanding of slip and fall accidents by examining the biomechanics related to heel control during walking and the tribological mechanisms of the shoe-floor-contaminant interface. The major contributions of this dissertation are:

1. Heel acceleration, a measure of heel control, at heel contact was identified as a contributing factor to falls. Knee flexion torque was strongly correlated with heel acceleration at the time of heel contact and is therefore thought to be most responsible for heel control at and around heel contact.
2. Mixed-lubrication was identified as the critical lubrication regime of the shoe-floor-contaminant interface relevant to human slip and fall accidents.
3. A physics-based computational model was developed for shoe-floor-contaminant friction based on mixed-lubrication theory and showed good agreement with experimental data.
4. The polar form of Reynolds equation was derived for non-symmetric entrainment velocities.

In addition, Chapter 6 proposed a hybrid approach to develop a model that can simulate the interaction between an entire shoe and a floor surface in the presence of a liquid contaminant. This hybrid model incorporates finite element analysis and custom code. This dissertation represents a first step towards developing a comprehensive understanding of biomechanical control of heel motion and tribology of the shoe-floor-contaminant interface during slip and fall accidents.

This final chapter will discuss how future research can build on the research presented in this dissertation. Specifically, this chapter outlines the most critical improvements to the shoe-floor-contaminant friction model. Additionally, the importance of this research and the utility of computational shoe-floor-friction models for reducing the number of slip and fall accidents are described. Furthermore, this chapter describes how the shoe-floor-contaminant friction model

can be coupled with biomechanics research for an integrated approach to heel contact control during slipping.

7.1 FUTURE DIRECTIONS FOR SHOE-FLOOR-CONTAMINANT FRICTION MODEL

While this dissertation achieved its primary purpose to improve the understanding of biomechanics and tribology for slip and fall accidents, additional work is needed to ensure that these efforts eventually result in a reduction of injuries due to slips. Specifically, the physical accuracy of the developed shoe-floor-contaminant friction model needs to be improved and the model needs to be expanded to include an entire shoe heel. This section also describes how future generation shoe-floor-contaminant friction models will become useful tools for reducing slip and fall accidents.

7.1.1 Necessary Improvements in the Model

Several improvements to the modeling efforts described in this dissertation are needed in order to develop a comprehensive shoe-floor-contaminant friction model. These improvements include increasing the physical accuracy of the models, particularly by including elastohydrodynamic lubrication (EHL) effects. In addition, the shoe-floor-friction model that was developed for a pin-on-disk apparatus needs to be expanded to model friction when an entire shoe heel is considered.

The primary limitation of the shoe-floor-contaminant friction model as described in Section 5.1.6 was that deformations due to hydrodynamic pressures were ignored. Therefore, EHL effects, which may play a critical role in the shoe-floor-contaminant interface, were not included in these preliminary modeling efforts. Including EHL effects into the shoe-floor-contaminant friction model requires altering the film thickness, h, to be a function of fluid pressures. While fluid pressures across the shoe surface can currently be solved using Reynolds equation as a system of linear equations (Equation 5.10), solving Reynolds equation while implementing EHL requires solving a system of highly non-linear equations. Thus, the current method of solving for hydrodynamic pressures with matrix-inversion cannot be used when EHL

effects are considered. Therefore, introducing EHL into the shoe-floor-contaminant friction model requires additional research to identify an algorithm that is capable of solving this set of non-linear equations.

Significant challenges also exist in trying to develop a shoe-floor-contaminant friction model that includes an entire shoe heel. The current shoe-floor-contaminant friction model estimates contact pressures based on Hertzian contact mechanics, which is only capable of modeling contact between a spherical surface and a flat surface. In response to this limitation, FEA was explored as an option for modeling the contact and lubrication effects between a shoe heel and floor surface. As described in Chapter 6, the FEA software was limited in its ability to model the interaction between the viscous fluid and the shoe and floor surfaces. Therefore, a hybrid model was proposed in order to combine the ability of custom code to model the viscous fluid while relying on FEA to model the contact between the shoe and floor surfaces. While the hybrid model may be relatively straight-forward to develop as proposed in Section 6.2, including EHL into this model would require the custom code and FEA model to interact, which may be difficult to implement. Additionally, to ensure that the shoe-floor-contaminant friction model accounts for transient effects, the Reynolds equation would have to be modified to include squeeze film effects. The squeeze film effect is often considered crucially relevant to slip and fall accidents [29, 82]. As the complexity of the shoe-floor-contaminant friction model increases, new testing protocols will need to be developed in order to validate each subsequent model. For example, the ability of the eventual whole-shoe model to capture transient effects will need to be validated with experiments that can capture the transient effects. The current friction testing protocol as described in Section 4.1 is poorly equipped for examining transient effects particularly because the device cannot accurately control normal force. Therefore, the current slip testing device would have to be adapted to better capture transient effects or a new device would have to be developed. Thus, significant challenges remain for expanding the currently developed shoe-floor-contaminant model into one that considers an entire shoe.

7.1.2 Long Term Plan for Model

The long term goal for this research effort beyond the thesis is to develop a tool that can aid in the reduction of slip and fall accidents. A predictive shoe-floor-contaminant friction model that

can capture the effects of macro-geometries (i.e. tread), shoe and floor surface topography, fluid properties and loading (shoe-floor angle, normal force, heel velocity) would be a valuable tool for achieving this goal. The envisioned shoe-floor-contaminant friction model will become a valuable tool:

1. For ergonomists by providing improved slip-resistance data for different shoe and floor combinations.
2. For shoe and floor manufacturers because it will aid in improving slip resistance of shoe and floor designs.
3. For future slip and fall research because it will improve understanding of how biomechanical factors such as gait style or post-slip postural responses affect the amount of shoe-floor-contaminant friction.

The current slip-testing devices that are available to ergonomists have numerous limitations (outlined in more detail in Section 2.3), particularly due to their inability to mimic slipping conditions and account for the variability of different walking styles. In fact, when comparing different shoe materials, the friction coefficient rank may depend on the testing conditions as shown in Sections 4.2 and 5.1. In addition to limitations in current slip testing device, the use of a single value of shoe-floor-contaminant friction as a measure of slip risk is flawed. The current approach of measuring slip resistance implies that a larger friction coefficient indicates better slip resistance; yet the amount of required friction even while walking on a severely sloped incline rarely exceeds 0.5. Therefore, shoe and floor designs that result in friction coefficients much above 0.5 may not improve slip resistance as would be indicated by the traditional approach to measuring slip resistance. In fact, excessive amounts of friction coefficients may result in the foot catching traction during the swing portion of gait and causing a trip. An improved approach to slip resistance would be to evaluate how a shoe or floor design performs in the presence of several different contaminants under a variety loading conditions, which would be more representative of the variable conditions experienced by either a shoe heel or floor surface. One advantage of a computational model for shoe-floor-contaminant friction is that friction coefficient can be efficiently evaluated under a large range of conditions, which may provide a more complete picture of the slip-resistance properties of a shoe-floor combination. Therefore, once the shoe-floor-contaminant friction model is developed, different tests will be

created so that this model can evaluate the slip-resistant properties across a wide range of conditions.

The shoe-floor-contaminant friction model would also be valuable to shoe and floor manufacturers for designing shoe heels and flooring with improved slip-resistance properties. Similar to ergonomists, shoe and floor manufacturers would benefit from the ability of the computational model to efficiently evaluate shoe-floor-contaminant friction across a large range of conditions relevant to slip and fall accidents. In addition, a shoe manufacturer would be able to rapidly test a shoe design against many different floor surfaces and contaminants to determine its ability to maintain adequate slip resistance for different conditions. Similarly, flooring design could also be tested with many fluids and shoe styles rapidly. A computational shoe-floor-contaminant friction model would also aid shoe designers by identifying the regions of the shoe with the highest hydrodynamic pressures. This feature would allow shoe manufacturers to focus on redesigning the tread in these regions in order to relieve the peak hydrodynamic pressures.

The fully developed shoe-floor-contaminant friction model may also be useful for evaluating how biomechanical factors affect shoe-floor-contaminant friction. For example, different researchers have determined that people use a smaller shoe-floor angle at heel strike to reduce their risk of slipping when they know that the floor is slippery [60, 133]. The mechanism by which this strategy reduces slip risk, however, is unknown. The computational shoe-floor-friction model would be able to determine if this strategy is effective in increasing the amount of shoe-floor-contaminant friction. Therefore, future research may involve using a computational shoe-floor-contaminant friction model to evaluate different walking styles and strategies to determine which, if any of these strategies, is capable of maximizing shoe-floor-contaminant friction.

7.2 INTEGRATED TRIBOLOGY AND BIOMECHANICS APPROACH TO HEEL CONTROL DURING SLIPPING

The control of heel motion during stance, either from shoe-floor friction forces or from lower leg joint torques, is critical to the stability of walking because the heel contact is the initiation of the base of support during a step. When the heel is positioned too far or moving too quickly away

from the center of mass, the body becomes unstable and the potential for a fall is increased [47]. The primary forces that act on the foot and can thus affect heel control are either due to lower body joint torques as described in Chapter 3 or shoe-floor frictional forces. While previous studies have considered shoe-floor-contaminant friction to be constant when considering slip risk [18, 19], this dissertation indicates that biomechanical factors such as shoe-floor angle, normal force and heel velocity may affect shoe-floor-contaminant friction. Therefore, through different biomechanical factors, the body may be able to control heel motion either directly through joint torques, particularly of the knee, and by using a gait style that maximized shoe-floor-friction.

The shoe-floor-contaminant friction modeling efforts described in this dissertation serve as a starting point towards developing a computational model that can predict the available frictional forces throughout a slip. This computational model will provide critical information regarding how different gait styles affect the amount of available shoe-floor friction. Previous research has only focused on how gait style affects the required coefficient of friction [45, 134] even though slip risk is dependent on the difference between required friction and available friction. Once developed, the shoe-floor-contaminant friction model will allow researchers to determine how gait style affects both the required friction coefficient but also the available friction coefficient, which has not yet been considered.

This dissertation also presents the opportunity for developing an integrated approach to understanding heel placement control by combining the effects of the leading leg joint torques and the available friction coefficient. Chapter 3 showed that in the absence of shoe-floor friction effects, heel acceleration resulted from the combined effects of the leading leg joint torques, particularly of the knee flexion torque. This analysis was limited to heel contact because the affects of shoe-floor friction could not be separated from the effects of the leg joint torques once the foot was in contact with the floor. The shoe-floor-contaminant friction model will help determine the relative contribution of shoe-floor-contaminant friction and the leading leg joint torques without being restricted to heel contact. This approach may shed light on the sequence of events that determine the outcome of a slip. For example, this integrated approach might determine whether the difference between subjects who slip versus subjects who do not slip while walking on a slippery surface is due to differences in available friction or differences in leg joint torques. In addition, different post-slip postural responses can be analyzed for their ability to directly control heel motion through joint torque generation as well as their ability to increase

the amount of available friction. The kinematics of the heel during slipping are critical to the outcome of the slip because if the body cannot remain above its base of support, a fall is imminent. Thus an integrated approach of considering both the joint torques generated by the body and shoe-floor friction would be a useful tool to improve understanding of slip and fall accidents.

7.3 CONCLUSIONS

This dissertation achieved its purpose of contributing towards the understanding of slip and fall accidents through the study of the biomechanics of heel control during slipping and the tribology of the shoe-floor-contaminant interface. Knee joint torque was determined to exhibit control over the heel, which was determined to be a contributor of slips and falls. In addition, the critical lubrication mechanisms relevant to slip and fall accidents were identified and modeled. The modeling efforts in this dissertation provide the framework for developing a comprehensive shoe-floor-contaminant friction model, which will be valuable to ergonomists, shoe and floor manufacturing companies and for future slip and fall research efforts. This research provides the opportunity to use an integrated approach to considering slip and fall accidents by considering both the way the body controls motion through joint torques and the tribological mechanisms at the shoe-floor-contaminant interface. While significant challenges remain, this dissertation provides a foundation as well as a plan for developing a computational model of shoe-floor-contaminant friction that can lead to a reduction in slip and fall accidents.

BIBLIOGRAPHY

1. Stellman, J.M., 1998. *Encyclopaedia of occupational health and safety*: International Labour Office.

2. Swedish Work Environment Authority and Statistics Sweden, 2000. *Occupational diseases and occupational accidents 1998*. Stockholm: SWEA.

3. U.S. Department of Labor- Bureau of Labor Services, 1999. *Workplace injuries and illnesses in 1998*. Washington, D.C.

4. Ruser, J.W., 2000. Nonfatal workplace injuries to older workers: Evidence from the BLS survey of occupational injuries and illness. in *National Occupational Injury Research Symposium (NOIRS)*. Pittsburgh, PA.

5. Leamon, T.B. and Murphy, P.L., 1995. Occupational slips and falls: More than a trivial problem. *Ergonomics* **38**(3): p. 487-498.

6. Hausdorff, J.M., Rios, D.A., and Edelberg, H.K., 2001. Gait variability and fall risk in community-living older adults: A 1-year prospective study. *Archives of Physical Medicine and Rehabilitation* **82**(8): p. 1050-1056.

7. Hornbrook, M.C., Stevens, V.J., Wingfield, D.J., Hollis, J.F., Greenlick, M.R., and Ory, M.G., 1994. Preventing falls among community-dwelling older persons: Results from a randomized trial. *The Gerontologist* **34**(1): p. 16-23.

8. Alexander, B.H., 1992. The cost and frequency of hospitalization for fall-related injuries in older adults. *Am Public Health Assoc* **82**(7): p. 1020-1023.

9. Sterling, D.A., O'Connor, J.A., and Bonadies, J., 2001. Geriatric falls: Injury severity is high and disproportionate to mechanism. *The Journal of Trauma: Injury, Infection, and Critical Care* **50**(1): p. 116.

10. CDC, 2008. *Web-based injury statistics query and reporting system (WISQARS)*. Center for Disease Control and Prevention National Center for Injury Prevention.

11. Courtney, T.K., Sorock, G.S., Manning, D.P., Collins, J.W., and Holbein-Jenny, M.A., 2001. Occupational slip, trip, and fall-related injuries--can the contribution of slipperiness be isolated? *Ergonomics* **44**(13): p. 1118-1137.

12. Filiaggi, A.J. and Courtney, T.K., 2003. Restaurant hazards: Practice-based approaches to disabling occupational injuries. *Professional Safety* **48**(5): p. 18-23.

13. Dempsey, P.G. and Filiaggi, A.J., 2006. Cross-sectional investigation of task demands and musculoskeletal discomfort among restaurant wait staff. *Ergonomics* **49**(1): p. 93-106.

14. Bentley, T., Tappin, D., Moore, D., Legg, S., Ashby, L., and Parker, R., 2005. Investigating slips, trips and falls in the new zealand dairy farming sector. *Ergonomics* **48**(8): p. 1008-1019.

15. Bentley, T.A. and Haslam, R.A., 2001. Identification of risk factors and countermeasures for slip, trip and fall accidents during delivery of mail. *Applied Ergonomics* **32**(2): p. 127-134.

16. Koepsell, T.D., Wolf, M.E., Buchner, D.M., Kukull, W.A., LaCroix, A.Z., Tencer, A.F., Frankenfeld, C.L., Tautvydas, M., and Larson, E.B., 2004. Footwear style and risk of falls in older adults. *Journal of the American Geriatrics Society* **52**(9): p. 1495-1501.

17. Menz, H.B., Lord, S.R., and McIntosh, A.S., 2001. Slip resistance of casual footwear: Implications for older adults. *Gerontology* **47**(3): p. 145-149.

18. Burnfield, J. and Powers, C., 2006. Prediction of slip events during walking: An analysis of utilized coefficient of friction and available slip resistance. *Ergonomics* **49**(10): p. 982-985.

19. Hanson, J.P., Redfern, M.S., and Mazumdar, M., 1999. Predicting slips and falls considering required and available friction. *Ergonomics* **42**(12): p. 1619-1633.

20. Powers, C.M., Burnfield, J.M., Lim, P., Brault, J.M., and Flynn, J.E., 2002. Utilized coefficient of friction during walking: Static estimates exceed measured values *Journal of Forensic Sciences* **47**(6): p. 1303-1308.

21. Siegmund, G.P., Heiden, T.L., Sanderson, D.J., Inglis, J.T., and Brault, J.M., 2006. The effect of subject awareness and prior slip experience on tribometer-based predictions of slip probability. *Gait & Posture* **24**(1): p. 110-119.

22. Tsai, Y.J. and Powers, C.M., 2008. The influence of footwear sole hardness on slip initiation in young adults. *Journal of Forensic Sciences* **53**(4): p. 884-888.

23. Redfern, M.S. and DiPasquale, J., 1997. Biomechanics of descending ramps. *Gait & Posture* **6**(2): p. 119-125.

24. Leclercq, S., Tisserand, M., and Saulnier, H., 1993. Quantification of the slip resistance of floor surfaces at industrial sites. Part II: Choice of optimal measurement conditions. *Safety Science* **17**: p. 41-55.

25. Redfern, M.S. and Bidanda, B., 1994. Slip resistance of the shoe-floor interface under biomechanically-relevant conditions. *Ergonomics* **37**(3): p. 511-524.

26. Wilson, M.P., 1990. Development of satra slip test and tread pattern design guidelines. *Slips, Stumbles, and Falls: Pedestrian Footwear and Surfaces*: p. 113-123.

27. Gronqvist, R., Matz, S., and Hirvonen, M., 2003. Assessment of shoe-floor slipperiness with respect to contact-time-related variation in friction during heel strike. *Occupational Ergonomics* **3**: p. 197-208.

28. Chang, W.R. and Matz, S., 2001. The slip resistance of common footwear materials measured with two slipmeters. *Applied Ergonomics* **32**(6): p. 549-558.

29. Gronqvist, R., 1995. Mechanisms of friction and assessment of slip resistance of new and used footwear soles on contaminated floors. *Ergonomics* **28**: p. 224-241.

30. Manning, D.P. and Jones, C., 2001. The effect of roughness, floor polish, water, oil and ice on underfoot friction: Current safety footwear solings are less slip resistant than microcellular polyurethane. *Applied Ergonomics* **32**(2): p. 185-196.

31. Li, K.W. and Chen, C.J., 2004. The effect of shoe soling tread groove width on the coefficient of friction with different sole materials, floors, and contaminants. *Applied Ergonomics* **35**(6): p. 499-507.

32. Li, K.W., Chen, C.J., Lin, C.H., and Hsu, Y.W., 2006. Relationship between measured friction coefficients and two tread groove design parameters for footwear pads. *Tsinghua Science & Technology* **11**(6): p. 712-719.

33. Chang, W.R., 1998. The effect of surface roughness on dynamic friction between neolite and quarry tile. *Safety Science* **29**: p. 89-105.

34. Chang, W.R., 1999. The effect of surface roughness on the measurement of slip resistance. *International Journal of Industrial Ergonomics* **24**: p. 299-313.

35. Chang, W.R., 2001. The effect of surface roughness and contaminant on the dynamic friction of porcelain tile. *Applied Ergonomics* **32**(2): p. 173-184.

36. Chang, W.R., 2002. The effects of slip criterion and time on friction measurements. *Safety Science* **40**(7-8): p. 593-611.

37. Chang, W.R., 2004. Preferred surface microscopic geometric features on floors as potential interventions for slip and fall accidents on liquid contaminated surfaces. *Journal of Safety Research* **35**(1): p. 71-79.

38. Chang, W.R., Gronqvist, R., Hirvonen, M., and Matz, S., 2004. The effect of surface waviness on friction between neolite and quarry tiles. *Ergonomics* **47**(8): p. 890-906.

39. Perkins, P.J., 1978. Measurement of slip between the shoe and ground during walking, in *Walkway surfaces: Measurement of slip resistance*. ASTM 649: Philadelphia, PA.

40. Strandberg, L. and Lanshammar, H., 1981. The dynamics of slipping accidents. *Journal of Occupational Accidents* **3**(1): p. 153-162.

41. Cham, R. and Redfern, M.S., 2002. Heel contact dynamics during slip events on level and inclined surfaces. *Safety Science* **40**(7-8): p. 559-576.

42. Brady, R.A., J. Pavol, M., Owings, T.M., and Grabiner, M.D., 2000. Foot displacement but not velocity predicts the outcome of a slip induced in young subjects while walking. *Journal of Biomechanics* **33**(7): p. 803-808.

43. Moyer, B.E., Chambers, A.J., Redfern, M.S., and Cham, R., 2006. Gait parameters as predictors of slip severity in younger and older adults. *Ergonomics* **49**(4): p. 329-343.

44. Lockhart, T.E., Woldstad, J.C., Smith, J.L., and Ramsey, J.D., 2002. Effects of age related sensory degradation on perception of floor slipperiness and associated slip parameters *Safety Science* **40**(7-8): p. 689-703.

45. Lockhart, T.E., Woldstad, J.C., and Smith, J.L., 2003. Effects of age-related gait changes on the biomechanics of slips and falls. *Ergonomics* **46**(12): p. 1136-1160.

46. Pai, Y.C. and Patton, J., 1997. Center of mass velocity-position predictions for balance control. *Journal of Biomechanics* **30**(4): p. 347-54.

47. Bhatt, T., Wening, J.D., and Pai, Y.C., 2005. Influence of gait speed on stability: Recovery from anterior slips and compensatory stepping. *Gait & Posture* **21**(2): p. 146-156.

48. Cham, R. and Redfern, M.S., 2001. Lower extremity corrective reactions to slip events. *Journal of Biomechanics* **34**: p. 1439-1445.

49. Marigold, D.S. and Patla, A.E., 2002. Strategies for dynamic stability during locomotion on a slippery surface: Effects of prior experience and knowledge. *Journal of Neurophysiology* **88**(1): p. 339-353.

50. Marigold, D.S., Bethune, A.J., and Patla, A.E., 2003. Role of the unperturbed limb and arms in the reactive recovery response to an unexpected slip during locomotion. *Journal of Neurophysiology* **89**(4): p. 1727-1737.

51. Moyer, B., 2006. *Slip and fall risks: Pre-slip gait contributions and post-slip response effects*. in *Bioengineering*. University of Pittsburgh: Pittsburgh.

52. Sandrian, P.N., 2006. *Arm movement during slipping*. in *Bioengineering*. University of Pittsburgh: Pittsburgh.

53. Kim, B. and Robinson, C., 2005. Postural control and detection of slip/fall initiation in the elderly population. *Ergonomics* **48**(9): p. 1065-1085.

54. Chambers, A.J. and Cham, R., 2007. Slip-related muscle activation patterns in the stance leg during walking. *Gait & Posture* **25**(4): p. 565-572.

55. Chang, W.R., Gronqvist, R., Leclercq, S., Brungraber, R.J., Mattke, U., Strandberg, L., Thorpe, S.C., Myung, R., Makkonen, L., and Courtney, T.K., 2001. The role of friction in the measurement of slipperiness, part 2: Survey of friction measurement devices. *Ergonomics* **44**(13): p. 1233-1261.

56. Gronqvist, R., Roine, J., Jarvinen, E., and Korhonen, E., 1989. An apparatus and a method for determining the slip resistance of shoes and floors by simulation of human foot motions. *Ergonomics* **32**(8): p. 979-995.

57. Beschorner, K.E., Redfern, M.S., Porter, W.L., and Debski, R.E., 2007. Effects of slip testing parameters or measured coefficient of friction. *Applied Ergonomics* **38**(6): p. 773-780.

58. Skiba, R., Kuschefski, A., and Cziuk, N., 1987. Entwicklung eines normgerechten prufverfahrens zur ermittlung der gleitsicherheit von schuhsohlen, forschung fb 526. *Schriftenreihe der Bundesanstalt fur Arbeitsschutz*.

59. DIN 51130, 2004. *Testing of floor coverings; determination of the anti-slip-properties; workrooms and fields of activities with slip danger; walking method; ramp test*. G.N.S. 2004.

60. Cham, R. and Redfern, M.S., 2002. Changes in gait when anticipating slippery floors. *Gait & Posture* **15**(2): p. 159-71.

61. McVay, E.J. and Redfern, M.S., 1994. Rampway safety: Foot forces as a function of rampway angle. *American Industrial Hygiene Association Journal* **55**(7): p. 626-634.

62. Redfern, M.S., Cham, R., Gielo-Perczak, K., Gronqvist, R., Hirvonen, M., Lanshammar, H., Marpet, M.I., and Pai, Y.C., 2001. Biomechanics of slips. *Ergonomics* **44**: p. 1138-1166.

63. Leamon, T.B. and Li, K.W., 1990. Microslip length and the perception of slipping. in *23rd International Congress on Occupational Health*. Montreal, Canada.

64. Leamon, T.B. and Son, D.H., 1989. The natural history of microslip. *Advances in Industrial Ergonomics and Safety I*: p. 633-638.

65. Kim, I.J., 2004. Development of a new analyzing model for quantifying pedestrian slip resistance characteristics: Part I–basic concepts and theories. *International Journal of Industrial Ergonomics* **33**(5): p. 395-401.

66. Kim, I.J., 2004. Development of a new analyzing model for quantifying pedestrian slip resistance characteristics: Part II—experiments and validations. *International Journal of Industrial Ergonomics* **33**(5): p. 403-414.

67. Kim, I.J. and Smith, R., 2000. Observation of the floor surface topography changes in pedestrian slip resistance measurements. *International Journal of Industrial Ergonomics* **26**(6): p. 581-601.

68. Proctor, T.D. and Coleman, V., 1988. *Slipping, tripping and falling accidents in great britain- present and future*. in *Journal of Occupational Accidents*.

69. Sun, Z., Howard, D., and Moatamedi, M., 2005. Finite-element analysis of footwear and ground interaction. *Strain* **41**: p. 113-115.

70. Higgs, C.F., Ng, S.H., Borucki, L., Yoon, I., and Danyluk, S., 2005. A mixed-lubrication approach to predicting CMP fluid pressure modeling and experiments. *Journal of The Electrochemical Society* **152**: p. G193.

71. Shan, L., Levert, J., Meade, L., Tichy, J., and Danyluk, S., 2000. Interfacial fluid mechanics and pressure prediction in chemical mechanical polishing. *Journal of Tribology* **122**: p. 539.

72. Greenwood, J.A. and Williamson, J.B.P., 1966. Contact of nominally flat surfaces. *Proceedings of the Royal Society of London. Series A, Mathematical and Physical Sciences (1934-1990)* **295**(1442): p. 300-319.

73. Patir, N. and Cheng, H.S., 1977. Average flow model for determining effects of three-dimensional roughness on partial hydrodynamic lubrication. *American Society of Mechanical Engineers (Paper)* (77-Lub-17): p. 6.

74. Bolander, N.W. and Sadeghi, F., 2007. Deterministic modeling of honed cylinder liner friction. *Tribology Transactions* **50**(2): p. 248-256.

75. Deolalikar, N., Sadeghi, F., and Marble, S., 2008. Numerical modeling of mixed lubrication and flash temperature in EHL elliptical contacts. *Journal of Tribology* **130**: p. 011004.

76. Beschorner, K.E. and Cham, R., 2008. Impact of joint torques on heel acceleration at heel contact, a contributor to slips and falls. *Ergonomics* **51**(12): p. 1799-1813.

77. U.S. Department of Labor- Bureau of Labor Services, 2005. *National census of fatal occupational injuries in 2004*. Washington, D.C.

78. U.S. Department of Labor- Bureau of Labor Services, 2005. *Lost-work time injuries and illnesses: Characteristics and resulting time away from work, 2004/ supplemental tables*. Washington, DC.

79. Layne, L.A. and Pollack, K.M., 2004. Nonfatal occupational injuries from slips, trips, and falls among older workers treated in hospital emergency departments, united states 1998. *American Journal of Industrial Medicine* **46**(1): p. 32-41.

80. Grönqvist, R., Abeysekera, J., Gard, G., Hsiang, S.M., Leamon, T.B., Newman, D.J., Gielo-Perczak, K., Lockhart, T.E., and Pai, C.Y.C., 2001. Human-centred approaches in slipperiness measurement. *Ergonomics* **44**(13): p. 1167-1199.

81. Gronqvist, R., Chang, W., Courtney, T.K., Leamon, T., Redfern, M.S., Strandberg, L., and Norrkoping, S., 2003. Measurement of slipperiness: Fundamental concepts and definitions. *Measuring Slipperiness: Human Locomotion and Surface Factors*.

82. Chang, W.R., Gronqvist, R., Leclercq, S., Myung, R., Makkonen, L., Strandberg, L., Brungraber, R.J., Mattke, U., and Thorpe, S.C., 2001. The role of friction in the measurement of slipperiness, part 1: Friction mechanisms and definition of test conditions. *Ergonomics* **44**(13): p. 1217-1232.

83. Chang, W.R., Kim, I.J., Manning, D.P., and Bunterngchit, Y., 2001. The role of surface roughness in the measurement of slipperiness. *Ergonomics* **44**(13): p. 1200-1216.

84. Irvine, C.H., 1976. Evaluation of some factors affecting measurements of slip resistance of shoe sole materials on floor surfaces. *Journal of Testing and Evaluation* **4**(2): p. 133-138.

85. Kim, B.J. and Robinson, C.J., 2006. Effects of diabetic neuropathy on body sway and slip perturbation detection in older population. *International Journal of Occupational Safety and Ergonomics* **12**(3): p. 241-254.

86. Brown, L.A., Doan, J.B., McKenzie, N.C., and Cooper, S.A., 2006. Anxiety-mediated gait adaptations reduce errors of obstacle negotiation among younger and older adults: Implications for fall risk. *Gait & Posture* **24**(4): p. 418-423.

87. Chen, H.C., Schultz, A.B., Ashton-Miller, J.A., Giordani, B., Alexander, N.B., and Guire, K.E., 1996. Stepping over obstacles: Dividing attention impairs performance of old more than young adults. *Journals of Gerontology Series A: Biological and Medical Sciences* **51**(3): p. 116-122.

88. McKenzie, N.C. and Brown, L.A., 2004. Obstacle negotiation kinematics: Age-dependent effects of postural threat. *Gait & Posture* **19**(3): p. 226-234.

89. Redfern, M.S., Jennings, J.R., Martin, C., and Furman, J.M., 2001. Attention influences sensory integration for postural control in older adults. *Gait & Posture* **14**(3): p. 211-216.

90. Redfern, M.S., Muller, M., Jennings, J.R., and Furman, J.M., 2002. Attentional dynamics in postural control during perturbations in young and older adults. *Journals of Gerontology Series A: Biological and Medical Sciences* **57**(8): p. 298-303.

91. Ferber, R., Osternig, L.R., Woollacott, M.H., Wasielewski, N.J., and Lee, J.H., 2002. Reactive balance adjustments to unexpected perturbations during human walking. *Gait & Posture* **16**(3): p. 238-248.

92. Tang, P.F. and Woollacott, M.H., 1998. Inefficient postural responses to unexpected slips during walking in older adults. *The Journals of Gerentology. Series A, Biological Sciences and Medical Sciences* **53**(6): p. M471-480.

93. Tang, P.F., Woollacott, M.H., and Chong, R.K.Y., 1998. Control of reactive balance adjustments in perturbed human walking: Roles of proximal and distal postural muscle activity. *Experimental brain research* **119**(2): p. 141-152.

94. Holbein-Jenny, M.A., Redfern, M.S., Gottesman, D., and Chaffin, D.B., 2007. Kinematics of heelstrike during walking and carrying: Implications of slip-resistance testing. *Ergonomics* **50**: p. 352-363.

95. Buczek, F.L. and Banks, S.A., 1996. High-resolution force plate analysis of utilized slip resistance in human walking. *Journal of Testing and Evaluation* **24**(6): p. 353-358.

96. Burnfield, J.M., Tsai, Y.J., and Powers, C.M., 2005. Comparison of utilized coefficient of friction during different walking tasks in persons with and without a disability. *Gait & Posture* **22**: p. 82–88.

97. Lockhart, T.E. and Kim, S., 2006. Relationship between hamstring activation rate and heel contact velocity: Factors influencing age-related slip-induced falls. *Gait & Posture* **24**(1): p. 23-34.

98. Winter, D.A., 2004. *Biomechanics and motor control of human movement*. New York, NY: John Wiley and Sons.

99. Winter, D.A., Patla, A.E., Frank, J.S., and Walt, S.E., 1990. Biomechanical walking pattern changes in the fit and healthy elderly. *Physical Therapy* **70**(6): p. 340.

100. Heiden, T.L., Sanderson, D.J., Inglis, J.T., and Siegmund, G.P., 2006. Adaptations to normal human gait on potentially slippery surfaces: The effects of awareness and prior slip experience. *Gait & Posture* **24**(2): p. 237-246.

101. ASTM F-1679-04, 2006. Standard test method for using a variable incidence triobometer (VIT), in *Annual book of ASTM standards 15.07*. ASTM: West Conshohocken, PA.

102. de Leva, P., 1996. Adjustments to Zatsiorsky-Seluyanov's segment inertia parameters. *Journal of Biomechanics* **29**(9): p. 1223-1230.

103. Pai, Y.C., 2003. Movement termination and stability in standing. *Exercise and Sports Sciences Reviews* **31**(1): p. 19-25.

104. Pavol, M.J. and Pai, Y.C., 2002. Feedforward adaptations are used to compensate for a potential loss of balance. *Experimental Brain Research* **145**: p. 528-538.

105. Iqbal, K. and Pai, Y., 2000. Predicted region of stability for balance recovery: Motion at the knee joint can improve termination of forward movement. *Journal of Biomechanics* **33**(12): p. 1619-1627.

106. Courtney, T.K., Chang, W.R., Gronqvist, R., and Redfern, M.S., 2001. The measurement of slipperiness--an international scientific symposium. *Ergonomics* **44**(13): p. 1097-1101.

107. Tisserand, M., 1985. Progress in the prevention of falls caused by slipping. *Ergonomics* **28**: p. 1027-1042.

108. Stevenson, M., 1997. Evaluation of the slip resistance of six types of women's safety shoe using a newly developed testing machine. *Journal of Occupational Health and Safety-Australia and New Zealand* **13**: p. 175-182.

109. Stevenson, M.G., Hoang, K., Bunterngchit, Y., and Lloyd, D., 1989. Measurement of slip resistance of shoes on floor surfaces. Part 1. Methods. *Journal of Occupational Health and Safety- Australia and New Zealand* **5**: p. 115-120.

110. Aschan, C., Hirvonen, M., Mannelin, T., and E., R., 2005. Development and validation of a novel portable slip simulator. *Applied Ergonomics* **36**: p. 585-593.

111. Skiba, R., Bonefeld, X., and Mellwig, D., 1983. Voraussetzung zur bestimmung der gleitsicherheit beim menschlichen gang. *Zeitschrift für Arbeitswissenschaft* **9**: p. 227-232.

112. Gronqvist, R., Hirvonen, M., Rajamaki, E., and Matz, S., 2003. The validity and reliability of a portable slip meter for determining floor slipperiness during simulated heel strike. *Accident: Analysis and Prevention* **35**(2): p. 211-225.

113. GmbH, K.R., 2004. Robots specification kr150 kr150w kr180 kr210.

114. Moller, U.J. and Boor, U., eds. 1996. *Lubricants in operation*. Mechanical Engineering Publications Limited: London.

115. Beschorner, K.E., Higgs, C.F., and Lovell, M., 2008. Solution of Reynolds equation in polar coordinates applicable to non-symmetric entrainment velocities. *Journal of Tribology* **in press.**

116. U.S. Department of Labor- Bureau of Labor Statistics, 2007. *Nonfatal occupational injuries and illnesses requiring days away from work, 2006*. Washington, D.C.

117. U.S. Department of Labor- Bureau of Labor Statistics, 2007. *2006 census of fatal occupational injuries, supplementary tables*. Washington, D.C.

118. Chang, W.R., 2003. *Measuring slipperiness: Human locomotion and surface factors*: CRC Press.

119. Strandberg, L., 1985. The effect of conditions underfoot on falling and overexertion accidents. *Ergonomics* **28**(1): p. 131-147.

120. Kim, I.J. and Nagata, H., 2008. Research on slip resistance measurements—a new challenge. *Industrial Health* **46**(1): p. 66-76.

121. Zhu, D. and Cheng, H.S., 1988. Effect of surface roughness on the point contact EHL. *Journal of Tribology* **110**(1): p. 32-37.

122. Zhao, J., Sadeghi, F., and Hoeprich, M.H., 2001. Analysis of EHL circular contact start up: Part I—mixed contact model with pressure and film thickness results. *Journal of Tribology* **123**: p. 67-74.

123. Terrell, E.J., Kuo, M., and Higgs, C.F., 2005. An approach to modeling particle-based and contact-based wear in CMP. *MRS Bulletin* **5**(V30): p. 0991-C06-04.

124. Johnson, K.L., 1987. *Contact mechanics*. Cambridge: Cambridge Univeristy Press.

125. Meyer, D., 2002. Reynolds equation for spherical bearings. *Journal of Tribology* **125**: p. 203-206.

126. Beschorner, K.E., Lovell, M.R., and Redfern, M.S., 2007. Shoe-floor frictional properties for varying sliding speed, pressure and contaminant. in *ASME/STLE Int. Joint Tribology Conf.* San Diego.

127. Bhushan, B., 1999. *Principles and applications of tribology*. New York: John Wiley & Sons, Inc.

128. Hamrock, B.J., Jacobson, B.O., and Schmid, S.R., 2004. *Fundamentals of fluid film lubrication*. New York: Marcel Dekker, Inc.

129. Pinkus, O. and Sternlight, B., 1961. *Theory of hydrodynamic lubrication*. New York: McGraw-Hill Book Company, Inc.

130. Park, S.-S., Cho, C.-H., and Ahn, Y., 2000. Hydrodynamic analysis of chemical mechanical polishing process. *Tribology International* **33**(10): p. 723-730.

131. Osorno, A., 2005. *Dynamic, in-situ pressure measurements during CMP*. Georgia Institute of Technology.

132. Ansys Inc., 2008, *Element reference: Fluid136*. Release 11.0 Documentation for ANSYS,

133. Bhatt, T. and Pai, Y.C., 2008. Can observational training substitute motor training in preventing backward balance loss after an unexpected slip during walking? *Journal of Neurophysiology* **99**(2): p. 843.

134. Cooper, R.C., Prebeau-Menezes, L.M., Butcher, M.T., and Bertram, J.E.A., 2008. Step length and required friction in walking. *Gait & Posture* **27**(4): p. 547-551.